CHALMERS
UNIVERSITY OF TECHNOLOGY

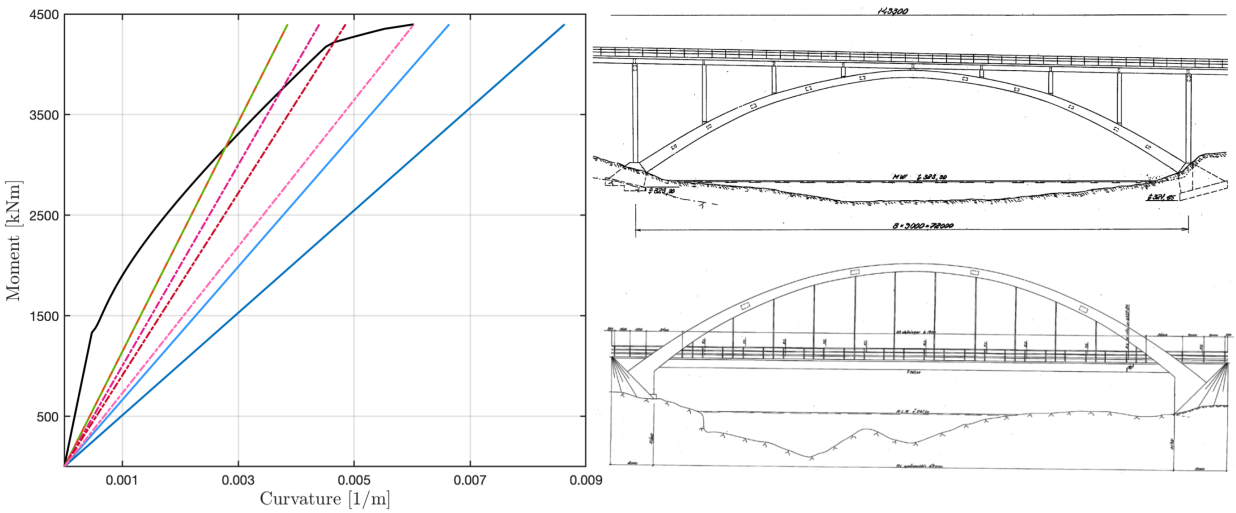

Calculation of stiffness in slender reinforced columns and arches in concrete bridges

A parametric study on stiffness calculation for isolated columns according to Eurocode

Master's thesis in the Master's Programme Structural Engineering and Building Technology

THERESE HAAR
MAJA LAGESON

DEPARTMENT OF ARCHITECTURE AND CIVIL ENGINEERING
DEVISION OF STRUCTURAL ENGINEERING AND BUILDING TECHNOLOGY

CHALMERS UNIVERSITY OF TECHNOLOGY
Master's thesis ACEX30
Gothenburg, Sweden 2025

MASTER'S THESIS ACEX30

Calculation of stiffness in slender reinforced columns and arches in concrete bridges

A parametric study on stiffness calculation for isolated columns according to Eurocode

Master's Thesis in the Master's Programme Structural Engineering and Building Technology

THERESE HAAR
MAJA LAGESON

Department of Architecture and Civil Engineering
Division of Structural Engineering and Building Technology
CHALMERS UNIVERSITY OF TECHNOLOGY
Gothenburg, Sweden 2025

Calculation of stiffness in slender reinforced columns and arches in concrete bridges
A parametric study on stiffness calculation for isolated columns according to Eurocode
Master's Thesis in the Master's Programme Structural Engineering and Building Technology

THERESE HAAR
MAJA LAGESON

Supervisor: Emanuel Trolin, Norconsult
Examiner: Carlos Gil Berrocal, Chalmers

Examensarbete ACEX30
Institutionen för Arkitektur och Samhällsbyggnadsteknik
Chalmers Tekniska Högskola, 2025

Department of Architecture and Civil Engineering
Division of Structural Engineering and Building Technology
Chalmers University of Technology
SE-412 96 Göteborg
Sweden
Telephone +46 31 772 1000

Cover:
Left: The non-linear and simplified stiffness of a cross-section. Right: Structural drawings of bridges over Ammerån and Indalsälven.
Department of Architecture and Civil Engineering
Göteborg, Sweden 2025

Calculation of stiffness in slender reinforced columns and arches in concrete bridges
A parametric study on stiffness calculation for isolated columns according to Eurocode

Master's thesis in the Master's Programme Structural Engineering and Building Technology

THERESE HAAR

MAJA LAGESON

Department of Architecture and Civil Engineering
Division of Structural Engineering and Building Technology
Chalmers University of Technology

ABSTRACT

For slender compressed reinforced concrete members such as bridge columns and arches, high stiffness is essential to limit deformations and ensure stability. However, increasing stiffness can generate significant restraint forces within the structure. Previous Norconsult projects on strengthening old bridges in Jämtland showed that the nominal stiffness values prescribed by EC2 are insufficient. Likewise, Norconsult's design of the Bukkestein Bridges demonstrated that when the superstructure deforms due to temperature changes and concrete shrinkage, it develops high forces that subject the substructure to loads beyond the intended design forces.

This thesis presents a parametric study of slender reinforced-concrete columns using nonlinear analysis in accordance with EC2's general method. The proposed calculation approach is validated by finite-element simulations in DIANA.

With the revised version of EC2 set to be adopted in the coming years, this study also evaluates its new provisions. The updated code replaces the nominal stiffness concept with an effective stiffness calculation that accounts for reinforcement yielding in the cross section and introduces a simplified global analysis method for column stiffness. Both revised-code approaches yield stiffness estimates comparable to those from the nonlinear analysis.

The parametric study examines how axial load, reinforcement ratio, and concrete strength influence stiffness and overall performance of slender columns. Results show that stiffness increases with higher axial force and reinforcement content. Analyses across various concrete-strength percentiles demonstrate that equivalent stiffness often exceeds nominal values making it possible to increase stiffness in capacity calculations by at least 29 %. The analysis shows that a reduction factor of approximately 0.45 can be applied to single, isolated columns, whereas columns with adjacent structural elements require a uniform reduction factor of 0.85 for all cases considered. By incorporating these factors into calculations, restraint forces can be mitigated, resulting in more efficient structures.

Key words: Equivalent stiffness, nominal stiffness, nonlinear analysis, concrete bridges, restraining forces, normal force, reinforcement content.

Beräkning av styvhet i slanka armerade pelare och bågar i betongbroar
En parameterstudie av beräkning av styvhet i enskilda pelare enligt Eurocode

Examensarbete inom masterprogrammet Structural engineering and buildning technology

THERESE HAAR

MAJA LAGESON

Institutionen för arkitektur och samhällsbyggnadsteknik
Avdelningen för konstruktion och byggnadsteknologi
Chalmers tekniska högskola

SAMMANFATTNING

För slanka, tryckta armerade betongmedlemmar, såsom bropelare och bågar, är hög styvhet avgörande för att begränsa deformationer och säkerställa stabilitet. Samtidigt kan ökad styvhet ge upphov till betydande tvångskrafter i konstruktionen. Tidigare Norconsult-projekt för förstärkning av gamla broar i Jämtland visade att EC2:s nominella styvhetsvärden inte ger tillräcklig kapacitet. Vid utformningen av Bukksteinbron noterades stora tvångskrafter orsakade av temperaturförändringar och krypning, vilket utsatte de bärande pelarna för betydande laster utöver huvudlasterna.

Denna avhandling presenterar en parametrisk studie av slanka armerade betongpelare med icke-linjär analys enligt EC2:s generella metod. Beräkningsmetoden valideras med FE-analys i DIANA.

Med den reviderade versionen av EC2, som väntas antas inom de närmaste åren, utvärderas även nya bestämmelser. Den uppdaterade koden ersätter nominell styvhet med en beräkning av effektiv styvhet som tar hänsyn till när armeringen flyter i tvärsnittet, och introducerar en förenklad global analysmetod för pelarstyvhet. Båda de reviderade metoderna ger styvhetsvärden som är jämförbara med dem som fås fram via icke-linjär analys.

Den parametriska studien undersöker hur axiell last, armeringskvot och betongens hållfasthet påverkar styvhet och prestanda hos slanka pelare. Resultaten visar att styvhet ökar med högre axiell kraft och mer armering. Analyser över olika betongstyrkepercentiler visar att ekvivalent styvhet ofta överstiger nominella värden, vilket möjliggör en ökning av beräknad styvhet med minst 29 %. Studien påvisar vidare att en reduktionsfaktor på cirka 0,45 kan användas för enskilda isolerade pelare, medan pelare med angränsande strukturella element kräver en enhetlig reduktionsfaktor på 0,85 i alla undersökta fall. Genom att inkludera dessa faktorer i beräkningarna minskas tvångskrafterna och effektiviteten i konstruktionen ökar.

Nyckelord: Ekvivalent styvhet, nominell styvhet, icke-linjär analys, betongbroar, tvångskrafter, normalkraft, armeringsmängd.

Contents

Preface

This master's thesis was carried out in 2025 as a collaboration between Norconsult and the Department of Structural Engineering and Building Technology at Chalmers University of Technology, in Gothenburg. This thesis aims to develop recommendations and guidelines for optimizing stiffness in bridge design.

The authors are grateful to the supervisor, Emanuel Trolin, Senior Bridge Engineer at Norconsult, for sharing his time, expertise and valuable insights throughout this work. We would also like to extend a sincere thanks to all colleagues in the Bridge and Analysis division at Norconsult, who patiently answered questions and provided practical guidance.

Finally, the authors thank the examiner, Carlos Gil Berrocal, for his clear, pedagogical guidance and for consistently providing constructive feedback throughout this thesis, which greatly enhanced the quality and clarity of the work.

Gothenburg, May 2025

Therese Haar and Maja Lageson

Definitions and acronymns

The following is a list of all acronyms and definitions used in this master's thesis, presented in alphabetical order.

EC2	Eurocode 2
EC2:2023	Eurocode 2 revision 2023
FE	Finite element
LEA	Linear Elastic Analysis
NLEA	Non-linear Elastic Analysis
NLFEA	Non-linear Finite Element Analysis
SLS	Service Limit State
State I	Uncracked state of reinforced concrete
State II	Cracked in tensile zone of reinforced concrete
State III	Fully cracked state of reinforced concrete
ULS	Ultimate Limit State

Notations

Below are all the notations used in the thesis, listed in alphabetical order:

Roman upper case letters

A	cross-section area $[m^2]$
E	modulus of elasticity $[Pa]$
F	load $[N]$
I	moment of inertia $[m^4]$
M	moment $[Nm]$
N	normal force $[N]$

Roman lower case letters

b	width of a cross section $[m]$
c	concrete cover thickness $[m]$
f_c	compression strength of concrete $[Pa]$
f_{cd}	design value of compression strength of concrete $[Pa]$
f_{ck}	characteristic compression strength of concrete $[Pa]$
f_{cm}	mean compression strength of concrete $[Pa]$
f_{ctk}	characteristic tensile strength of concrete $[Pa]$
f_{ctm}	mean tensile strength of concrete $[Pa]$
f_{yd}	design value of tensile strength for reinforcing steel $[Pa]$
f_{yk}	characteristic tensile strength for reinforcing steel $[Pa]$
h	height of a cross-section $[m]$
k_h	notional size coefficient
l, L	length of a member $[m]$
$1/r$	curvature $[1/m]$
t	time $[s, day]$
u	circumference $[m]$

Greek letters

α	coefficient [-]
β	coefficient [-]
γ	partial coefficient [-]
δ	deformation or deflection [m]
ζ	distribution coefficient [-]
ε	strain [-]
θ	rotation [rad]
κ	curvature [1/m]
λ	slenderness [-]
ρ	density $[kg/m^3]$
σ	stress [Pa]
ϕ	diameter [m]
φ	creep $[1/m]$

1 Introduction

For slender, compressed reinforced concrete members, such as columns and arches in bridges, achieving high stiffness is essential for reducing the influence of second-order effects. While this increased stiffness helps control deformations and maintain stability under load, it also introduces a challenge related to thermal expansion and shrinkage. These deformation-induced loads, which are typically not considered as the primary loads on a bridge, can still lead to severe load effects, especially if the bridge is highly restrained. As the concrete expands or contracts due to temperature changes and shrinkage, internal forces develop within the structure. These forces arise because the rigidity of the member restricts the free movement of adjacent structural components, such as the superstructure and foundations. The stiffness of a bridge substructure plays a significant role, as it connects the superstructure to the foundations. A decrease in the stiffness of the bridge substructure generally leads to a proportional decrease in restraining forces.

It is complex to calculate the correct stiffness due to the non-linear response of reinforced concrete, and as a result, the calculation is often simplified for practicality, as it can be too time-consuming to perform in every case. With better guidance on how to incorporate stiffness reduction, restraining forces could be further minimized, leading to potential material and cost savings within the field of concrete bridge engineering. At the same time, there are situations where higher stiffness is beneficial, particularly for slender members subjected to significant second-order effects. In such cases, simplified methods outlined in Eurocode for nominal stiffness or nominal curvature, are often used. However, more detailed stiffness calculations based on the general method in Eurocode, may lead to a higher stiffness, which in turn results in increased capacity. Understanding how different parameters affect the stiffness of a bridge structure is crucial, as it offers opportunities for innovative solutions that enhance both performance and cost-effectiveness.

It is important to ensure that structures are not over-engineered, as reducing the amount of material used is better for the environment. In Sweden alone, the construction sector accounted for 22.1% of the country's total greenhouse gas emissions in 2022 [1]. This highlights the need for sustainable design practices that minimize material use without compromising structural safety. By optimizing design, engineers can contribute to significant reductions in emissions while also lowering construction costs.

1.1 Background

In early design stages, simplified methods of calculating stiffness are often used as they are time-effective. In Eurocode 2 [2], from this point forward referred to as EC2, two simplified methods are provided, nominal stiffness and nominal curvature. Both methods are considered conservative and yield results on the safe side, which often returns structures with excessive dimensions. It has been discussed

whether the simplified methods are accurate enough [3], and the discussion concluded that practical usability was considered important. It is also noted that in later design stages, a non-linear analysis should be performed for more accurate results.

Norconsult has undertaken two projects in Jämtland focusing on arch bridges to assess whether their load-bearing capacity can be enhanced through refurbishment. Older bridges often suffer from capacity limitations stemming from the simplified design practices used at the time of their original conception. There are several factors that contribute to this, traffic loads have increased since the bridges were built, modern finite-element analysis enables far more detailed studies, and the understanding of structural instability has improved significantly. In addition, today's reinforcement materials and detailing differ in both design and quality from those used when these bridges were constructed.

The first bridge is located over the river Ammerån in Åre. Figure 1.1 shows a structural drawing of the bridge. This is a deck arch bridge, where the arch is positioned below the deck, supporting it from underneath. The bridge deck spans 143.3 m and the arch span is 72 m, the bridge is 4 m wide.

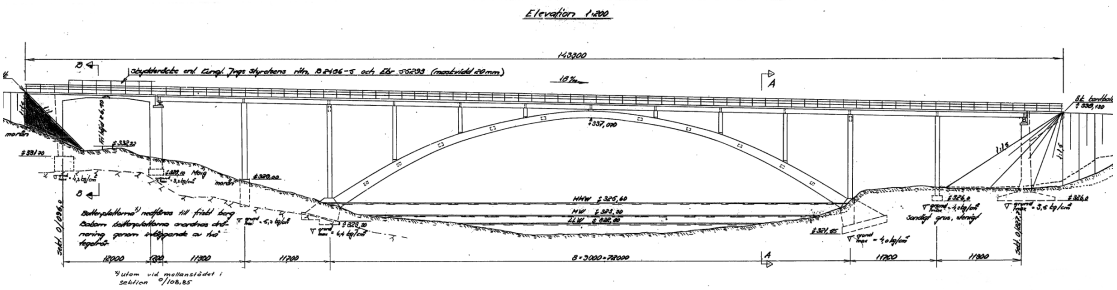

Figure 1.1: Structural drawing of the bridge over Ammerån in Åre, provided by Norconsult.

In total, five vertical supports rest on the arch, creating four intermediate spans in addition to the two end spans at the abutments. Notably, the supports are not symmetrical as the right support does not rest on a solid foundation. This asymmetry introduces a potential for rotational and stability issues. Furthermore, the arch lacks a transverse brace at its crown, resulting in a structurally weaker point at the top. This makes the crown more susceptible to out-of-plane deformation and increases the risk of local buckling under compressive forces. Figure 1.2 shows a photograph taken from the site in 2017.

Figure 1.2: Photograph taken of site, bridge over Ammerån in Åre, provided by Norconsult.

The second bridge crosses the river Indalsälven in Ragunda. Figure 1.3 presents the structural drawings of this bridge. It is a through arch bridge, where the arch rises above the deck and the deck is suspended from the arch using vertical hangers. The bridge is shorter than the bridge over Ammerån, and the deck spans 58 m and the arch span is 49 m. The bridge deck is slightly wider at 6 m.

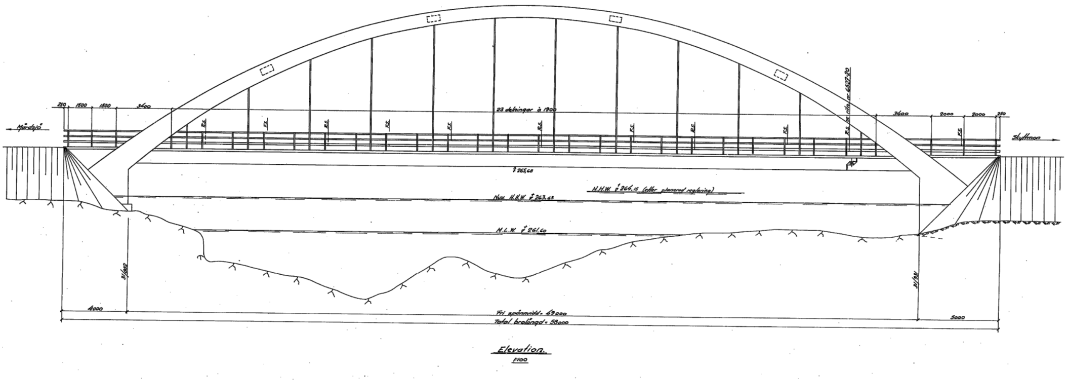

Figure 1.3: Structural drawing of the bridge over Indalsälven in Ragunda, provided by Norconsult.

The bridge was constructed in 1950 and the deck is suspended from the arch using 23 vertical hangers spaced at 1.8 meter intervals. This arrangement allows for efficient load transfer from the deck to the arch, enabling an unobstructed span across the river. Figure 1.4, which shows a photograph taken from the site in 2022.

Figure 1.4: Photograph taken on site, bridge over Indalsälven, provided by Norconsult.

During the investigations of the bridges, it was found that when applying the simplified method for nominal stiffness from EC2 [2], the bridges were deemed to lack sufficient capacity. This was surprising, considering that the bridges have been in service for 76 and 62 years, respectively. To more accurately assess the stiffness of the bridges, the general method in EC2 was used, which requires additional parameters and is more complex. This method provided a more accurate estimation of the remaining stiffness of the studied bridges. However, it also introduced certain methodological contradictions, which were challenging to interpret, particularly regarding how the calculations should be performed considering long-term effects like creep, a factor required by the current code.

Another problem that has been prevalent in projects at Norconsult is the occurrence of restraining forces. As a designer, it can be unclear what degree of stiffness to assume, since it depends on boundary conditions, interaction with other structural parts, and time-dependent effects. An incorrect assumption may result in either over- or underestimation of internal forces, which can compromise the safety or economy of the design. Here, the calculation of an equivalent stiffness is of importance. It is a simplified way to express the global, non-linear stiffness, with a constant stiffness. In this way, calculations can be carried out with reasonable accuracy while maintaining a manageable level of complexity.

The Bukkestein bridges, situated in Norway and designed by Norconsult is an example of a project that had issues with restraining forces. The bridges are multi-span continuous concrete girder bridges with the total length of 114.5 m, all divided into four main spans measuring 22 m, 28 m, 35 m, and 29.5 m. Figure 1.5 displays the structural drawing of one of the bridges.

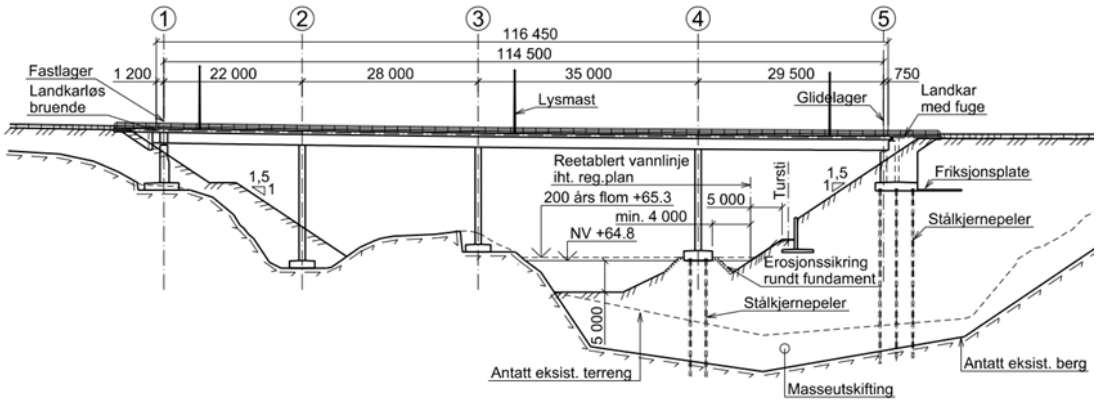

Figure 1.5: Structural drawing of one of the Bukestein bridges, provided by Norconsult.

The bridge decks are carried by slender columns of approximately 15-20 meters high, and fixed at both ends. The superstructures are equipped with a fixed bearing at one end and a sliding bearing at the other, allowing the bridge decks to move at one end. The design of the bridge structure induced large restraining forces in the columns, as they are forces to move in the longitudinal direction when the structure is subjected to loads from temperature variations and creep. Reducing stiffness to alleviate restraint forces in this type of structure is important, yet the columns must still maintain enough rigidity to support the bridge-deck load without risking buckling failure. Figure 1.6 shows a photograph taken from the site, showcasing the substructure of the bridge.

Figure 1.6: Photograph taken on site, Bukkestein bridges part of highway E39 in Norway, provided by Norconsult.

These projects demonstrate the complexity in structural design were there is a contradictory demand to both increase and decrease stiffness within the same structure, depending on the design objective. On one hand, increased stiffness

may be desired to ensure adequate load-bearing capacity, especially in elements critical for strength verification. On the other hand, reduced stiffness can be beneficial for minimizing restraining forces, which arise due to imposed deformations, boundary conditions, or differential movements. This duality creates a design dilemma, particularly in continuous or restrained structures where stiffness assumptions strongly influence internal force distribution. Balancing these opposing requirements requires a deep understanding of the structural behavior and the implementation of appropriate stiffness models, particularly in cases involving time-dependent effects such as creep and shrinkage.

The idea for this master's thesis originated from Norconsult, partly based on the insights gained from these projects, and is being conducted as a collaboration with Chalmers University of Technology.

1.2 Aim

This master's thesis seeks to examine the methodology for stiffness calculation in accordance with EC2, the current and revised version, focusing on the general and nominal stiffness method, while considering long-term effects. The main aim of this thesis is to develop recommendations and guidelines for optimizing stiffness in bridge design. The primary objective is to assess, through hand calculations, how the simplified method for stiffness calculation compare to the general non-linear method. This comparison will focus on evaluating the accuracy and reliability of the simplified methods when applied to different load cases, reinforcement configurations and boundary conditions. The hand calculations will be verified through non-linear finite element analysis, which provide understanding of the effectiveness and limitations of the methods, with the aim of evaluating the impact of using simplified methods for stiffness calculations in practical bridge design. Additionally, effective stiffness which is used when designing for retraining forces will be evaluated. The complexity of the need for high stiffness and reduction of stiffness in the same structure will be discussed.

Specific questions related to the investigation that will be answered in this master thesis are:

- How should material parameters be chosen in detailed calculations?
- How does the stiffness from detailed analysis compare to the uncracked stiffness, dependent on reinforcement amount and loading?
- How does a detailed calculation of stiffness of a compressed concrete member compare to the stiffness given by the method of nominal stiffness in EC2?
- How does hand calculations according to EC2 correspond to detailed non-linear finite element analysis?
- How can effective stiffness be calculated to reduce restraining forces? Is there a general reduction of column stiffness that can be used in design?

1.3 Scope and limitations

The scope of this thesis includes performing stiffness calculations following the general and nominal stiffness methods presented in EC2 using hand calculation. The study will focus on the stiffness of single, isolated columns in compression, where the geometry of the cross-section will be limited to 1 by 1 meter, with tensile reinforcement amounts of 7 and 9 bars, with diameters of 20, 25, and 32 mm. The applied axial loads will be limited to 1, 3, 6, and 12 MN. Triangular load distribution is assumed at maximum load. The investigation will not address second-order effects. A discussion will be held on whether the proposed methods are suitable for practical application and how they affect the overall structural performance. In addition, the investigation will explore how the stiffness can be reduced to an effective stiffness to mitigate the degree of restraining force. The general non-linear stiffness calculation performed will be verified against a finite element analysis in order to verify the method. The analysis will be performed for one example case, a cantilever column with $7\phi25$ reinforcement with an applied axial force of 6 MN. A finite element analysis of second-order effects will not be performed due to time constraints and the challenges associated with accurately interpreting the results from such an investigation. By narrowing the scope to isolated columns the study can maintain a focused approach on stiffness within the given time frame. This limitation ensures a manageable and practical analysis while addressing the primary objectives.

1.4 Ethical aspects

This following section describes the ethical considerations of this thesis, such as compliance with standards, academic integrity, and the social- and environmental-impacts. This is to ensure the integrity and reliability of the work. Ethical aspects are carefully addressed to maintain transparency, honesty, and adherence to academic standards throughout the process.

1.4.1 Compliance with standards

All calculations, including hand calculations and non-linear finite element analysis, are conducted in accordance with EC2 standards, with clear documentation of assumptions, limitations, and methods.

1.4.2 Academic integrity

In this project, the AI tool ChatGPT will be used to assist in editing and refining original text written by the the authors, specifically for tasks such as checking spelling, grammar, and sentence structure. This will help ensure that the final text has clarity, coherence, and readability. However, it is important to note that ChatGPT will not be used for tasks such as gathering information or conducting independent research. Furthermore, the AI will not be used to generate original content or write any sections of the project.

1.4.3 Environmental and social impact

Detailed stiffness calculations can improve material use and resource efficiency by enabling optimized designs that more accurately estimate loads, enhance structural performance, and slow degradation, ultimately extending the service life of a structure. In this thesis, environmental impact is addressed in the design of concrete columns by identifying methods that estimate stiffness more precisely, thereby reducing material consumption. Applying these refined calculations to restoration of existing bridges instead of demolishing and rebuilding conserves the embodied energy and materials such as steel, concrete and asphalt already invested and reduces greenhouse gas emissions from new production while minimizing demolition waste and transport emissions and preserving historical and cultural value. This approach also lessens demand on quarrying and manufacturing operations, which further cuts carbon emissions across the supply chain. Extending a bridge's service life through targeted repairs and upgrades lowers life cycle emissions and supports sustainable circular economy practices in the construction sector. Also, by reducing material procurement and waste management costs, communities benefit economically and infrastructure resilience is improved, ensuring safer and more reliable transport networks over time.

1.5 General methodology

The approach for this project involves a series of key steps designed to ensure thoroughness and accuracy throughout the process. These steps will be presented in the following sections, providing a clear and general overview of the methodology to be followed.

1.5.1 Literature study

To gather comprehensive and relevant information regarding the topic, a literature study will be conducted. This study will include a range of relevant publications, including scientific articles, technical papers, and other academic resources that have specifically investigated stiffness in the context of concrete structures. The aim is to obtain a broad understanding of the existing research and methodologies surrounding the topic. Additionally, both the current and forthcoming versions of EC2 will be thoroughly analyzed. This analysis will help in gaining a deeper insight into the methods and guidelines provided by EC2 for managing stiffness in calculations. The collected information from the literature study, which is directly relevant to the project, will then be compiled and structured into a dedicated theory chapter. This chapter will not only provide a theoretical foundation for the project but also serve to explain the significance of the research and establish the context for this thesis, ensuring that the work is grounded in existing knowledge and practices.

1.5.2 Calculations

The hand calculations in this study follow both the general and nominal stiffness approaches specified in EC2, as well as the stiffness calculation procedures introduced in the revised code. The aim is to determine the stiffness of concrete cross-sections under four axial load scenarios, four reinforcement configurations, and two boundary condition sets.

Initially, a numerical calculation method based on the general approach is executed. This process involves integrating the concrete and steel material models to derive the moment capacity, from which equivalent stiffness is computed. The equivalent stiffness from the non-linear analysis is then compared to the stiffness obtained via the nominal method. The purpose of these calculations is to assess the applicability and relevance of both the current and revised standards. All hand calculations are carried out using Mathcad Prime, and the results for one example case are validated against a non-linear finite element analysis in DIANA.

1.5.3 Non-linear finite element analysis

Non-linear finite element analyses (NLFEA) will be conducted as part of this master thesis to provide a detailed comparison with hand calculations. These analyses will be crucial in evaluating and contrasting the results obtained from the hand calculation methods, ensuring accuracy and reliability of the chosen approach. The FE analysis will assess both the uncracked and cracked stiffness of the concrete members, taking into account factors such as the non-linear material properties of the concrete and reinforcement. The FE analysis will be performed using the software DIANA (DIsplacement ANAlysis), which is well-suited for modeling the complex behavior of reinforced concrete structures and performing detailed simulations. This software will allow for a more accurate and in-depth analysis of the structural behavior.

2 Theory

This chapter presents the theoretical framework underlying the analysis and design of reinforced concrete columns subjected to axial and bending loads. Initially, fundamental structural analysis methods are introduced, including linear elastic analysis, non-linear analysis, and considerations of second-order effects. Subsequently, key material properties and their influence on structural behavior are discussed, focusing on concrete's compressive and tensile strengths, modulus of elasticity, and phenomena like creep and shrinkage. The use of partial factors in structural design is also addressed. Additionally, various concrete material models used for structural analysis are presented and compared.

Furthermore, the chapter examines the response of concrete sections under load, addressing critical aspects such as cracking stages, moment-normal (M-N) force interaction, cracking moment, moment capacity, stress calculation in cracked concrete (state II), and crack width control. Subsequently, the global structural response of columns is described, focusing on critical aspects including the contribution of uncracked concrete, deflection, slenderness, and stability against buckling. The general method for stiffness calculation and obtaining exact responses is described, as well as simplified second-order analysis methods specified in EC2, including the methods of nominal stiffness and nominal curvature. Important recent revisions introduced in Eurocode 2:2023 (EC2:2023), particularly regarding stiffness methods and second-order linear elastic analysis, are presented, as well as a review of prior studies in the field to offer a broader context for this thesis.

2.1 Structural analysis

This section introduces basic structural analysis concepts crucial for understanding the behavior of reinforced concrete columns. Initially, linear elastic analysis is discussed, highlighting idealized structural responses based on linear material properties. Subsequently, non-linear analysis is presented, emphasizing the role of material and geometrical non-linearities, such as concrete cracking and reinforcement yielding, in accurately predicting column behavior. Finally, the importance of second-order effects is outlined, explaining how axial loads, combined with lateral displacements, lead to additional deformations and stability considerations essential for safe structural design.

2.1.1 Linear elastic analysis

Linear elastic analysis (LEA) of concrete structures is presented in Section 5.4 in EC2 [2]. LEA is based on the assumption of uncracked cross-sections and a linear stress-strain relationship for materials. The mean modulus of elasticity, E_{cm}, should be used. Under the assumption of linear elasticity, the material deforms linearly when loaded and if the load is removed the deformation follows the same linearity back to zero. The superposition principle can be applied, which means that effects of different loads can be added directly.

2.1.2 Non-linear analysis

Section 5.7 of EC2 [2] covers non-linear analysis of concrete structures (NLEA), considering both material and structural non-linearity for a more accurate structural assessment. Material non-linearity includes the plastic behavior of concrete, crack formation, and subsequent softening, while reinforcement is modeled using an elastoplastic curve, see Figure 2.6. Geometrical non-linear effects, such as second-order effects, are crucial for large deformations, especially in slender structures. Analysis is typically performed numerically using the finite element method to account for complex behaviors such as cracking, creep, and stability issues. Such an analysis is made in iterations where equilibrium equations are solved for each load step. In this way, the analysis captures the redistribution of stiffness when the structure deforms. NLEA can be used in both serviceability state (SLS) and ultimate limit state (ULS).

2.1.3 Second-order effects

Second-order effects are non-linear behaviors in a structure that occur when deformations influence internal forces. These effects must be considered in structures where the axial force are of significant magnitude to alter the equilibrium state and affect load-bearing capacity. Geometric non-linearity can cause an additional 2nd order moment, this is commonly found in high-rise buildings, columns and frames. This additional moment amplifies the initial curvature of the structure. Figure 2.1 illustrates how the curvatures of the 1st and 2nd order moments adds to one total moment. If the deformations are large, they can cause the original equilibrium equation to no longer be valid, requiring more advanced analysis methods.

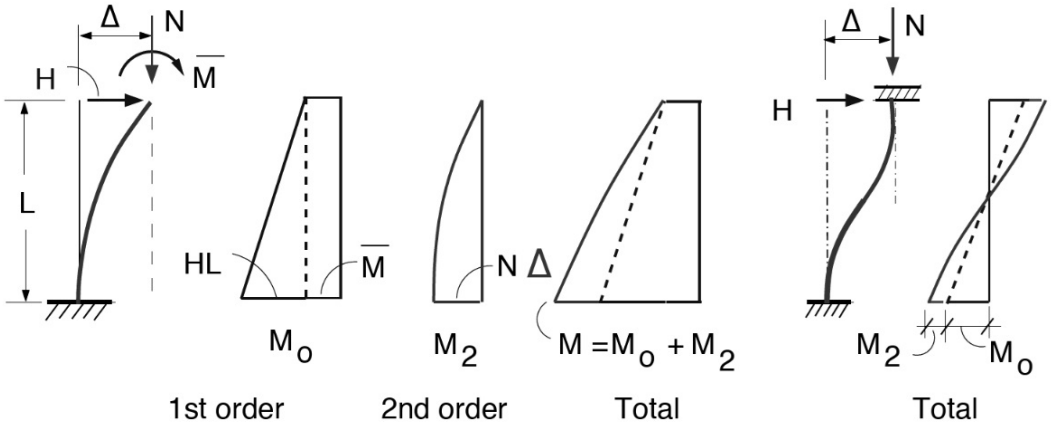

Figure 2.1: First and second-order moments of unbraced and braced columns. Figure 2.4 from [4].

Second-order effects can be particularly problematic in slender columns, as the additional moment can accelerate failure. Slenderness will be discussed more in-depth in Section 2.4.3. These second-order effects contribute to the total moment of a column, and if this contribution becomes excessive, it can compromise the stability of the column. Stability depends on the equilibrium between the applied and resisting moments, as illustrated in Figure 2.2. If equilibrium is not achieved, no solution exists, leading to instability or failure, as shown in Figure 2.2a. In contrast, Figure 2.2b illustrates a stable case, where the column is less slender and possesses sufficient stability to carry the additional moment without the risk of failure by buckling. Buckling is the lateral bending caused by axial loads due to initial imperfections, out-of-plane straightness deviations, initial curvature, or bending produced by a simultaneous bending moment.

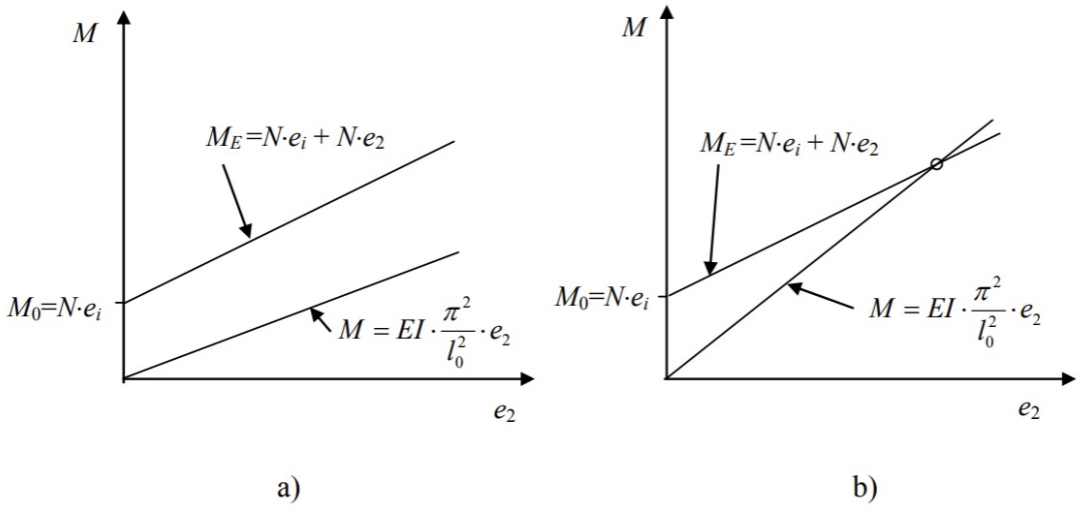

Figure 2.2: The response of columns with different slenderness a) unstable column, where the resisting moment is insufficient b) stable column in equilibrium. Figure K2.15 from [5].

If the second-order effects are smaller than 10% of the corresponding first-order effects, no consideration to second-order effects needs to be taken according to 5.8.2(6) in EC2 [2], for single columns.

2.2 Material behaviour

This section covers the key factors influencing material behaviour, including partial safety factors, compressive and tensile strength, modulus of elasticity, creep, shrinkage, and material models. These aspects are essential for accurately modelling and analyzing the response of materials and structures under various load conditions.

2.2.1 Partial factors

Table 2.1 shows the partial factors for concrete and reinforcing steel as presented in Section 2.4.2.4 in EC2 [2]. For serviceability state, the values of γ_c and γ_s should be set to 1.0.

Table 2.1: Partial factors for materials in ultimate limit states.

Design situations	γ_c **for concrete**	γ_s **for reinforcing steel**	γ_s **for prestressing steel**
Persistent & Transient	1,5	1,15	1,15
Accidental	1,2	1,0	1,0

Partial factors are used in structural design to account for uncertainties in loads, material properties, and calculation models. They ensure that the structure has sufficient safety and robustness without excessive dimensions.

2.2.2 Compressive strength

Figure 2.3 illustrates the variability of concrete compressive strength. The characteristic strength, $f_{ck0.05}$, corresponds to the 5th percentile of the distribution, i.e., the value exceeded by at least 95 % of specimens in standardized testing and represents the lowest expected strength for that concrete class, while the 95th percentile, $f_{ck0.95}$, denotes the highest strength likely to be observed under the same testing regime.

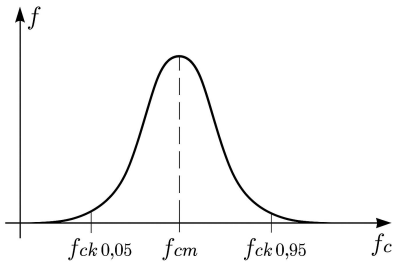

Figure 2.3: Standard deviation for concrete strength. Figure 9.4 from [6].

For concrete of an age of 28 days or more, the characteristic strength can be found in Table 3.1 in EC2 [2]. The compressive strength depends on the age of the concrete, the concrete type, the temperature and the curing conditions. The mean compressive strength, f_{cm}, for concrete younger than 28 days, can be determined by:

$$f_{cm}(t) = \beta_{cc}(t)\, f_{cm} \tag{2.1}$$

Where:

$$f_{cm} = f_{ck} + 8\,\text{MPa} \tag{2.2}$$

$$\beta_{cc}(t) = \exp\left\{ s \left[1 - \left(\frac{28}{t} \right)^{1/2} \right] \right\} \tag{2.3}$$

And:	$\beta_{cc}(t)$	is a coefficient that accounts for the concrete age
	s	is 0.20, 0.25 or 0.38 depending on concrete type
	t	is time, in days

The design compressive strength is dependent on the characteristic compressive strength, and is reduced by safety factors according to:

$$f_{cd} = \frac{\alpha_{cc} f_{ck}}{\gamma_C} \tag{2.4}$$

Where:	α_{cc}	is a coefficient that accounts for long-term effects on the compressive strength, values are given in the national annex
	γ_C	is the partial safety factor for concrete, see Section 2.2.1

2.2.3 Tensile strength

The characteristic value of tensile strength, f_{ctk}, represents the value that is exceeded by at least 95% of tested specimens in a standardized test. For concrete of an age of 28 days or more, the characteristic strength can be found in Table 3.1 in EC2 [2]. The tensile strength depends on the age of the concrete, the concrete type, the temperature and the curing conditions. The mean compressive strength, f_{ctm}, for concrete younger than 28 days, can be determined by:

$$f_{ctm}(t) = (\beta_{cc}(t))^{\alpha} f_{ctm} \tag{2.5}$$

Where:

$$f_{ctm} = f_{ctk} + 8\,\text{MPa} \tag{2.6}$$

And:	$\beta_{cc}(t)$	is a coefficient that accounts for the concrete age according to expression (2.3)
	α	is 1 for t $<$ 28 days
	α	is 2/3 for t $\geq$ 28 days

The design tensile strength is dependent on the characteristic tensile strength, and is reduced by safety factors according to:

$$f_{ctd} = \frac{\alpha_{cc} f_{ctk}}{\gamma_C} \tag{2.7}$$

Where:	α_{cc}	is a coefficient that accounts for long-term effects on the tensile strength, values are given in the national annex
	γ_C	is the partial safety factor for concrete, see Section 2.2.1

2.2.4 Modulus of elasticity

The mean modulus of elasticity, E_{cm}, is determined by the material's ability to resist deformation under load, it depends on the mean compressive strength of the concrete according to:

$$E_{cm} = 22 \left(\frac{f_{cm}}{10} \right)^{0.3} \tag{2.8}$$

For concrete under the age of 28 days, the mean modulus of elasticity is determined by:

$$E_{cm}(t) = \left(\frac{f_{cm}(t)}{f_{cm}} \right)^{0.3} E_{cm} \tag{2.9}$$

The design modulus of elasticity is determined by dividing the mean modulus of elasticity by the partial factor γ_C for concrete:

$$E_{cd} = \frac{E_{cm}}{\gamma_C} \tag{2.10}$$

2.2.5 Creep

Creep depends on the age of the concrete when the load is applied, as well as the load duration and size. The creep deformation after a long time is determined from:

$$\varepsilon_{cc}(\infty, t_0) = \varphi(\infty, t_0) \cdot \frac{\sigma_c}{E_c} \tag{2.11}$$

Here, the creep coefficient found in Appendix B in EC2 [2] is calculated as:

$$\varphi(t, t_0) = \varphi_0 \cdot \beta(t, t_0) \tag{2.12}$$

Where $\beta(t, t_0)$ is a parameter considering the load duration. The notional creep coefficient φ_0 is determined by:

$$\varphi_0 = \varphi_{RH} \cdot \beta(f_{cm}) \cdot \beta(t_0) \tag{2.13}$$

Where:
- φ_{RH} is a parameter considering the relative humidity, see expression (B.3) [2]
- $\beta(f_{cm})$ is a parameter considering the compressive strength of concrete, see expression (B.4) [2]
- $\beta(t_0)$ is a parameter considering the age of the concrete when the load is applied, see expression (B.5) [2]

To calculate the effective creep factor, φ_{ef}, the notional creep coefficient is multiplied by the ratio of the load that is assumed to be acting on the structure for a long time and the total load:

$$\varphi_{ef} = \varphi_0(\infty, t_0) \cdot load\,ratio \tag{2.14}$$

The effect of creep may be disregarded if all three conditions specified in Section 5.8.4(4) of EC2 [2] are satisfied. This applies when the creep factor is less than 2, the slenderness ratio does not exceed 75, and the ratio between the design moment and the design normal force remains below the height of the cross-section. Though, it is mentioned that precaution should be taken if creep is to be neglected at the same time as second-order effects are neglected, as it can yield results on the unsafe side. If the mechanical reinforcement ratio, ω ($A_s f_{yd}/A_c f_{cd}$), is at least 0.25, it is safe to neglect both creep and second-order effects according to the same section.

2.2.6 Shrinkage

Shrinkage depends on the difference in humidity content in the structure and in the surrounding air as well as the dimensions of the structure. The total shrinkage ,ε_{cs}, consists of drying shrinkage and autogenous shrinkage. The autogenous shrinkage starts as soon as the concrete is cast, while drying shrinkage typically starts at de-moulding when the structure is exposed to the surrounding air. The total shrinkage is therefore is determined by:

$$\varepsilon_{cs} = \varepsilon_{cd} + \varepsilon_{ca} \tag{2.15}$$

The drying shrinkage ε_{cd} is determined by:

$$\varepsilon_{cd} = \beta(t, t_s) \cdot k_h \cdot \varepsilon_{cd,0} \tag{2.16}$$

Where:
- $\beta(t, t_s)$ is a parameter considering the drying time, see expression (3.10) [2]
- k_h is a coefficient depending on the notional size ($2A_c/u$) of the structure, see Table 3.3 [2]
- $\varepsilon_{cd,0}$ is the nominal unrestraint drying shrinkage, see Table 3.2 [2]

The autogenous shrinkage is determined by:

$$\varepsilon_{ca} = \beta_{as}(t) \cdot \varepsilon_{ca}(\infty) \tag{2.17}$$

Where:
- $\beta_{as}(t)$ is a parameter considering the age of the concrete, see expression (3.13) [2]
- $\varepsilon_{ca}(\infty)$ is a coefficient considering the characteristic strength of concrete, see expression (3.12) [2]

2.2.7 Material models

EC2 provides two material models for concrete design. Figure 2.4 shows the general stress-strain material model, which should be used in cases where non-linear analysis is applied [6]. For concrete members, the design value for compressive strength, f_{cd}, and modulus of elasticity, E_{cd}, should be used.

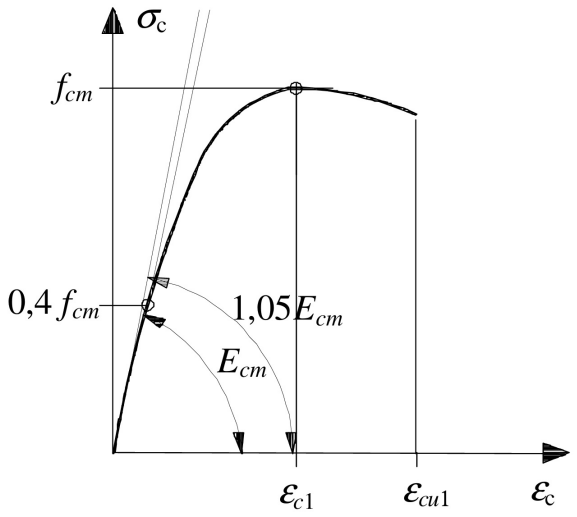

Figure 2.4: General stress-strain relation for structural analysis. Figure 9.4 from [6].

At low stress levels, the general stress-strain model follows an elastic relationship, where the slope of the curve is defined by the secant modulus, E_{cm}. Which is set at 40 % of the maximum strength, f_{cm}. This model also accounts for the softening behavior after the maximum strength is reached. The following formula describes the relation showcased in the figure:

$$\frac{\sigma_c}{f_{cm}} = \frac{k\eta - \eta^2}{1 + (k-2)\eta} \tag{2.18}$$

Where:	η	is equal to $\frac{\varepsilon_c}{\varepsilon_{c1}}$
	ε_{c1}	is the strain at peak stress according to Table 3.1 [2]
	k	is equal to $1.05E_{cm}\frac{\lvert\varepsilon_{c1}\rvert}{f_{cm}}$, f_{cm} according to Table 3.1 [2]

Figure 2.5 shows the second material model presented in EC2. This is a bilinear model, which is a simplified version of the non-linear curve intended for the design of cross-sections [6]. The two curves represent the relation between stress and strain, and follows the characteristic compressive strength, f_{ck}, and the design compressive strength, f_{cd}.

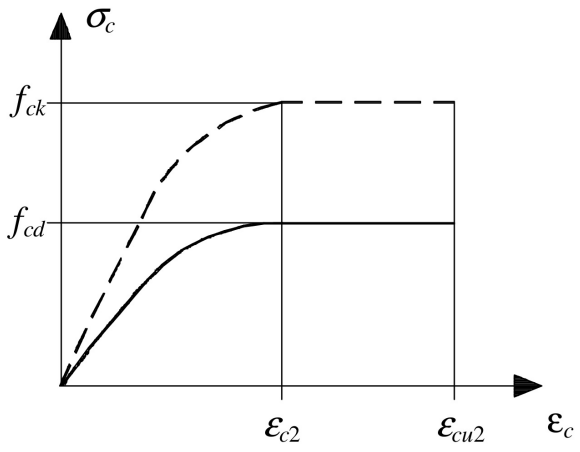

Figure 2.5: Simplified stress-strain relation for cross-section design. Figure 9.5 from [6].

The dashed curve in the figure represents the characteristic compressive strength, and the solid curve corresponds to the design compressive strength. For structural design, the lower solid curve is used, as it accounts for material variability and safety considerations.

The first part of the curves increases non-linearly until reaching the strain at peak stress, ε_{c2}. At this point, the corresponding stress is the design compressive strength, f_{cd}. After the design strength is reached, the curve flattens and remains constant until the ultimate strain, ε_{cu2}, is reached. The following formula describes the relation showcased in the figure:

$$\sigma_c = \begin{cases} f_{cd}\left[1 - \left(1 - \frac{\varepsilon_c}{\varepsilon_{c2}}\right)^n\right], & \text{for } 0 \leq \varepsilon_c \leq \varepsilon_{c2} \\ f_{cd}, & \text{for } \varepsilon_{c2} \leq \varepsilon_c \leq \varepsilon_{cu2} \end{cases} \tag{2.19}$$

Where:	n	is an exponent given in Table 3.1 in [2]
	ε_{c2}	is the the strain at peak stress
	ε_{cu2}	is the the ultimate strain

One notable difference between the two models is that the non-linear model is more accurate and follows the actual behavior of concrete more closely, requiring iteration during calculation. The simplified model is less complex but easier to apply in hand calculations. The non-linear model accounts for strain-softening behavior after the peak is reached while the simplified model assumes perfect plasticity after design compressive strength, f_{cd}, is reached.

The material model for reinforcing steel is illustrated in Figure 2.6. The curve shows both the idealized (dashed line) and the design (solid line) stress-strain relations. The idealized model simplifies the real behavior of steel, which makes it easier to use in analytical calculations.

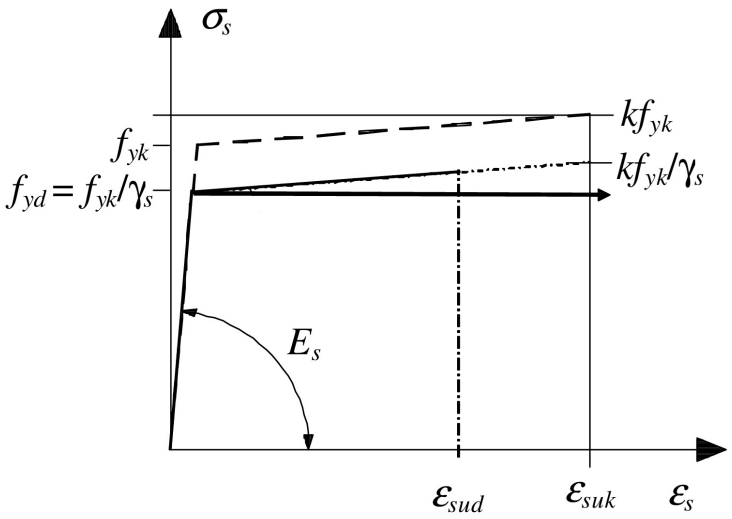

Figure 2.6: Idealized and design stress-strain diagrams for reinforcing steel. Figure 9.11 from [6].

Initially, the steel behaves linear elastically according to the modulus of elasticity, E_s. This is followed by yielding at characteristic yield strength, f_{yk}. The model applies to both hot rolled and cold worked reinforcing steel. The design strength of steel is reduced by safety factors, and is determined by the following formula:

$$f_{yd} = \frac{f_{yk}}{\gamma_s} \tag{2.20}$$

Where: f_{yk} is the characteristic steel strength
γ_s is the partial safety factor for steel, see Section 2.2.1

2.3 Response of concrete sections

The structural response of reinforced concrete sections is crucial for understanding how loads are resisted and distributed within a structure. Concrete exhibits a non-linear behavior, primarily due to its limited tensile strength and the formation of cracks under increasing load. The interaction between concrete and reinforcement determines the overall stiffness, strength, and failure mechanisms of the section.

This section outlines the different cracking stages a concrete section undergoes, the influence of axial load on moment capacity, and how cracking affects stiffness and deformation. Additionally, methods for estimating cracking moments, moment capacity, and crack widths are presented, providing a comprehensive framework for analyzing reinforced concrete sections.

2.3.1 Cracking stages

As load is increased on a structure, its cross-sections enter different cracking stages. At stage I the critical cross-section remains uncracked and both concrete and re-

inforcing steel have a linear elastic response. In stage II the cross-section is partly cracked, but the material responses of concrete and steel remains linear elastic. When the cross-section enters stage III it is considered cracked and either one or both materials have started to plasticize and shows a non-linear response. For cross-sections subjected to axial compression, stage III can be reached even if the section remains uncracked, since axial force has a favorable effect on crack formation and propagation.

Figure 2.7 shows a moment-curvature diagram illustrating how the moment increases with curvature until failure occurs for a section subjected to bending. The spans for the different states are marked, and the linear elastic material behavior of state I and state II is clearly illustrated. The slope of the curve represents the stiffness of the cross-section, which decreases as cracking and plastic deformations develop. If the section is also subjected to an axial compression force, the moment capacity increases. The section will be able to sustain a higher load before cracking, and the maximum moment will increase. With a high axial compressive force the plastic deformations in state III decrease, elevating the risk of brittle failure since the concrete may reach failure before all of the reinforcement yields [6].

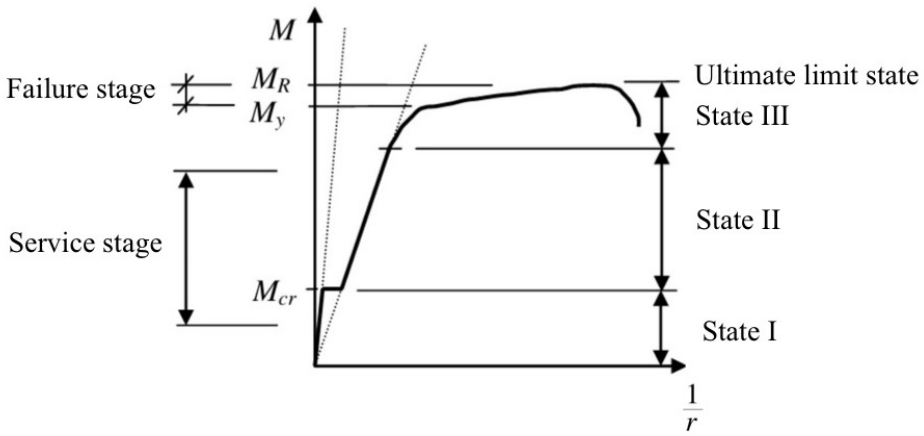

Figure 2.7: Cracking stages for a concrete cross-section. Figure B3.12 from [7]. Modified by the author.

2.3.2 M-N interaction

For a given reinforced concrete column section, the bending moment capacity is influenced by the axial load acting on the column. The moment capacity is therefore not a fixed sectional property but varies depending on the specific load case. Figure 2.8 illustrates the principal moment-curvature relationships for the same cross-section subjected to different magnitudes of axial compressive loads. The figure depicts typical ductile failures, where the tensile side of the column section is the critical part. In such failures, the presence of compressive load increase the moment capacity.

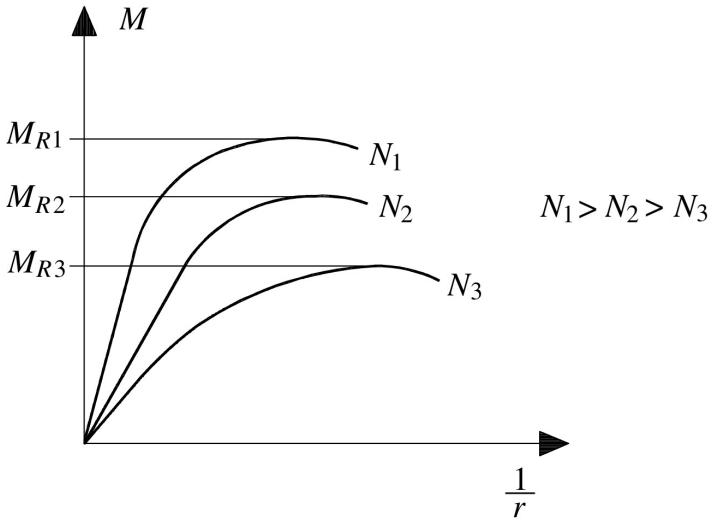

Figure 2.8: Moment-curvature relation for different load cases. Figure 13.6 from [6].

Figure 2.9 shows the interaction between moment and an axial compressive force N. The bending moment capacity is analyzed in state III and the different combinations of M and N inside of the curve will not lead to failure, while those outside of the curve will fail. At the point of balanced failure, the compressive strength of the concrete and the tensile strength of the reinforcing steel are both reached. In the case of a pure compression failure, the strain distribution remains uniform across the section and continues to increase until the section ultimately fails due to concrete crushing.

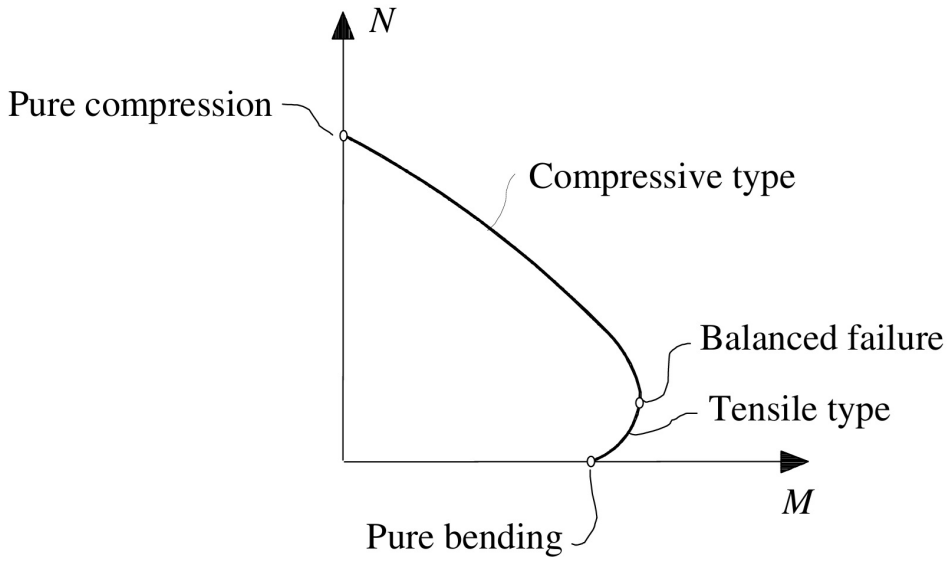

Figure 2.9: Moment-normal force interaction curve. Figure 13.7 from [6].

2.3.3 Cracking moment

When the cross-section is in stage I the material responses are linear elastic and the cracking moment, M_{cr}, depends on the tensile strength of the concrete, the axial compressive force and the moment of inertia, I_I of the uncracked section. Figure 2.10 shows an uncracked section subjected to an external moment and an axial compressive force.

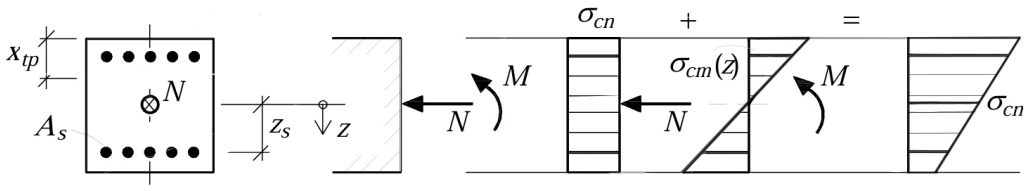

Figure 2.10: Cross-section in state I.

The cracking moment is calculated as:

$$M_{cr} = \left(f_{ct} + \frac{N}{A_I}\right) \frac{I_I}{h/2} \tag{2.21}$$

Where:
- f_{ct} is the tensile strength of the concrete
- I_I is the moment of inertia for the uncracked cross-section
- A_I is the transformed concrete section
- h is the height of the cross-section

The moment of inertia for an uncracked rectangular cross-section is calculated as:

$$I_I = I_c + I_s\,(\alpha - 1) \tag{2.22}$$

$$I_c = \frac{b\,h^3}{12} \tag{2.23}$$

$$I_s = \Sigma A_{si}\,(z_i - h/2)^2 \tag{2.24}$$

Where:
- I_c is the moment of inertia for the concrete
- I_s is the moment of inertia for the reinforcement
- α is modular ratio of steel and concrete E_s/E_c

The transformed concrete section is calculated as:

$$A_I = A_c + A_s(\alpha - 1) \tag{2.25}$$

Where:	A_c	is the gross concrete cross-section
	A_s	is the area of the reinforcement bars
	α	is modular ratio of steel and concrete E_s/E_c

To calculate the concrete stress at any height of the section, Navier's formula for bending and compression can be used:

$$\sigma_c = \frac{N}{A_I} + \frac{N \cdot e + M}{I_I} z \tag{2.26}$$

Where:	N	is the axial force
	A_I	is the area of the transformed concrete section
	e	is the eccentricity of the applied axial force
	M	is the moment
	I_I	is the moment of inertia of the uncracked section
	z	is the position of the cross-section where the stress is evaluated

2.3.4 Moment capacity

Figure 2.11 shows a cross-section in state III where the materials have started to plasticize, and the concrete has reached ultimate strain. To simplify the calculations, the stress block factors, α and β, are used to replace the non-linear stress distribution with an equivalent compression block.

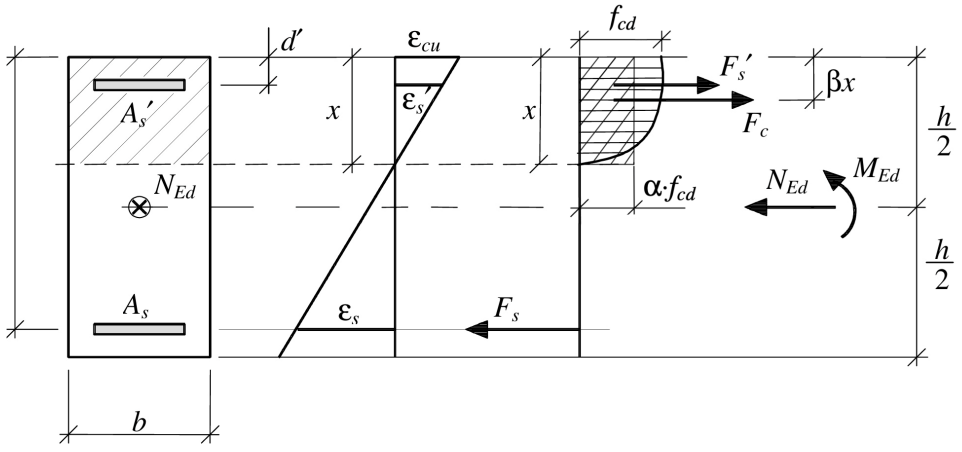

Figure 2.11: Cross-section in state III. Modified figure B5.28 from [5].

For a known normal force, N_{Ed}, the moment capacity, M_{Rd}, can be found through equilibrium equations. The height of the compressive zone is found through horizontal equilibrium which is determined as:

$$\alpha \cdot f_{cd} \cdot b \cdot x + \sigma'_s \cdot A'_s = \sigma_s \cdot A_s + N_{Ed} \tag{2.27}$$

Where:

α	is the average horizontal stress block factor
f_{cd}	is the design compressive strength of concrete
b, x	are measures according to Figure 2.11
σ'_s, σ_s	is the stress in the reinforcement
A'_s, A_s	is the area of the reinforcement steel
N_{Ed}	is the design normal force

The x can be extracted and the moment equation is taken about the tensile resultant to find the moment capacity according to:

$$M_{Rd} = \alpha \cdot f_{cd} \cdot b \cdot x(d - \beta \cdot x) + \sigma'_s \cdot A'_s(d - d') - N_{Ed}\left(d - \frac{h}{2}\right) \tag{2.28}$$

Where:

d, d', h	are distances according to Figure 2.11
β	is the average vertical stress block factor

2.3.5 Stress calculation in state II

For a concrete cross-section subjected to bending and normal force, the neutral axis is effected by the magnitude of loading. Since the equivalent cross-section is unknown, the analysis must begin by iterating the stresses. By guessing an x, the sectional properties can be calculated for the equivalent concrete cross-section. The transformed concrete section in state II is calculated as:

$$A_{II} = bx + (\alpha - 1)A'_s + \alpha A_s \tag{2.22}$$

The centroid of gravity for the compressive zone is calculated as:

$$x_{tp} = \frac{bx\,\frac{x}{2} + (\alpha - 1)\,A'_s\,d' + \alpha\,A_s\,d}{A_{II}} \tag{2.29}$$

The state II moment of inertia is non-linear and dependent on the applied normal force and the corresponding moment, it is calculated as:

$$I_{II} = \frac{bx^3}{12} + bx\left(\frac{x}{2} - x_{tp}\right)^2 + (\alpha - 1)A'_s(x_{tp} - d')^2 + \alpha A_s(d - x_{tp})^2 \tag{2.24}$$

Where:

bx	is the gross area of the compressive zone
A_s, A'_s	are the areas of the reinforcement bars
α	is the modular ratio E_s/E_{cm}

d, d' are the distances from the reinforcements and the top of the cross-section

The concrete stress is then calculated at the neutral layer $z = x - x_{tp}$. If $\sigma(z) \neq 0$ the x-value is incorrect and the calculation needs to be repeated, starting with a new value for x.

The stress is calculated using Navier's formula:

$$\sigma_c(z) = \frac{N}{A_{II}} + \frac{N \cdot e + M}{I_{II}} z \tag{2.25}$$

Where:
- N is the applied normal force
- A_{II} is the transomed concrete section
- e is the eccentricity $(\frac{h}{2} - x_{tp})$
- M is the applied moment
- I_{II} is the moment of inertia in state II

When the concrete stress at the neutral layer is equal to zero, the concrete stress can be calculated at steel level, where $z = d - x$. The steel stress can then be calculated at the same level as:

$$\sigma_s(z) = \alpha \, \sigma_c(z) \tag{2.30}$$

2.3.6 Crack spacing and crack width

It is natural for cracks to appear during SLS for reinforced concrete structures. Reinforcement is placed to ensure equilibrium after cracking. The following section will present how crack width, spacing and limitation is calculated according to EC2.

The characteristic crack spacing can be estimated with the following equation:

$$s_{r,\max} = k_3 c + k_1 \cdot k_2 \cdot k_4 \frac{\phi}{\rho_{p,ef}} \tag{2.31}$$

Where:
- c is the concrete cover of the longitudinal reinforcement
- k_1 factor accounting for the surface properties of the reinforcement
  - $k_1 = 0.8$ for ribbed bars
  - $k_1 = 1.6$ for smooth bars (e.g., prestressing steel)
- k_3 $7\phi/c$ according to national annex
- k_4 0.425 (national parameter, recommended value)
- ϕ is the diameter of the reinforcement

$\rho_{p,ef}$ is a parameter that describes the effective reinforcement ratio, which influences crack spacing and width in reinforced concrete structures. It is dependent on the reinforcement amount and A_{ef}, which is the area of the effective concrete between cracks. $\rho_{p,ef}$ is determined by the following:

$$\rho_{p,ef} = \frac{A_s}{A_{ef}} \tag{2.32}$$

The characteristic crack width for reinforced concrete structures is calculated according to EC2 as:

$$w_k = s_{r,\max}(\varepsilon_{sm} - \varepsilon_{cm}) \tag{2.33}$$

Where:
- $s_{r,\max}$ is the characteristic crack spacing
- ε_{sm} is the mean strain in the steel, including the effect of imposed deformation
- ε_{cm} is the mean strain in the concrete between cracks

The difference in mean strain between steel and concrete can be estimated as:

$$\varepsilon_{sm} - \varepsilon_{cm} = \frac{\sigma_s - k_t \frac{f_{cm}(t)}{\rho_{p,ef}}(1 + \alpha\,\rho_{p,ef})}{E_s}, \quad \text{but at least} \quad 0.6\,\frac{\sigma_s}{E_s} \tag{2.34}$$

Where:
- σ_s is the steel stress in the cracked section, calculated in stage II
- k_t is a factor accounting for the duration of loading
  - $k_t = 0.6$ for short-term loading
  - $k_t = 0.4$ for long-term loading
- α is the modular ratio of steel and concrete E_s/E_c

For columns subjected to both bending moment and axial force, cracks may close if the bending moment decreases sufficiently for the cross-section to be in compression at the level of the reinforcement. Even if the structure cracks under the design load in SLS, it may still be considered crack-free under lower loads. However, cracking still needs to be considered, especially because it can significantly affect the load-bearing capacity of columns.

EC2 states requirements for crack limitation. The requirements accounts for both the durability and appearance. Maximum allowable characteristic crack width w_k is discussed in Section 7.3 in EC2 [2], specific values are provided in the national annex. For long-term loading, the calculated characteristic crack width must be limited to certain permissible values, or the structure must be demonstrated to be crack-free in SLS.

Another method for limiting cracking, according to EC2, is by restricting the maximum allowable stress in both the concrete and the reinforcement. These limits are

given in Section 7.2 in EC2 [2]. By ensuring that stresses remain within acceptable levels, excessive cracking can be prevented, contributing to both structural performance and durability.

2.4 Global Response

The global response of a column is governed by its deformation behavior, stiffness, and stability. This section describes the influence of uncracked concrete, how deflections are calculated, the effects of slenderness, and the risk of buckling. These factors are essential for assessing the overall structural behavior and ensuring that stability requirements are met.

2.4.1 Contribution of uncracked concrete

Structural elements that are not anticipated to experience loads leading to stresses exceeding the concrete's tensile strength at any point should be regarded as uncracked. Elements expected to develop cracks but not fully crack will exhibit behavior that falls between the uncracked and fully cracked states. The concrete between cracks gives a small contribution to the capacity, so called tension stiffening. For elements primarily subjected to bending, their response can be reasonably estimated using the following expression:

$$\alpha = \zeta \alpha_{II} + (1 - \zeta)\alpha_I \tag{2.35}$$

Where α_I and α_{II} is the relevant deformation parameter. This can be strain, curvature or rotation. Where the distribution coefficient ζ is given by:

$$\zeta = 1 - \beta \left(\frac{\sigma_{sr,\mathrm{II}}}{\sigma_{s,\mathrm{II}}} \right)^2 \tag{2.36}$$

Where:
- β is 1.0 for short-term loading and 0.5 for long-term or frequently repeated loading
- $\sigma_{s,II}$ is the stress in the reinforcement calculated for the cracked cross-section
- $\sigma_{sr,II}$ is the corresponding stress for the cracking load

The distribution factor represents the extent to which a structure is cracked. It describes how the total deformation is divided between the cracked and uncracked sections of the element. As the stress in the reinforcement within the cracked section increases, the contribution of the cracked deformation becomes more significant. This means that a larger portion of the structure undergoes cracking, leading to a redistribution of internal forces and affecting the overall stiffness and deformation behavior of the member.

2.4.2 Deflection

The deflection of a structure can be determined by integrating the curvature along its length. This process, illustrated in Figure 2.12, involves summarizing the contributions from the slope at each section of the column. Each segment contributes to the overall deflection based on its curvature and the distance to the section of interest.

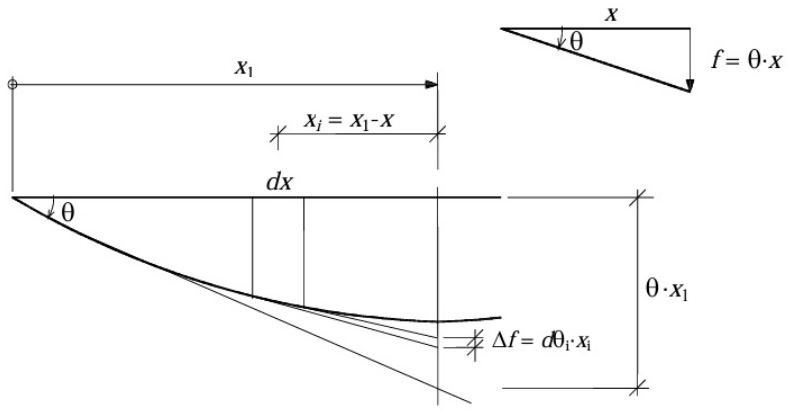

Figure 2.12: Calculation of the deflection in a section x_1. Figure 3.3 in [6].

As shown in the figure, the deflection in a section x_1 can be calculated by integrating the curvature and can be described by the following expression:

$$\delta(x_1) = \theta \cdot x_1 - \int_0^{x_1} \frac{1}{r(x)}(x_1 - x)\, dx \tag{2.37}$$

where the curvature $1/r(x)$ is integrated along the length of the column and the distance between the element x_i and the section x_1 is accounted for in the formula. As an example, for a case with a cantilever column, the maximum defection will be at the top of the column, and can be calculated as:

$$\delta(l) = \theta \cdot l - \int_0^{l} \frac{1}{r(x)}(l - x)\, dx \tag{2.38}$$

The integration is now carried out from 0 to l, which is the length of the column. If the support rotation θ, is equal to zero, the final equation becomes:

$$\delta(l) = -\int_0^{l} \frac{1}{r}(x)(l - x)\, dx = -\int_0^{l} \frac{M}{EI}(l - x)\, dx = -\int_0^{l}\int_0^{l} \frac{M}{EI}\, dx\, dx \tag{2.39}$$

With the moment and stiffness known, the maximum deflection can be calculated. To calculate the deflection along the column a numerical approach can be implicated. Expression 2.40 is used along with M(x) and I(M(x)), since the stiffness of the column varies with increased moment, as illustrated earlier in Figure 2.7.

$$\delta(x) = \int_0^{l}\int_0^{l} \frac{M(x)}{EI(M(x))}\, dx\, dx \tag{2.40}$$

2.4.3 Slenderness

A slender member in structural engineering refers to a structural element, such as a column, beam, or frame, that has a high length-to-thickness ratio. A slender member can buckle before the materials reach their strength limits. The slenderness ratio is calculated according to Section 5.8.3.2 in EC2[2] as:

$$\lambda = \frac{l_0}{i} \tag{2.41}$$

The effective length, l_0, is calculated based on if the member is braced or unbraced according to the same section. These formulas depend on degree of fixation at the end supports. For single columns the Euler modes for buckling shown in Figure 2.13 can decide the effective length directly. A shorter effective length is favorable as it gives the applied load a smaller lever arm, and therefore subjects the system to a reduced moment.

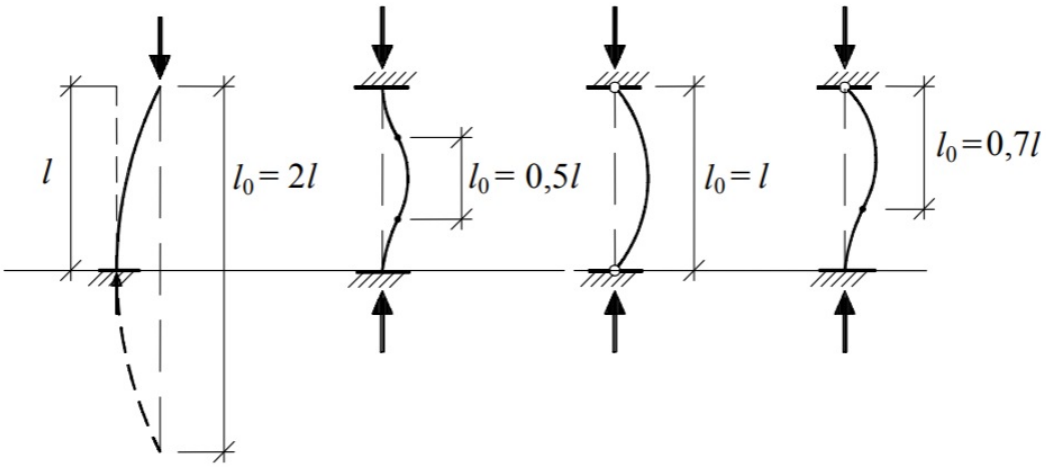

l

Figure 2.13: Resulting effective length depending on boundary conditions. Figure K2.16 from [5].

The radius of gyration i, describes how a cross-section's area is distributed around its centroidal axis, and calculated as the square root of the ratio between the moment of inertia and the area of the uncracked section.

$$i = \sqrt{\frac{I_c}{A_c}} \tag{2.42}$$

If the slenderness ratio of a concrete member is less than the limit, λ_{lim}, which is specified in the same section and calculated for the specific case, second-order effects may be ignored. According to Section 5.8.3.1(2) in EC2 [2] in the case of bi-axial bending the slenderness ratio must be checked in both directions separately, and second-order effects can then be excluded in one or two directions.

2.4.4 Buckling

Buckling is an instability phenomenon that arises in slender members, such as columns, when subjected to a compressive axial load, causing them to bend outward. This phenomenon is of great importance since it can lead to catastrophic collapse of structures if not accounted for in design.

When a slender column is subjected to a compressive axial load, equilibrium between internal and external forces are established. The critical buckling load can be calculated using Euler's fomula:

$$P_{cr} = \frac{\pi^2 EI}{l_0^2} \tag{2.43}$$

Where: P_{cr} is the critical buckling load
E is the modulus of elasticity
I is the moment of inertia around the weak axis
l_0 is the effective length of the column

Euler buckling considers an idealized case and does account for imperfections. A real column can buckle earlier due to material properties, geometric imperfections, and other practical factors that are not considered in an idealized analysis.

2.5 Second-order analysis in EC2

Second-order analysis, chapter 5 in EC2 [2], provides three methods to calculate stiffness for reinforced concrete structures. The methods include one general method, and two simplified methods to calculate stiffness. The methods are the following:

- General method
- nominal stiffness method
- Nominal curvature method

In the commentary to EC2 [3] the authors argue that certain methods are more appropriate for specific structural conditions, while others emphasize simplified approaches for practical use. In the following sections, a comprehensive presentation of the two methods will be provided.

2.5.1 General method

Section 5.8.6 [2] in EC2 presents the general method to calculate stiffness for reinforced concrete structures. The general method relies on non-linear analysis to evaluate structural behavior. For axial loading, the section is assessed in state III, assuming that the load is applied at the center of the concrete cross-section. Creep effects are considered using the same approach as described in Section 2.2.5, by

applying an effective modulus of elasticity to account for time-dependent deformations. The method also includes second-order effects, which influence structural response under load, and is carried out through an iterative process to improve accuracy. According to EC2 [2] the material model that should be applied in calculation of the general method is the one presented in Section 2.2.7, Figure 2.4. Where the modulus of elasticity, E_{cd}, should be calculated as E_{cm}/γ_{CE} according to 5.8.6(3) in [2], and the recommended value for γ_{CE} is 1.2. By following the general method, the exact stiffness for the cross-section is obtained. And it is possible to see how the stiffness varies with increasing moment.

2.5.2 nominal stiffness

The nominal stiffness method is a simplified method that estimates the stiffness conservatively. The method estimates the stiffness for an arbitrary cross-section, including contributions from both the concrete and reinforcement. The method is explained in Section 5.8.7 in EC2 [2] and the stiffness is estimated using the following formula:

$$EI = K_c E_{cd} I_c + K_s E_s I_s \tag{2.44}$$

Where:
- E_{cd} is the design value for the modulus of elasticity for the concrete section
- I_c is the moment of inertia of the gross concrete section
- E_s is the design value for the modulus of elasticity of the steel
- I_s is the moment of inertia of the steel
- K_c is a factor accounting for cracking, shrinkage, etc
- K_s is a factor accounting for the effect of the reinforcement

For an approximate analysis (as a preliminary step), given that the reinforcement content $\rho \geq 0.01$, which is $\rho = A_s/A_c$. The values for K_c and K_s are the following:

$$K_s = 0 \quad \text{and} \quad K_c = \frac{0.3}{1 + 0.5 \cdot \varphi_{\text{ef}}} \tag{2.45}$$

Where:
- φ_{ef} is the effective creep coefficient

For an improved value of nominal stiffness it is recommended, given that the reinforcement content $\rho \geq 0.002$, the values for K_c and K_s are as following:

$$K_s = 1 \quad \text{and} \quad K_c = \frac{k_1 k_2}{1 + \varphi_{\text{ef}}} \tag{2.46}$$

Where:
- k_1 is a factor that depends on the concrete strength class, see expression (5.23) in EC2 [2]

k_2 is a factor that depends on the axial force and slenderness, see expression (5.24) in EC2 [2]

Second-order effects are considered globally using the nominal stiffness method. These effects are accounted in the formula for the design moment, which is done by amplifying the first-order bending moment. The formula is as follows:

$$M_{Ed} = M_{0Ed}\left[1 + \frac{\beta}{\frac{N_B}{N_{Ed}} - 1}\right] \tag{2.47}$$

Where:
- M_{0Ed} is the first-order bending moment.
- β is a factor accounting for the ratio between the first- and second-order moments, see expression (5.28) [2]
- N_{Ed} is the design value of the normal force
- N_B is the buckling force based on a nominal stiffness

2.5.3 Nominal curvature

The nominal curvature method should be used in cases of isolated structural elements, with a constant normal force and a defined effective buckling length according to Section 5.8.8 in EC2 [2]. The method estimates second-order effects by increasing the curvature. The design moment is calculated by the following formula:

$$M_{Ed} = M_{0Ed} + M_2 \tag{2.48}$$

Where:
- M_{0Ed} is the first-order moment
- M_2 is the second-order moment

The second-order effects are accounted for in the second-order moment, which is calculated according to the following formula:

$$M_2 = N_{Ed} \cdot e_2 \tag{2.49}$$

Where:
- N_{Ed} is the normal force
- e_2 is the eccentricity

The column's lateral deflection under load is estimated using an assumed curvature distribution, this gives the second-order eccentricity. The eccentricity of the second-order moment is expressed as:

$$e_2 = \frac{1}{r} \cdot \frac{l_0^2}{c} \tag{2.50}$$

Where:	$\frac{1}{r}$	is the curvature
	l_0	is the effective length
	c	is the factor that depends on the curvature distribution

The curvature at failure of the critical section is determined based on the curvature of a balanced section. The curvature of the critical section at failure is calculated by the following formula:

$$\frac{1}{r} = K_r K_\varphi \frac{1}{r_0} \tag{2.51}$$

Where:	K_r	is a correction factor depending on axial load, and considers the type of failure, see Section 5.8.8.3 in [2]
	K_φ	is a factor that accounts for creep, see Section 5.8.8.3 in [2]
	$1/r_0$	is $\varepsilon_{yd}/(0.45\text{d})$, the curvature of critical section in case of balanced failure, see Section 5.8.8.3 in [2]

2.6 Revisions in EC2:2023

A revised 2nd generation of Eurocode 2, EC2:2023, was released in 2023, it is used as a pre-standard between 2023 and 2027 and the complete set of Eurocode standards will be published in 2028 [8]. This new version is significantly revised from the current code and will be updated in several areas in addition to having a considerably wider scope [9]. The wider scope will in certain areas mean more complicated models to allow for a more general application. Some key changes to the code include updates based on the latest research and methods, there will be a reduction in the number of nationally determined parameters [8]. Additionally, provisions will be introduced for the assessment, re-use, and retrofitting of existing structures. The provisions for robustness have been improved. Furthermore, three new Eurocodes will be added, focusing on glass, fiber-reinforced polymers (FRP), and membranes. The following sections presents the changes that are relevant to this thesis.

2.6.1 General revisions of stiffness methods

Section 7.4.3.1 in EC2:2023 [10] describes that the nominal curvature method and second-order linear elastic analysis should use an effective stiffness. A conservative approach is to take the stiffness at the point where reinforcement starts yielding, as in Figure 2.14a. For multiple layers of reinforcement, where yielding occurs at multiple locations, the stiffness corresponding to the final plastic formation can also be used, according to Figure 2.14b. The revision makes it easier to understand how local and global effects should be taken into account.

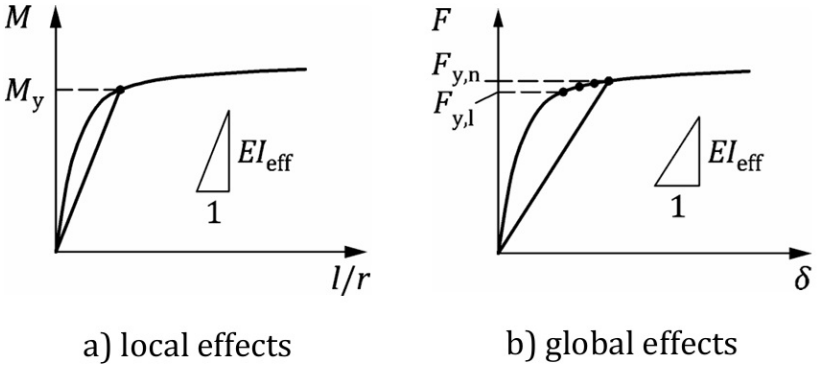

Figure 2.14: Possible equivalent stiffness. Figure 7.4 from [10].

2.6.2 Second-order linear elastic analysis

Instead of nominal stiffness, the revised code recommends the calculation of an effective stiffness corresponding to the moment when the reinforcement yields. This effective stiffness is calculated in the critical section as:

$$EI_{yield} = \frac{M_{Rd.y}}{\kappa_{y.steel}} \tag{2.52}$$

Where: $M_{Rd.y}$ is the moment corresponding to the curvature at yielding
$\kappa_{y.steel}$ is the curvature at yielding

It is unclear whether the code refers to if both tensile and compressive reinforcement should yield or only the tensile reinforcement. The revised version also allows for calculation of stiffness with set reduction values for each category of specific elements. In this thesis, this is referred to as a simplified global analysis and is calculated accordingly:

$EI = 0.4E_{cd}I_c$ for walls and columns;
$EI = 0.3E_{cd}I_c$ for reinforced concrete beams and slabs;
$EI = E_{cd}I_c$ for uncracked concrete beams and slabs due to prestressing

2.6.3 Nominal curvature

In Annex O of the revised version of EC2:2023 [10], the modification made to the nominal curvature method concerns the definition of the curvature at the critical section.

$$\frac{1}{r_0} = \frac{2\,\varepsilon_{sy}}{d - d'} \tag{2.53}$$

In the current code, 0.45d is used as a simplification to estimate the position of the neutral axis. In the revised version, both the tensile and compressive resultants are taken into account, providing a more detailed and accurate calculation.

2.7 Prior studies

In the following section, previous studies that are relevant to the project are presented in chronological order.

Westerberg (2008)
This doctoral thesis by Westerberg [11] concerns the effect of time-dependent concrete properties, in non-linear analysis. The author has done an extensive compilation of data from experimental tests spanning the years 1956 to 2005. Several of the tests are compared to hand calculations made by the author to investigate if the simplified methods for stiffness calculations are accurate enough, the conclusion is that high degree of agreement is found in most cases.

Andreatta & Kofler (2009)
Andreatta & Kofler makes a parameter study [12] on single columns using the different methods provided in EC2 [2]. Their investigation demonstrates the influence of material, slenderness and eccentricity of the axial force. They conclude that both simplified methods ensure accurate calculations for single columns, but for highly precise results or complex cases, the general method is recommended to meet structural design requirements.

Luo et al (2009)
Luo et al [13] investigates how stiffness of a reinforced concrete pier can be reduced, by numerical integration with non-linear material characteristics. The study includes rectangular cross-sections and the reason for this investigation is to fill the gaps in the research for stiffness reduction. The paper mainly describes their method of calculation which is later compared to experimental tests. Their conclusion is that the stiffness reduction factor for rectangular cross-sections, on average for different axial compression ratios can be set to 0.3.

Zhang et al (2010)
Zhang et al [14] refer to Luo et al [13] as previous work on the topic, it also has three of the same co-authors. In this paper the same methodology is used, but the investigation concerns the reduction factor for circular cross-sections which they mean seems to be missing in corresponding research. Their conclusion is that the stiffness reduction factor for circular cross-sections, on average for different axial compression ratios can be set to 0.7.

Bonet et al (2011)
In this paper, Bonet et al [15] presents a new equation for determining the effective stiffness of slender concrete columns. This is an extension of earlier work from the same authors from 2004. The method they used was compared to 613 exper-

imental tests from previous literature and a strong accuracy was obtained. The author means that their method can verify and design slender reinforced concrete columns for any shape of cross-section.

Hellesland et al (2013)
In this book by Hellesland et al [4] there is a section comparing the nominal stiffness method, both the approximate and the improved approaches including the moment magnification factor, with the method of nominal curvature. Their conclusion is that the design moment for the nominal stiffness method exceeds that of the nominal curvature method in both cases.

Várdai & Bódi (2014)
Várdai & Bódi's investigation [16] concerns the design of reinforced concrete columns according to the stiffness methods provided in EC2. They make a case study where flexural stiffness and deformation varies for the three different methods, nominal stiffness, nominal curvature and the non-linear general, for different magnitudes of axial load. They determine that the effective stiffness for the general method increases with increased axial load. The deflection in the nominal stiffness method deviates significantly compared to a linear elastic analysis, while the general method aligns with the deflection magnitude observed in a linear analysis. The authors conclude that the simplified methods overestimates the second-order deflections and moments.

Gebauer et al (2018)
Gebauer et al [17] investigates the complexity of stiffness of semi-integral bridges. The complexity being that the piers need to be stiff to have the needed load bearing capacity, but ductile to not cause large restraint forces in the structure. In this investigation, the failure behavior, constraint moments and the moment-curvature relation in the structure were evaluated. Gebauer et al used this investigation to generate design criteria, in a new investigation on normal force and reinforcement amount [18] for semi-integral bridges.

Das et al (2021)
Das et al [19] has developed a Gene Expression Programming (GEP) model to obtain a precise estimation of the effective stiffness, as it influences the distribution of forces in non-linear dynamic analysis. Their findings suggest that the GEP model delivers accurate predictions of the effective stiffness ratios for reinforced concrete columns.

3 Method

In the following chapter, the methodology is presented in detail. A numerical calculation method developed to determine the capacity and precise response of a concrete cross-section under axial load is introduced. The methodologies used to calculate and estimate displacements and stiffness is then presented. Additionally, all assumptions and input parameters are introduced, along with how the FE analysis was conducted to verify the numerical calculation method.

3.1 Model compositions and input parameters

This section presents the different parameters investigated in the study. To ensure that the selected parameter combinations are appropriate, the chosen dimensions align with those used in previous and upcoming projects at Norconsult.

Table 3.1 presents the parameters that remain constant throughout all calculations. The concrete cover thickness and center-to-center spacing exceed the minimum requirements specified by EC2 [2]. The selected reinforcement arrangement and cross-sectional dimensions were chosen to simplify calculations and simulations while simultaneously representing realistic conditions. The concrete class used in all calculations in this thesis is C45/55, as it is commonly used in bridge design.

Table 3.1: Set parameters in hand calculation.

Set parameters	
CC distance reinforcement $[mm]$	125
Height of column $[m]$	10
Cross-section area $[m^2]$	1x1
Concrete class $[-]$	C45/55
Steel strength $[MPa]$	500

The main cross-section analyzed consists of two single rows reinforcement of 7 bars each. A second case was also analyzed, where an additional row of reinforcement was added, consisting of 2 more bars. The cases are illustrated in Figure 3.1. The height of the cross-section is denoted by h and the width by b. The concrete cover is represented by c.

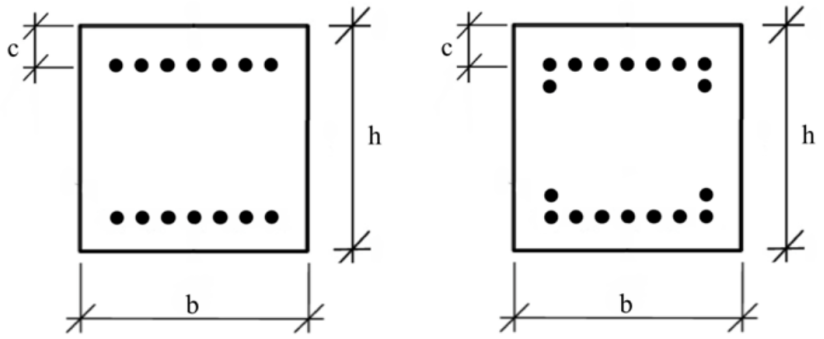

Figure 3.1: Chosen analyzed cross-sections, 7 and 9 bars (tensile reinforcement).

The selected reinforcing bar diameters are presented in Table 3.2. These diameters have been chosen based on standard dimensions relevant to projects at Norconsult. Additionally, the chosen bar diameters and corresponding number of bars ensure a reinforcement ratio that exceeds 0.2%, in compliance with the requirement in EC2 [2]. Since Norconsult is a Norwegian company, the Norwegian national standards are also interesting to review. These standards impose stricter requirements regarding minimum reinforcement amounts compared to EC2. The Norwegian requirement for minimum reinforcement is 1%, resulting in $7\phi32$ and $9\phi32$ being the only reinforcement quantity analyzed exceeding the Norwegian national requirements, which will be discussed in later sections.

Table 3.2: Variable parameters in hand calculation.

Variable parameters	
Reinforcing bar diameter $[mm]$	20, 25, 32
Concrete cover thickness $[mm]$	115, 112.5, 109
Number of reinforcement bars (tensile) $[-]$	7, 9
Normal force $[MN]$	1, 3, 6, 12
Effective height (from boundary conditions) $[m]$	10, 20
Creep coefficient $[-]$	0, 2
Concrete strength $[MPa]$	45(γ), 53, 61

Two different column models were analyzed, both of which are presented in Figure 3.2. The figure illustrates the boundary conditions, the expected deformation and the effective lengths that were used in the calculations. The first case is a simple cantilever, in this case the buckling length is double the actual length of the beam which is illustrated in the figure. The second case is a column that is fixed at both ends but allowed to move horizontally at the top.

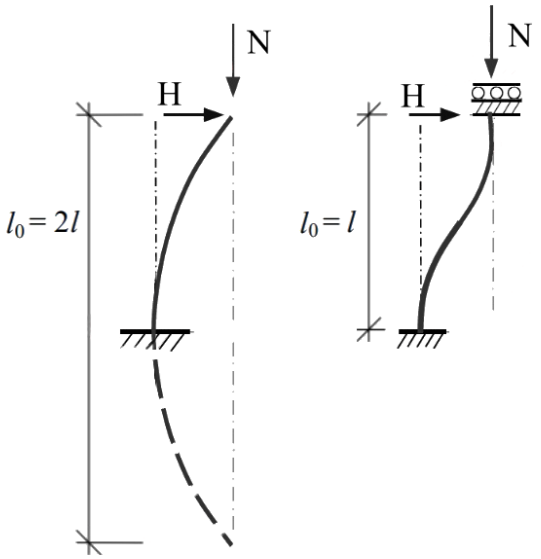

Figure 3.2: Boundary conditions for the studied columns. The left column is the cantilever case and the right is the fixed case.

The range of design axial loads was determined based on the critical buckling load for each column and are presented in Table 3.2. Using Expression 2.43 from Section 2.4.4, these critical buckling loads are approximately 6.2 MN and 24.7 MN for the cantilever and fixed column, respectively. This ensures that relevant load cases are investigated.

All calculations were done with and without the effect of creep. The creep coefficient of 2 is the recommended value from EC2 [2], if no other information is available.

To account for the variation in material strength, analyses were carried out for different cases. Characteristic values with partial factors (γ), mean values and the 95th percentile were the different concrete strengths analyzed, represented by 45(γ), 53 and 61 MPa in Table 3.2. These three strengths will from here on out be denoted as 5th(γ), 50th and 95th percentile. These cases were carried out in SLS and ULS. All analyses were carried out with concrete strength C45/55.

3.2 Numerical calculation process

Linear calculation methods are typically used to determine the cross-sectional response of a concrete section. The stiffness in Stage I and II, together with the moment capacity and cracking moment, are used to estimate the stiffness behavior of the cross-section. Figure 3.3 illustrates how stage I and II stiffness, along with the cracking moment and moment capacity, can describe the simplified behavior of a concrete cross-section.

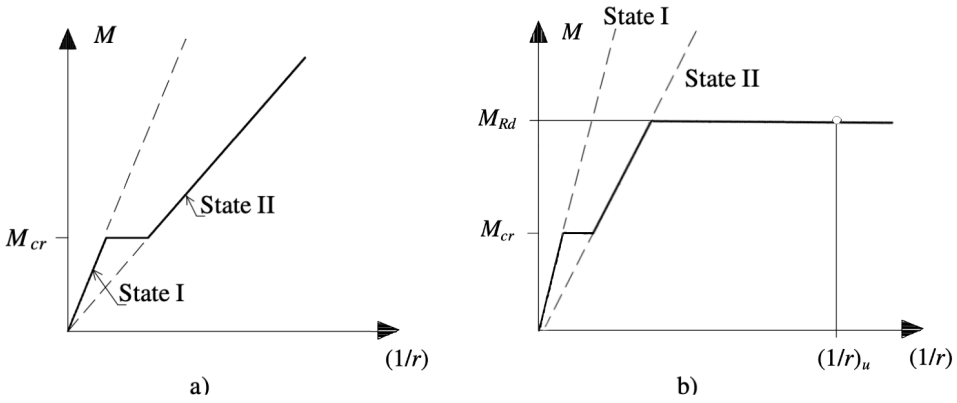

Figure 3.3: The simplified behavior of a concrete cross-section. a) showcases how the stiffness changes when the first crack appears. b) illustrates the simplified behavior from an uncracked cross-section all the way until failure.

In the theory chapter, all necessary calculation methods to determine the simplified response for a cross-section were presented. In Section 2.2.4, the stage I stiffness was introduced, while Section 2.3.5 covered stage II stiffness. The cracking moment was presented in Section 2.3.3, and the calculation of moment capacity was addressed in Section 2.3.4. The contribution of concrete between cracks was described in Section 2.4.1. Figure 3.4 illustrates which sections of the theory chapter correspond to different parts of the cross-sectional response.

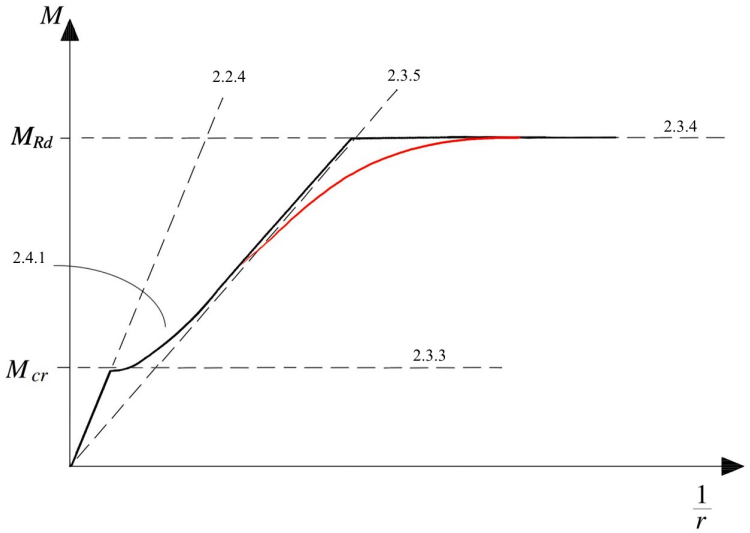

Figure 3.4: Sections in the theory chapter and how they relate to determining the cross-sectional response of a concrete section.

However, to determine the exact response of a concrete section, illustrated by the red line in Figure 3.4, a new calculation process must be introduced. The capacity of a compressed cross-section, can be determined numerically by integrating the contribution of concrete over the cross-section and the contributions from the rein-

forcement bars. The moment capacity was obtained by taking moment equilibrium around the top edge and is decided by the following equation:

$$M_{\mathrm{Rd}}(\varepsilon_1, \varepsilon_2) = \int_0^h x \cdot b_c(x) \cdot \sigma_c\left(\varepsilon(x, \varepsilon_1, \varepsilon_2)\right) dx + \sum_i \left(x_{s,i} \cdot A_{s,i} \cdot \sigma_s\left(\varepsilon(x_{s,i}, \varepsilon_1, \varepsilon_2)\right)\right) + N_{\mathrm{Rd}}(\varepsilon_1, \varepsilon_2) \cdot \frac{h}{2} \tag{3.1}$$

Where:

$b_c(x)$	is the width of the cross-section at depth x
σ_c	is the concrete stress based on the strain distribution
$A_{s,i}$	is the area of reinforcement bars
σ_s	is the reinforcement stress corresponding to the concrete strain
$x_{s,i}$	are the positions of reinforcement bars i within the cross-section
ε_1, ε_2	are the strains at respective edges of the concrete cross-section

The last term in the equation accounts for the contribution of the axial force to the moment equilibrium, where h is the height of the cross-section. The axial force was calculated using the following equation:

$$N_{\mathrm{Rd}}(\varepsilon_1, \varepsilon_2) = -\int_0^h b_c(x) \cdot \sigma_c\left(\varepsilon(x, \varepsilon_1, \varepsilon_2)\right) dx + \sum_i \left(A_{s,i} \cdot \sigma_s\left(\varepsilon(x_{s,i}, \varepsilon_1, \varepsilon_2)\right)\right) \tag{3.2}$$

The strain distribution in the cross-section was decided by the following expression:

$$\varepsilon(x, \varepsilon_1, \varepsilon_2) = \varepsilon_1 + (\varepsilon_2 - \varepsilon_1)\frac{x}{h} \tag{3.3}$$

The calculation process used in this thesis is presented summarized in the following steps:

Material model
Which material model that was used is defined by comparing the material models available in EC2. Creep was modeled by multiplying the strain values in the material model diagram with a factor $(1+\phi_{ef})$.

Moment capacity
The moment capacity was calculated by assuming ultimate strain at the top edge of the concrete. The strain in the bottom edge was then iteratively increased from the ultimate strain in compression to a value ten times larger in tension, using the relationships defined in Equations 3.1-3.3. For the strain distribution, the corresponding M-N interaction curve for the cross-section was obtained. For a set axial

force, the moment capacity was then extracted from the M-N curve.

Moment-curvature relationship
Moment-curvature relation was calculated by solving for the strain distribution in Equations 3.1-3.3 using a moment stepping from 0 up to the calculated moment capacity at the applied axial force.

Displacement
The displacement was determined by integrating the curvature distribution along the two columns. The moment distribution varies for the columns since they have different boundary conditions.

Force-displacement
The force-displacement relation was extracted by applying a horizontal force equal to the moment capacity of the cross-section from the 5th(γ) percentile.

Stiffness calculations
The equivalent stiffness was calculated in SLS and ULS for both columns. The applied horizontal force in SLS corresponds to the moment at which the reinforcement reaches a stress of 150 MPa, an assumption made to limit crack width. The applied horizontal force in ULS corresponds to 95 % of the moment capacity for the cross-section. The nominal stiffness was calculated according to EC2, only in ULS. From EC2:2023 the effective stiffness was calculated in SLS and ULS at yielding of the first and second row of reinforcement. The stiffness allowed for simplified global analysis was also calculated according to the revised code.

The following sections describes the different steps of the calculation process in detail. The hand calculations were performed numerically using Mathcad, and follow the general method according to Section 2.5.1, see Appendix A .

3.2.1 Material model

When performing non-linear structural analysis, the material model presented in Figure 2.4 should be used. However, at Norconsult, the similar but simpler curve shown in Figure 2.5 intended for cross-sectional design, has been used. To investigate the differences between these material models, the initial calculation step involved plotting both curves for various concrete strength classes and comparing their behavior. Figure 3.5 illustrates the stress-strain relationship between the curves for concrete classes 35, 45 and 55. All three curves are plotted with design values, and the curves for all concrete classes is presented in Appendix B.

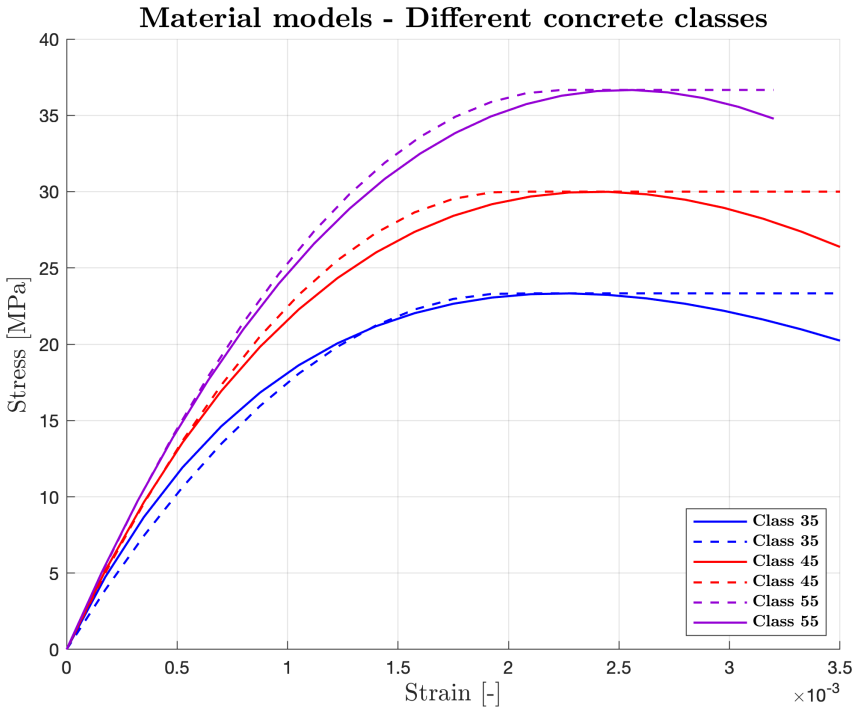

Figure 3.5: Material curve for non-linear structural analysis shown as solid lines; material curve for cross-sectional design shown as dashed lines; concrete classes 35, 45, 55.

It can be observed that the non-linear curve, the solid line, exhibits a higher initial modulus of elasticity for concrete classes 35 and below, see Appedix B. For all classes above 35, the cross-section design curve shows a higher modulus of elasticity, which could result in overestimation in calculation. This apparent inconsistency, despite the formula only varying with concrete strength, underscores the non-linear nature of the material behavior. Figure 3.6 compares the M–N interaction curves for both material models, for C45/55, and shows that the simplified design curve provides a higher moment capacity under large axial loads. Because the initial slope of the non-linear curve depends on the concrete strength class, the shape of the corresponding M–N interaction also varies with strength. In the case studied here (C45/55), the maximum difference occurs at an axial force of 12 MN, where the capacity of the simplified curve exceeds the capacity of the non-linear curve by approximately 2 %.

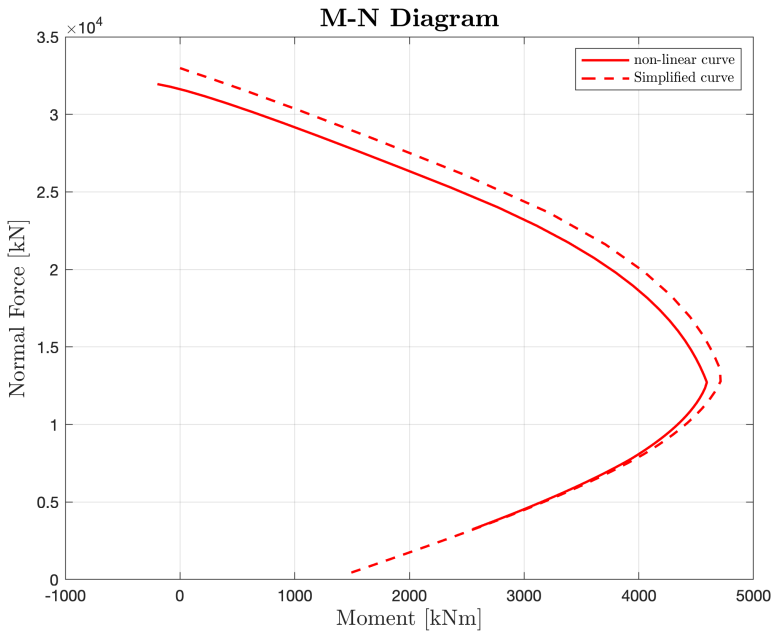

Figure 3.6: M-N interaction curves for the non-linear and simplified material models, C45/55.

After comparing the different curves, all calculations were made with the non-linear model in accordance with EC2 presented in Figure 2.4. To account for creep, a simplified approach was used where the strain values were adjusted by a factor $(1+\varphi_{ef})$ in accordance with EC2. Figure 3.7 shows the modified material model using design values.

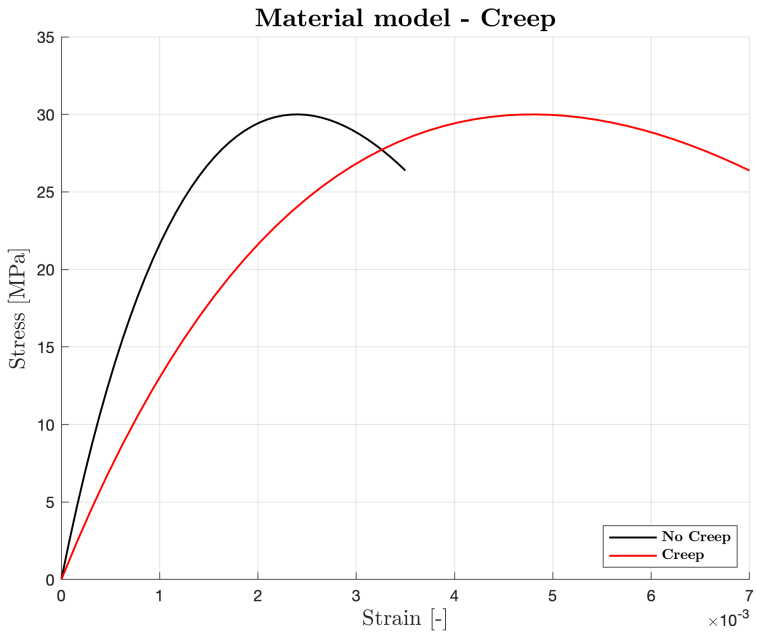

Figure 3.7: Material model modified for creep.

The tensile strength of concrete was ignored in the material model and in the calculation of moment capacity. This is a reasonable simplification, as EC2 does not explicitly state whether it should be accounted for in the material model. Furthermore by not adding it in the material model calculations are on the safe side. The effect of tension stiffening is accounted for in the calculation of the contribution of concrete between cracks, which is recommended by EC2. Lastly, the model used for steel in the hand calculations is the idealized elastic perfectly plastic illustrated in Figure 2.6 in Section 2.2.7, in accordance with EC2. Hand calculations assume full interaction between reinforcement and concrete.

3.2.2 Calculation of moment capacity

With the material behavior defined by the material models, the capacity of the cross-section was calculated. The capacity is decided by the interaction curve of the maximal normal force N_{Rd} and the maximum resisting moment M_{Rd}. Calculations displaying this process can be found in Appendix A.

The moment capacity was calculated using Equations 3.1-3.3 and by gradually assuming strains in the concrete at the edges of the cross-section, ε_1 and ε_2. Then the maximum axial force acting on the cross-section was calculated for each specific stress distribution.

For the concrete, ultimate strain was assumed at the top edge of the cross-section. On the opposite side, the strain was iterated from the concrete's ultimate strain (ε_{cu}) to a much higher tensile strain, which in this case, 10 times the ultimate strain. This strain iteration process is illustrated in Figure 3.8 below. Since the stress distribution in the cross-section is non-linear, these calculations are performed using numerical methods. From the M-N interaction curve, for each applied normal force the moment capacity was calculated.

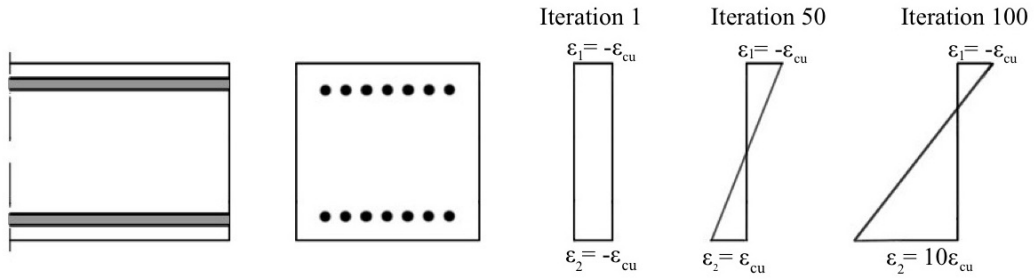

Figure 3.8: Strain iteration process.

3.2.3 Calculation of moment-curvature

The exact response of a cross-section can be determined by calculating the strain response for every set of normal force and moment. This was done numerically by

solving a system of equations. Calculations of the exact response can be found in Appendix A.The system was defined by the following equations:

$$\begin{aligned} N_{Rd}(\varepsilon_1, \varepsilon_2) &= N_d \\ M_{Rd}(\varepsilon_1, \varepsilon_2) &= M_d \end{aligned} \tag{3.4}$$

$N_{Rd}(\varepsilon_1, \varepsilon_2)$ and $M_{Rd}(\varepsilon_1, \varepsilon_2)$ were the defined as expressions 3.2 and 3.1 in Section 3.2. The terms N_d and M_d are known values, where N_d is the applied normal force (1, 3, 6 or 12 MN). To capture the full structural behavior, the strains were evaluated at multiple points by incrementally increasing the moment M_d from 0 to M_{Rd}. By solving this system numerically, the strain values ε_1 and ε_2 at the edges of the cross-section were obtained. These strain values were then used to determine the curvature and the strain distribution in the reinforcement and concrete, which is crucial when accessing the structural response in both SLS and ULS. From the strain distribution in the concrete, the strains in the reinforcement were obtained with the following expression:

$$\varepsilon_s = \varepsilon(x_s, \varepsilon_1, \varepsilon_2) \tag{3.5}$$

Where $\varepsilon(x_s, \varepsilon_1, \varepsilon_2)$ was calculated using Expression 3.3, for strain, in Section 3.2. With the strain distribution in the reinforcement, the stress in the reinforcement σ_s was determined by Hookes law:

$$\sigma_s = \sigma_s(\varepsilon_s) = E_s\, \varepsilon_s \tag{3.6}$$

With the strains $(\varepsilon_1, \varepsilon_2)$ solved from the system of equations, the curvature in any state can then be calculated with the following expression, in this case, state II was examined:

$$\kappa_{II} = \frac{\varepsilon_1 - \varepsilon_2}{h} \tag{3.7}$$

Where: $\varepsilon_1, \varepsilon_1$ are the strains at respective edges

When calculating the response using the general method, tensile stresses in the concrete between cracks can be considered, as specified in EC2 [2]. This was accounted for using the method presented in Section 2.4.1. By considering the contribution of concrete between cracks a slightly higher stiffness was attained in SLS. The contribution of concrete between cracks was then combined with the curvature of both state I and state II to obtain the actual behavior of the cross-section, κ_{tot}.

3.2.4 Calculation of displacement

The displacement was determined by integrating the curvature distribution along the column. The calculation method for displacement builds on the previous calculation of capacity. A detailed calculation of the displacement can be found in Appendix A. The displacement along the column was calculated with the following

expression:

$$\delta(H,x) = -\int_0^x \int_0^x \kappa_f(M(H,x))\,dx\,dx \tag{3.8}$$

Where: $\kappa_f = \frac{1}{r_f}$ is the curvature along the column
$M(H,x)$ is the unction for moment variation along the column

The curvature along the column κ_f, was obtained through linear interpolation between the moment-curvature relationship ($M_{Ed} - \kappa_{tot}$) and the moment along the column, generated by applying a horizontal force, proportional to a moment distribution where the maximum moment is equivalent to the moment capacity, at the top of the column. The magnitude of the horizontal force H depends on the applied moment, M_{Ed}. To calculate the deformation for each axial load, the horizontal force was incrementally increased until the moment capacity is reached. The moment distribution along the two different columns investigated varies and is illustrated in Figure 3.9.

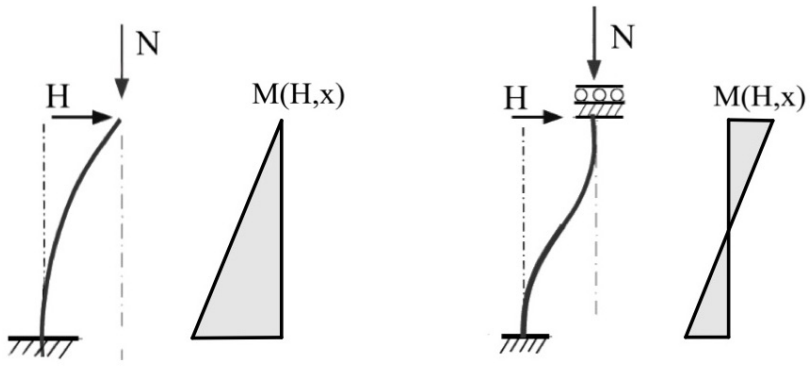

Figure 3.9: Moment distribution for cantilever and fixed column.

The moment distribution was described using the following formulas, where the first formula is for the case with a cantilever and the second case is for fixed connection:

$$M(H,x) = H(l-x) \tag{3.9}$$

$$M(H,x) = H\left(\frac{l}{2} - x\right) \tag{3.10}$$

Where: H is the horizontal force acting at the top of the column
l is the column length

3.2.5 Force-displacement

The force-displacement relation was calculated according to Appendix A, and was used to generate a plot to verify the calculation method against the FE analysis made in DIANA. The maximum applied horizontal force used to generate the force-displacement relation corresponds to 95 % of the moment capacity for the cross-section in the 5th(γ) percentile in ULS. This is the load that the columns are designed for, and therefore the largest load that the structures will be exposed to.

3.2.6 Equivalent stiffness

The equivalent stiffness is a fictive stiffness used to represent the actual, often non-linear response of a structure or structural element. By replacing the true, variable stiffness with an equivalent constant value it becomes possible to approximate the global response of a structure in a simplified way. The calculation method for the equivalent stiffness builds on the non-linear calculation of deformation in Section 3.2.4. By solving the second order derivative for the deformation, using the boundary conditions for the two different columns, the moments from Section 3.2.4, along with the non-linear maximum displacements from the same section, the equivalent stiffness was determined. This calculation process is displayed in Appendix D.

$$\delta''(x) = -\frac{M(H,x)}{EI_{ekv}} \tag{3.11}$$

Equations 3.12 and 3.13 are the result of the derivation and represents the linear equivalent stiffness for the respective columns.

$$EI_{\text{ekv.cantilever}} = \frac{H_{\text{Ed}} \cdot l^3}{3 \cdot \delta_{\text{max}}} \tag{3.12}$$

$$EI_{\text{ekv.fixed}} = \frac{H_{\text{Ed}} \cdot l^3}{12 \cdot \delta_{\text{max}}} \tag{3.13}$$

Where:
- l is the column length
- δ_{max} is the maximum deformation calculated according to Section 3.2.4
- H_{Ed} is the applied horizontal force

The equivalent stiffness was calculated in SLS and ULS for both columns. The applied horizontal force in SLS corresponds to the moment at which the reinforcement reaches a stress of 150 MPa for the 50th percentile, an assumption made to limit crack width. The applied horizontal force in ULS corresponds to the ultimate load from the 5th(γ) percentile, M_{Rd}/l for the cantilever and $2M_{Rd}/l$ for the fixed column.

3.2.7 Nominal stiffness

The nominal stiffness provides a linearized approximation of the actual structural stiffness. The nominal stiffness was calculated according to Expression 2.44 in Section 2.5.2 which comes from the current code [2]. The formula accounts for slenderness of the columns, which effects the nominal stiffness.

3.2.8 Stiffness according to EC2:2023

The effective stiffness from Expression 2.52 in Section 2.6.2 was calculated. This was achieved by identifying the curvatures at which the different rows of reinforcement yield in the non-linear analysis and their corresponding moments. All calculations were made with the assumption that the tensile reinforcement yielded. When presenting the results from this section, stiffness values corresponding to both the first and last row of reinforcement yielding will be provided when more than one layer of reinforcement is present. The revised version also allows for calculation of stiffness presented in Section 2.6.2 as:

$$EI = 0.4E_{cd}I_c \tag{3.14}$$

This stiffness can be used in simplified global analysis for columns and walls and was calculated based on different concrete strengths and reinforcement contents.

3.3 FE-analysis DIANA

Non-linear finite element analyses was conducted as part of this master thesis to provide a detailed comparison with hand calculations. These analyses is crucial in evaluating and contrasting the results obtained from the hand calculation method, ensuring accuracy and reliability of the chosen approach.

The software DIANA FEA (DIsplacement ANAlysis) is an advanced finite element tool used to perform numerical analysis in structural engineering [20]. It is particularly suited for non-linear analysis of materials such as concrete, soil and masonry. In this project, DIANA has been used to perform structural analyses of reinforced concrete, where both cracking and plastic behavior are modeled. The software enables detailed simulation of the interaction between reinforcement and concrete and stress-induced cracking, providing a more realistic representation of the actual structural behavior compared to linear analyses. The software allows for import of user-defined material models, making it possible to enter a material model of choice.

This section describes the setup of the FE model used in the DIANA software. It presents the choices and assumptions made during the modeling process, including verification of material behavior, model geometry, material definitions, element types, loads and supports, and the meshing and analysis methods. The section provides an overview of the key steps required to build and perform the FE analysis in DIANA.

3.3.1 Chosen parameters

To achieve comparable results, one set of parameters from Table 3.2 is chosen for all analyses done in DIANA. Reinforcement bar diameter is set to 25 mm and the axial force is set to 6 MN. The other set parameters in Table 3.1 are also used. Only the case of the cantilever column will be analyzed. Creep effects are not considered in the FE analysis, and all concrete strength values are entered as mean values.

3.3.2 Verification of material behavior in DIANA

To verify that the correct material behavior is used in DIANA, a test for different material models was carried out. A 2D model was set up in DIANA, a square with the measures 1x1 m^2 with a depth of 1 meter. The model was restrained vertically in both bottom nodes, with the left bottom node restrained in the horizontal direction. A prescribed displacement, ε_{cu}, was then applied in the two top nodes, and the mesh size was set to one element. Figure 3.10 shows the model.

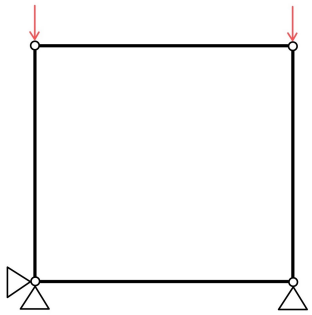

Figure 3.10: Structural model for test of material model.

The stress-strain relation from the analyses was plotted, see Figure 3.11. The plot contains the results from four different material models in DIANA. The user defined curve matches the one used in hand calculations from EC2, varifying that it is implemented in a correct way in DIANA. It can be observed that curve from EC2 directly from DIANA is the same as the one implemented manually. The curve from CEB FIB 2010 [21] shows less softening and stops at a higher capacity. The curve from CEB FIB 1990 [22] shows a significant deviation from the other curves. These results show that it is possible to use the material model from EC2 directly in DIANA as it is equivalent to the user-defined curve (EC2).

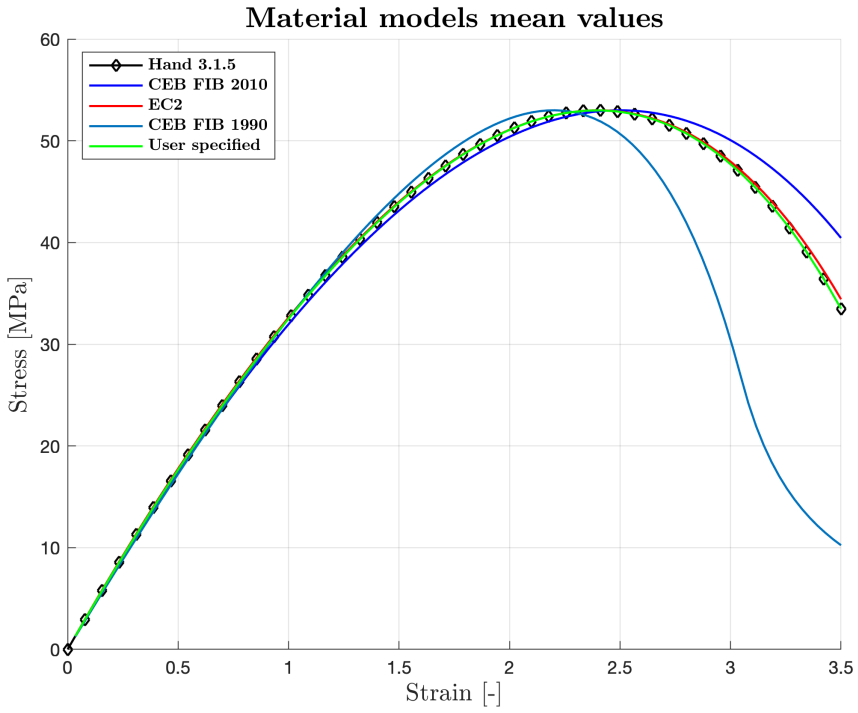

Figure 3.11: Material models from DIANA compared to EC2 hand calculations.

3.3.3 Geometry

The geometry of the structural model was defined in two dimensions, representing a vertical concrete column with embedded reinforcement, see Figure 3.12. The column was modeled as a 2D plane stress element, assuming unit thickness in the out-of-plane direction. This approach is suitable for analyzing the cross-sectional behavior and capturing cracking and non-linear effects within the plane.

The column geometry consists of a rectangular shape with a height of 10 meters and a width of 1 meter, defined using two separate shapes, the main column body and a top segment used for applying boundary conditions and loads. Both shapes were assigned the element class Regular Plane Stress.

To investigate the interaction between reinforcement and concrete, two different modeling approaches were implemented for bond behavior. Embedded reinforcement was defined in a separate geometric object. The reinforcement was modeled using the Embedded Bar method. The reinforcement was distributed on opposing faces of the column to represent vertical reinforcement. No anchorage lengths or interface reduction settings were applied at the bar ends. In the second case, a bond–slip model was applied using an interface behavior between the reinforcement and the concrete. The bond-slip relationship was defined according to a bilinear law, where parameters such as maximum bond stress, slip at peak stress, and residual bond strength were specified. This approach enables simulation of partial interaction and local slip effects, which is particularly important for studying anchorage behavior, crack spacing, and slip-induced deformations.

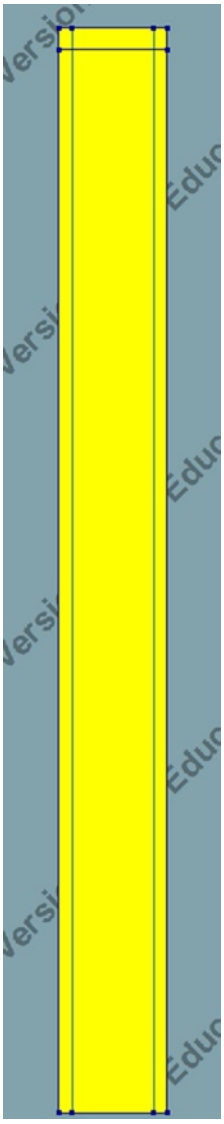

Figure 3.12: Modeled geometry in DIANA.

3.3.4 Materials

The main column was modeled using a physically non-linear concrete material. The material was defined with a total strain-based crack model, incorporating both tensile and compressive non-linear behavior. For the tensile behavior, two softening curves were tested, a brittle model and a Hordijk tension softening model. In the latter case while in the user specified case, the crack bandwidth was calculated and specified manually as 0.127 m, see Appendix C. Following the methodology proposed by the model code for concrete structures [21] and recommended by Plos et al [23], the fracture energy was calculated as 149 N/m. The compressive response was modeled using a multi-linear stress-strain relationship based on the curve presented in Figure 2.4 enabling accurate representation of non-linear com-

pressive behavior according to EC2, including softening. Young's modulus was set to 36 GPa and Poisson's ratio to 0.2. The compression material model from EC2 directly in DIANA was also used, with the same input as for the user defined curve, to use as verification that the used defined curve and its input were correctly implemented.

The top segment of the column was assigned a simplified linear elastic concrete material, to avoid problems with local stress concentration. This material was defined according to the CEB-FIP 1990 model code with direct input of elastic properties. Young's modulus was again set to 36 GPa, and Poisson's ratio was 0.2. Both tensile and compressive behaviors were modeled as linear, which is appropriate for the top segment, as its main purpose is to ensure numerical stability during load application.

The reinforcement was modeled using a bilinear Von Mises plasticity model. Linear elasticity was defined with a Young's modulus of 200 GPa. A yield stress of 500 MPa was used, and no hardening was assumed beyond yielding, representing the idealized elastic–perfectly plastic behavior presented in Figure 2.6.

A case with a bond–slip model was also applied using an interface behavior between the reinforcement and the concrete. The bond-slip relationship was defined according to a bilinear law, where parameters such as maximum bond stress, slip at peak stress, and residual bond strength were specified. This approach enables simulation of partial interaction and local slip effects, which is particularly important for studying anchorage behavior, crack spacing, and slip-induced deformations.

3.3.5 Element geometry and data

The element geometry of the finite element model was defined separately for the concrete column and the reinforcement. The concrete section was assigned a thickness of 1 meter, representing the out-of-plane depth in the 2D plane stress model. Since the model geometry aligns with the global coordinate system, no local element axes were specified.

The embedded reinforcement was defined using the embedded reinforcement method in DIANA, where a total reinforcement area of 0.00343437 m^2 was specified. This value represents the total cross-sectional area of the reinforcement bars placed on each side of the column. Anchorage effects and stiffness modifications at the bar ends were not included in this model. The bond-slip reinforcement was defined using the Truss bond-slip option in DIANA. A total reinforcement area of 0.00343437 m^2 was specified, corresponding to the combined cross-sectional area of the reinforcement bars. The contact perimeter between the reinforcement and the concrete was set to 0.5495 m, which governs the interaction surface for bond-slip behavior. The bond-slip formulation allows for relative movement between steel and concrete, but anchorage effects through bond-slip anchor surface area were not defined in this model.

Element data settings was set to predefined settings for integration for the concrete. The embedded reinforcement elements were defined using default integration parameters, which were considered sufficient given the simplified embedded modeling approach. The bond-slip reinforcement was modeled using truss elements, for which the INTERF option was activated to account for interface behavior between the reinforcement and the surrounding concrete.

3.3.6 Loads and supports

The axial load of 6MN was applied as a distributed force along the top edge. At the top vertex of the top segment, to simulate the horizontal load that is applied in the hand calculation, a prescribed displacement of 130 mm was applied. The magnitude of the displacement is related to the applied axial force and the corresponding moment capacity in the hand calculation. Boundary conditions were defined to constrain the model and prevent rigid body motion. The bottom edge of the column was fully fixed, restraining translation in both horizontal and vertical directions and rotations in the plane. This simulates a fully clamped base. In addition, a deformation support was applied to the top vertex of the column. This support is required in DIANA in order to use displacement-controlled loading. Figure 3.13 shows horizontal and vertical supports in red triangles, rotation supports are depicted as orange circles, and the applied normal force and deformation are orange and green arrows, respectively.

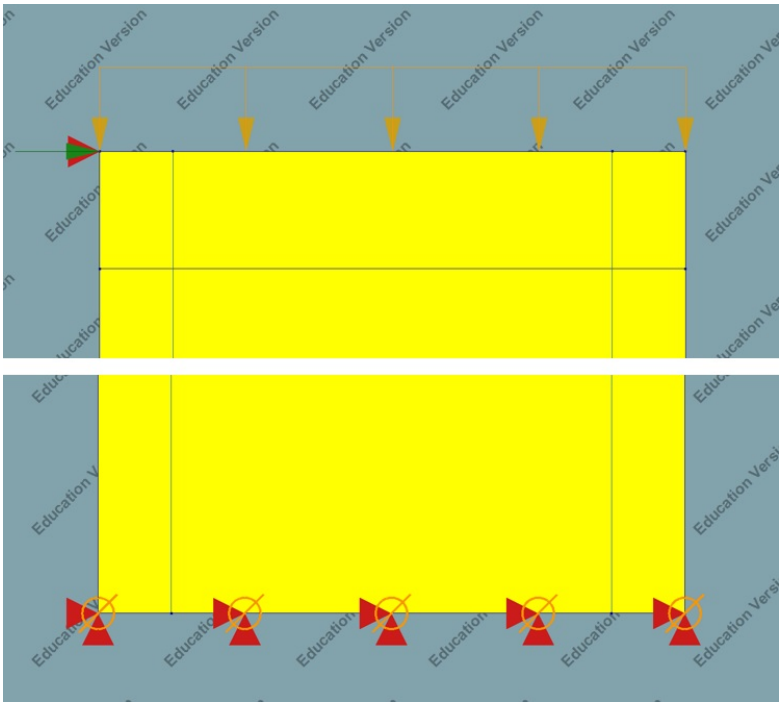

Figure 3.13: Picture illustrating loads and supports in DIANA.

3.3.7 Mesh and Analysis

The default mesh consisting of hexahedral/quadrilateral elements with a linear mesh order was used. An element size of 0.05 meters resulted in 4000 elements in total, Figure 3.14 shows the modeled mesh. To ensure mesh independence, additional analyses were carried out using finer meshes of up to 25,000 elements. The results showed negligible variation compared to the coarser mesh, indicating that the 4000-element mesh provides sufficient accuracy for the analysis.

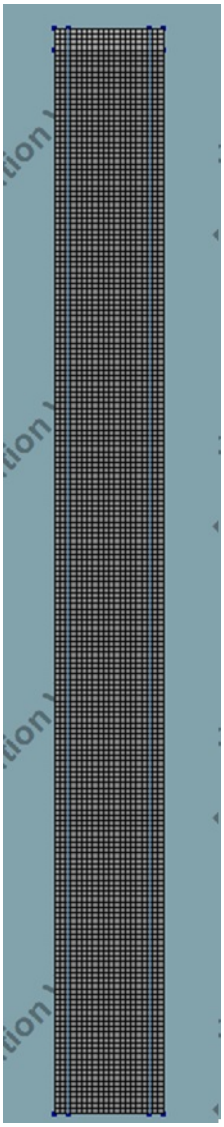

Figure 3.14: Modeled mesh in DIANA.

The analysis was created as structural non-linear with only physical non-linearity effects. The equilibrium equations were solved using the Parallel Direct Sparse Method, which provides an accurate and robust solution while ensuring computational efficiency through parallel processing. In the equilibrium iteration settings for both load cases, the Newton-Raphson method was used, with a maximum number of iterations set to 60. The convergence norm used was displacement and force, both set to continue even if convergence was not reached within all steps, to be able to run the analysis until failure. To get a valid analysis, the steps that did not converge needed to be linked to an event like cracking of concrete or pull through of reinforcement.

The axial load was applied incrementally over 100 steps, while the prescribed displacement was introduced in 200 steps to ensure a stable and controlled progression of the analysis. Additional simulations with a total of up to 2000 steps were performed to assess the sensitivity to step size. These analyses produced equivalent results, confirming that the chosen step distribution is sufficient for achieving accurate and reliable outcomes.

4 Results

This chapter presents the outcomes of the analysis and calculations. It begins with the presentation of results from hand calculations based on a reference case, including the M-N interaction curve, exact response, force-displacement, deformation and stiffness. The chapter then moves on to the verification of the hand calculations through FE analysis, comparing force-displacement results and examining loading stages in DIANA. Relevant results from the hand calculations are compiled, covering moment-curvature, force-displacement data and stiffness results for the geometry with an additional reinforcement row. Finally, the chapter concludes with the stiffness results, analyzing stiffness for different percentiles of concrete strength and utilization ratios, with varying applied axial load and reinforcement amounts as described in Section 3.1.

4.1 Hand calculation: Results from example case

In the following section, the calculation process is presented for the case with $7\phi25$ reinforcement, and with a normal force of magnitude 6 MN acting on the cross-section. This section is presented in SLS (50th percentile) and ULS (5th(γ)) percentile. This section is included in the results to provide complete overview of the calculation procedure. The calculation was performed using Mathcad Prime and is presented in Appendix A.

4.1.1 M-N interaction curve

Using the calculation method described in Section 3.2.2, the M-N interaction curve was derived. This curve illustrates the relationship between the applied normal force and the corresponding moment capacity for the cross-section. Figure 4.1 depicts the M-N interaction with and without the effect of creep in SLS. When creep is considered, a small contribution along the whole curve can be observed. When the applied normal force is in the range of 20–30 MN, a more pronounced increase in capacity can be observed. This is due to the fact that creep has a beneficial effect as long as the concrete remains uncracked. At higher load levels, the influence of creep becomes more significant, as it helps redistribute internal stresses and delay the onset of cracking. The maximum capacity of the cross-section is identified as the intersection between the solid and dashed horizontal lines. The resulting moment capacity, denoted as M_{Rd}, with the applied normal force of 6MN is 3885 kNm. When the effect of creep is considered, the capacity is slightly higher at 3895 kNm.

Figure 4.2 illustrates the M-N curve in ULS, with and without creep. Here, it can be observed that the curves have the same shapes as the curves in Figure 4.1, but with decreased values. The effect of creep increases the capacity significantly in the normal force span of 13-20 MN. The resulting moment capacity when applying 6 MN is 3458 kNm without the effect of creep, and 3479 kNm with the effect of creep.

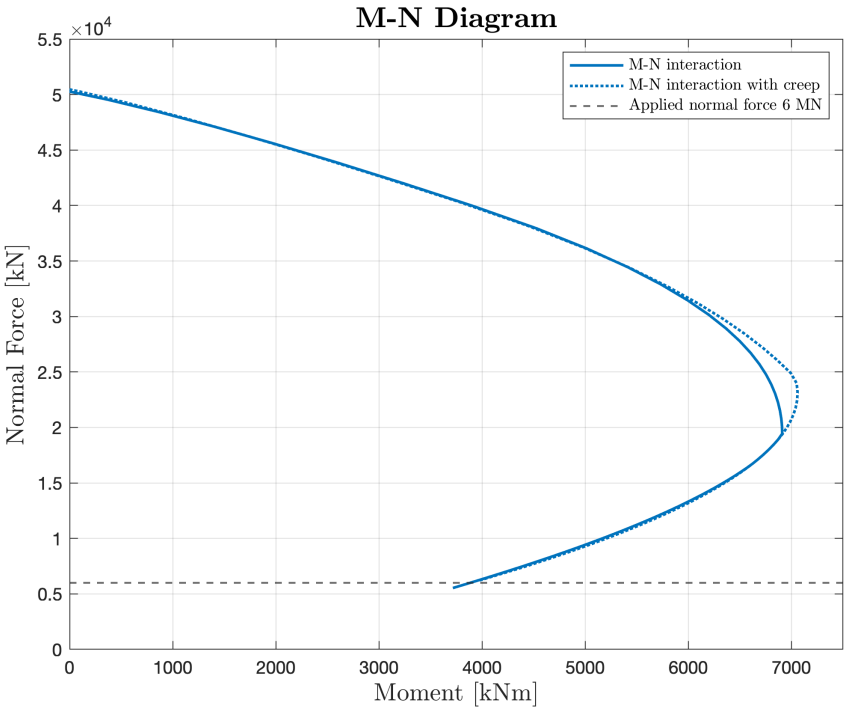

Figure 4.1: M-N interaction curve for 7ϕ25 in SLS.

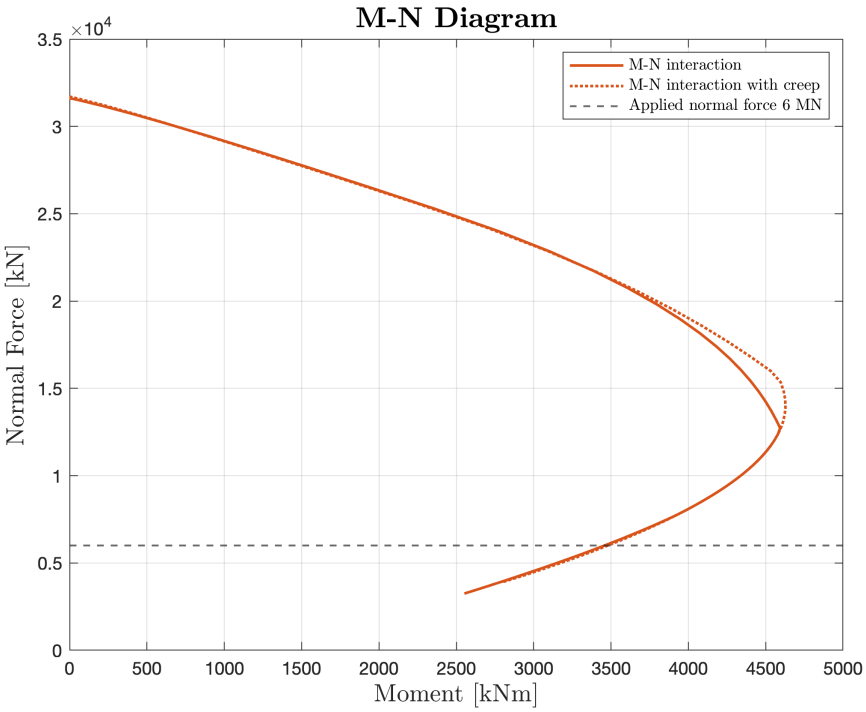

Figure 4.2: M-N interaction curve for 7ϕ25 in ULS.

4.1.2 Moment-curvature

Using the calculation method described in Section 3.2.3, both the moment-curvature relation and the stress-curvature relation of the reinforcement were determined. Figure 4.3 shows the moment-curvature diagram, the exact response of the cross-section in SLS and ULS. The solid lines shows the capacity with the consideration of concrete between cracks, while the dotted line is without this consideration. For this combination of reinforcement configuration and applied normal force, the contribution of uncracked concrete has a small influence. The first change in stiffness marks the point where the first crack occurs, and the second significant change in stiffness corresponds to the point at which yielding in the reinforcement starts.

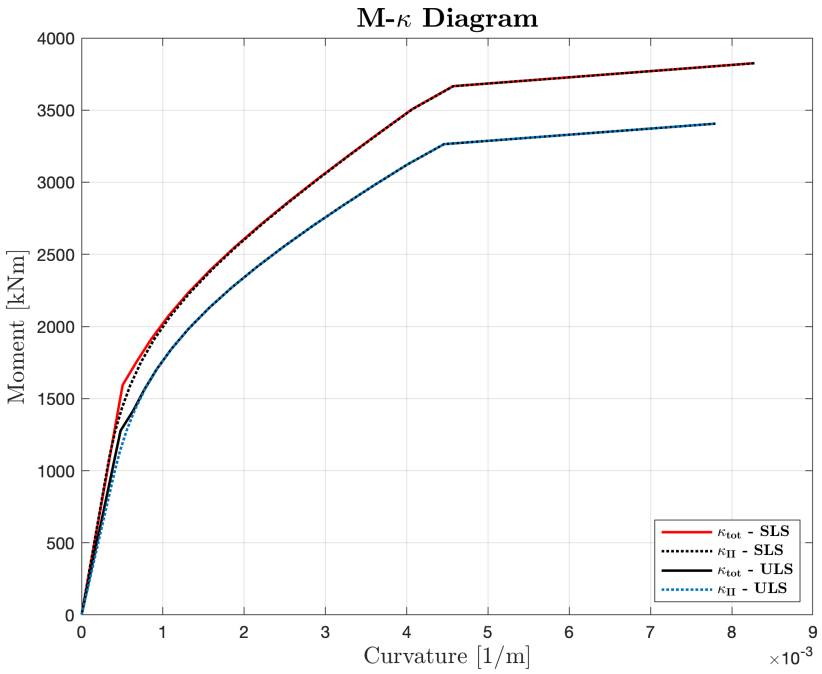

Figure 4.3: Moment-curvature diagram in SLS and ULS.

Figure 4.4 shows the moment-curvature relation in SLS with and without the effect of creep, highlighting a reduction in stiffness when creep is accounted for. The red solid line is the moment-curvature with consideration of concrete between cracks and the dashed black line denotes the same curve with the effect of creep. It can be noted that the cracking moment with the effect of creep is slightly higher at 1751 kNm compared to 1687 kNm without the effect of creep. Once the concrete have cracked the effect of creep becomes unfavorable. Creep can initially benefit concrete by redistributing stresses and delaying cracking, but it also contributes to increased long-term deformations and crack widths. Even after cracking, creep leads to greater deformations and wider cracks. This is the reason why yielding of the reinforcement occurs at a lower moment and at a higher curvature.

Figure 4.5 shows the moment-curvature relation in ULS, with and without the effect of creep. The solid blue line considers the contribution of concrete between cracks and the black dashed line considers creep. The cracking moment is 1340 kNm without the effect of creep, and 1391 kNm with the effect of creep.

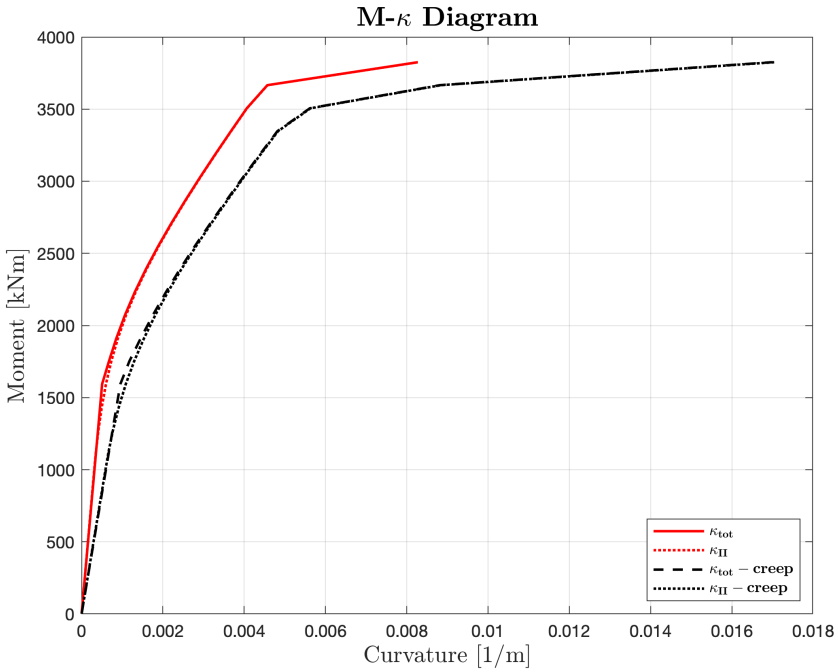

Figure 4.4: Moment-curvature diagram in SLS, with and without the effect of creep.

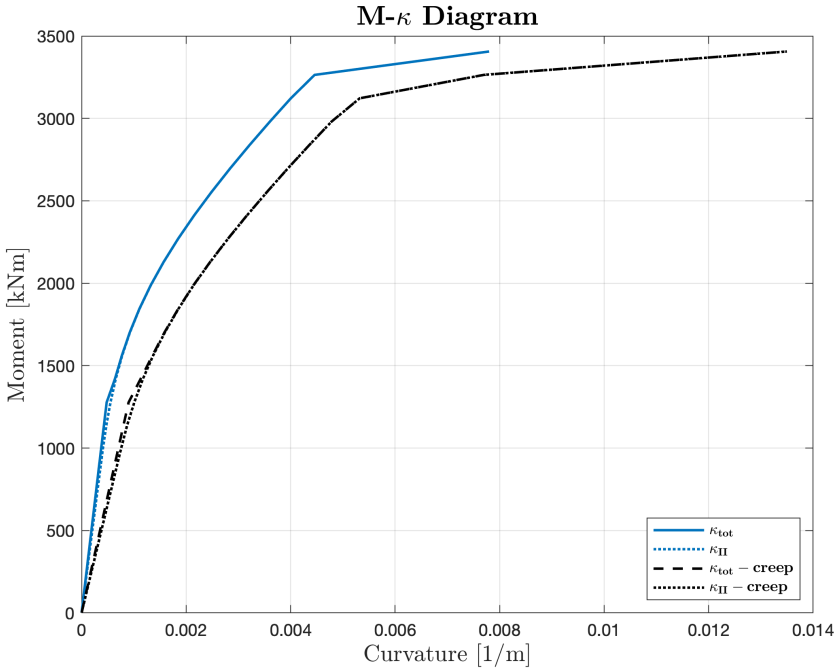

Figure 4.5: Moment-curvature diagram in ULS, with and without the effect of creep.

Figure 4.6 illustrates how the stresses in the tensile and compressive reinforcement vary with curvature. The red curve denotes the characteristic stress, used in the SLS calculation. The black curve denotes design stress used in ULS calculation. When the stress plateaus at 500 and 435 MPa, respectively, the tensile reinforcement has reached yielding. The horizontal dashed line at 150 MPa is a set limit to calculate the moment capacity in SLS, with the assumption that the cross-section meets the requirements of minimum crack widths.

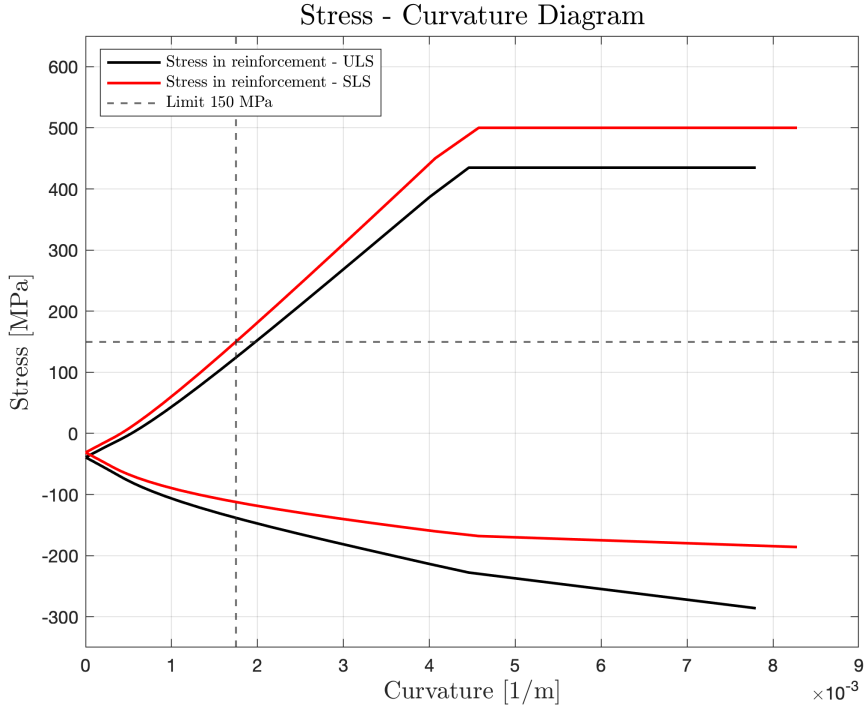

Figure 4.6: Stress-curvature diagram for the reinforcement in characteristic and design values.

4.1.3 Force-displacement

Figure 4.7 illustrates the force-displacement of the column in the 50th and 5th(γ) percentile. When creep is considered, an increase in deflection can be observed. The left subplot shows the 50th percentile, where the maximum deflection with the effect of creep is 128 mm, compared to 90 mm without creep. Like the moment-curvature relation diagrams, the bends in the force-displacement diagram also illustrates the points of cracking and yielding. The first change corresponds to the first crack, and the second change corresponds to yielding in the reinforcement. The right subplot in Figure 4.7 illustrates the force-displacement of the column in the 5th(γ) percentile, with and without the effect of creep. The maximum deflection with the effect of creep is 198 mm, and the maximum deflection without the effect of creep is 128 mm.

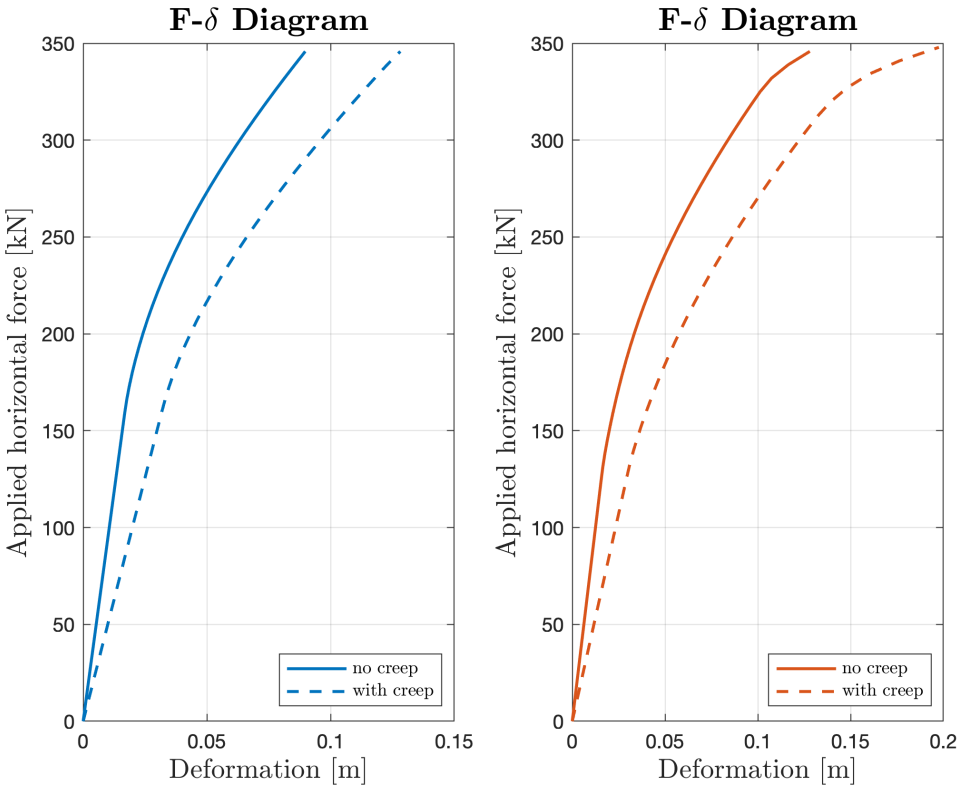

Figure 4.7: Force-displacement diagram in the 50th and 5th(γ) percentile with and without the effect of creep.

4.1.4 Deformation

Figure 4.8 illustrates the deformation for the cantilever column in the left subplot. The deformation curves in the graph show a difference in behavior between the actual and equivalent deformations. The actual deformation curves deforms more at the bottom of the column, reflecting the influence of material non-linearity and stiffness changes due to cracking. In contrast, the equivalent deformation curves exhibit a smoother deformation along the length of the column, a result of the constant stiffness. The right subplot in Figure 4.8 shows the deformation for the fixed column. The curves behave in the same way as for the cantilever column, but the boundary conditions limit the magnitude of the maximum deflection.

Figure 4.9 illustrate the effect of using an equivalent and the actual stiffness for the cantilever and fixed column, respectively, with and without the effects of creep in SLS. Both curves demonstrate that the deformations increases when creep is considered.

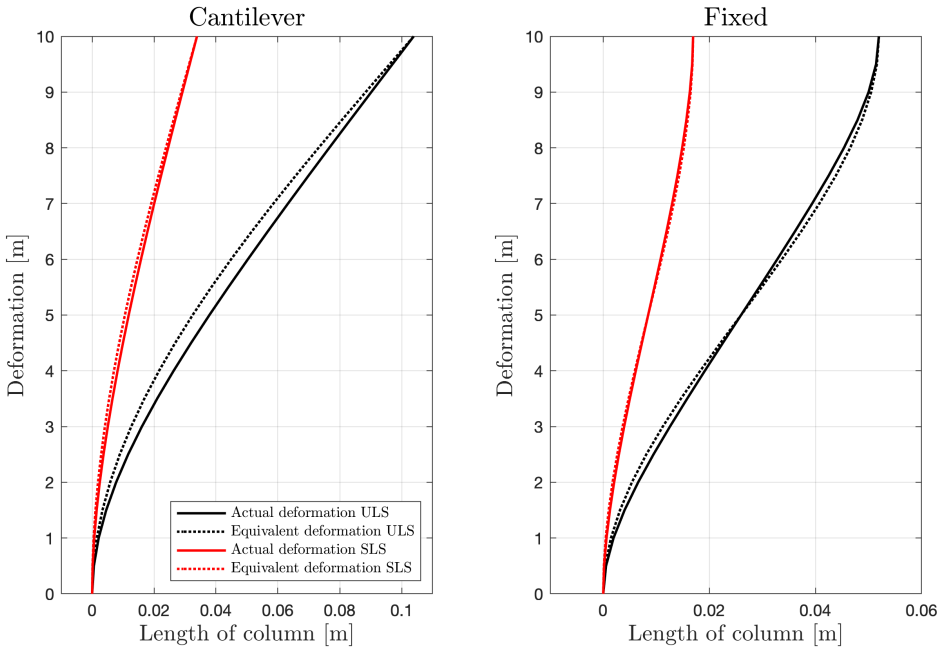

Figure 4.8: Deformation in SLS and ULS, cantilever column in left subplot and fixed column in right subplot.

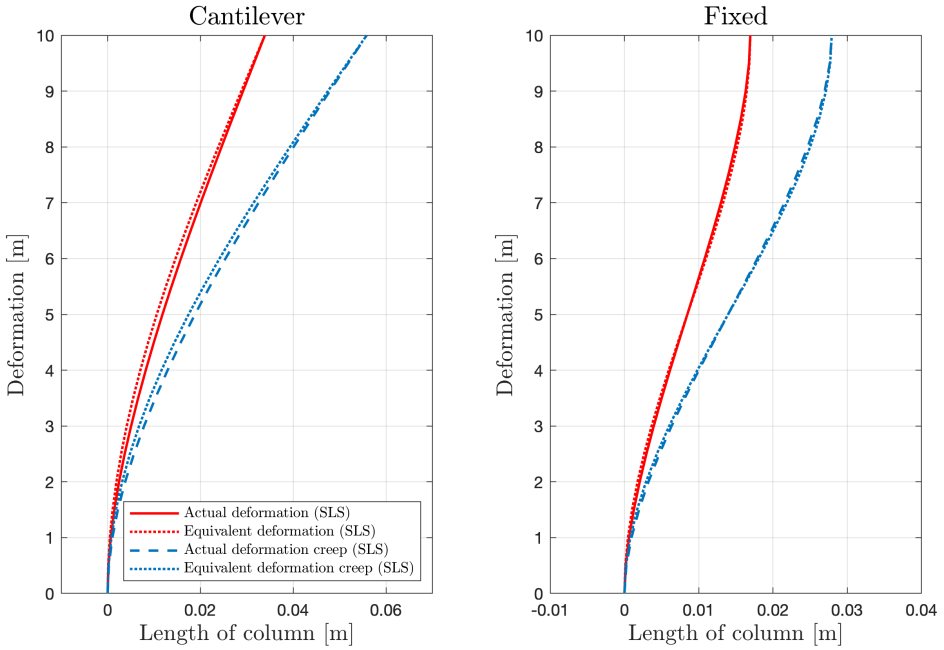

Figure 4.9: Deformation in SLS with and without creep, cantilever column in left subplot and fixed column i right subplot.

Table 4.1 presents the calculated top displacements for the cantilever and fixed column in SLS and ULS, with and without the effect of creep. For the cantilever column, deformation increases from 34 mm to 56 mm in the SLS case and from 104 mm to 153 mm in the ULS case when creep is included. For the fixed column, the corresponding increases are from 18 mm to 28 mm (SLS) and from 52 mm to 77 mm (ULS). It is evident that long-term creep effects amplify deformations by roughly 45–65 %, that the ULS load case produces significantly larger deflections than the SLS case, and that cantilever columns generally exhibit greater top displacements than fixed columns. When the concrete cracks the reinforcement significantly contributes to the stiffness of the cross-section.

Table 4.1: Deformation with and without creep for different column types.

$7\phi25$	**Deformation [mm]**		
Column type	**Without creep**	**With creep**	**Increase [%]**
Cantilever column SLS	34	56	65%
Cantilever column ULS	104	153	47%
Fixed column SLS	18	28	56%
Fixed column ULS	52	77	48%

4.1.5 Stiffness

Table 4.2 shows how the calculated stiffness varies with limit state, with and without the effect of creep. The equivalent stiffness is the same for both columns. The nominal stiffness for the two different columns are only valid in ULS, as design values are used in EC2 [2]. EC2:2023 is unclear in describing how to modify E_{cd} for design values and how to account for creep in revised approach. In all calculations with design values, E_{cd} is set to $E_{cm}/1.2$, as that is what the current code specifies. When creep is accounted for, the modulus of elasticity is divided by $1.2(1+\phi_{ef})$ for design values, and $(1+\phi_{ef})$ for all analyzes without safety factors. The stiffness from when the first reinforcement yields comes from the non-linear analysis according to expression 2.52 in Section 3.2.7.

Table 4.2: Linear stiffness in MNm^2 for $7\phi25$ and 6 MN, with and without creep.

Stiffness [MNm^2]	**SLS**	**SLS$_{creep}$**	**ULS**	**ULS$_{creep}$**
EI_{ekv}	2113	1386	1053	719
$\text{EI}_{nom.cantilever}$	-	-	499	346
$\text{EI}_{nom.fixed}$	-	-	346	270
$\text{EI}_{global.EC2:2023}$	1200	600	1000	500
$\text{EI}_{first.yield.EC2:2023}$	-	-	725	605

The actual stiffness applies only to the cross-section. The nominal, equivalent, and global stiffness values are calculated for the entire column. Figures 4.10 and 4.11 show the equivalent stiffness in SLS and ULS. The equivalent stiffness is the same for both columns for the respective limit states.

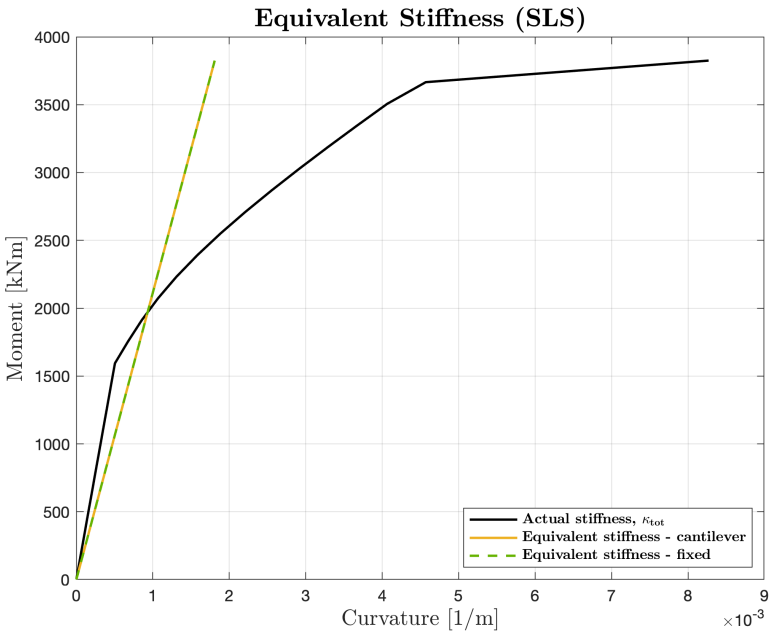

Figure 4.10: Actual and equivalent stiffness for 7ϕ25 in SLS.

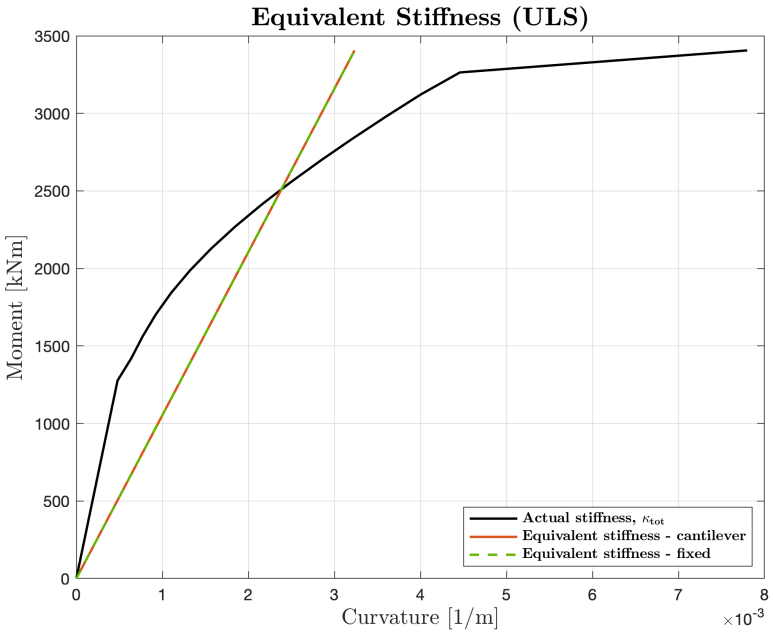

Figure 4.11: Actual and equivalent stiffness for 7ϕ25 in ULS.

Figure 4.12 shows the nominal and actual stiffness. The nominal stiffness is valid only in ULS and increases with increased slenderness. Since the cantilever column has an effective length twice that of the fixed column, its nominal stiffness is higher.

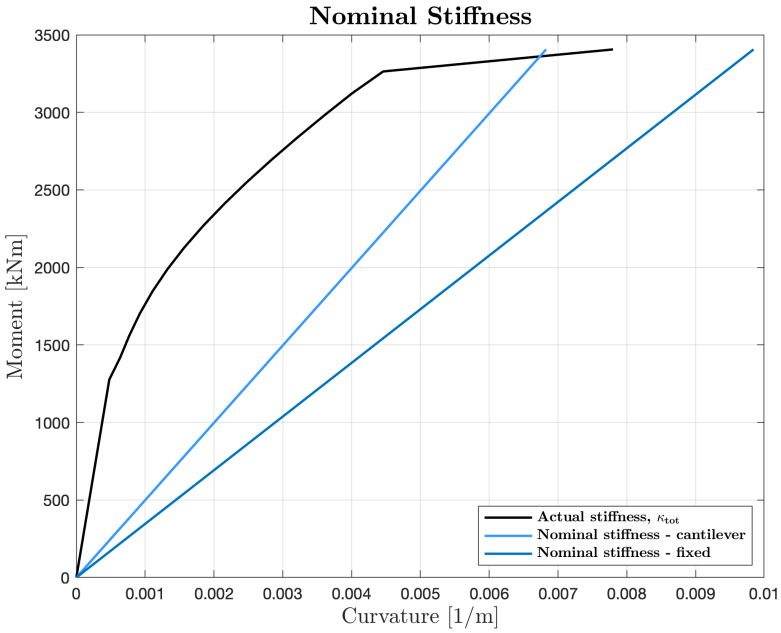

Figure 4.12: Actual and nominal stiffness for 7ϕ25 in ULS.

Figure 4.13 shows the effective stiffness and the stiffness for simplified global analysis from EC2:2023. The effective stiffness corresponds to the point when the first reinforcement yields, which in all cases aligns with the second inflection point of the moment-curvature (M-κ) diagram. The effective stiffness from where the first reinforcement yields is lower than that of the global analysis.

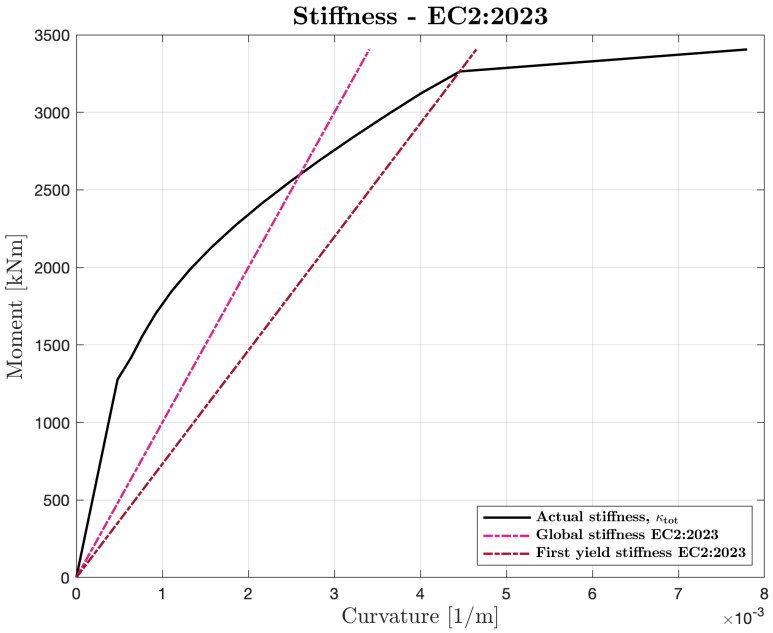

Figure 4.13: Effective stiffness and the stiffness for simplified global analysis from EC2:2023.

Figure 4.14 shows every stiffness calculated for the both columns with different boundary conditions. The stiffness from the simplified global analysis from EC2:2023 aligns close to the calculated equivalent stiffness.

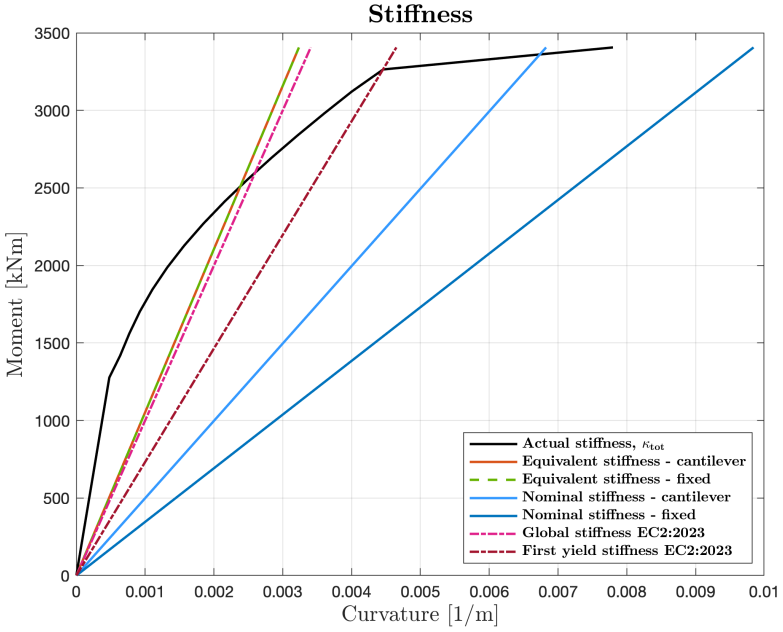

Figure 4.14: Every stiffness calculated for $7\phi25$ in ULS, cantilever and fixed column.

4.2 FE verification of hand calculations

To verify that the chosen hand calculation method reflects the actual behavior of a reinforced concrete column, the results from the hand calculation were compared to the FE analysis performed in DIANA. Various analyses were done, some to learn how the parameters affected the results, and some to test different methods. Figure E.1 in Appendix E shows a compilation of the analyses done in DIANA, only to illustrate the amount of analyses done. The results that deviate significantly are either from tests with varying strength properties or differences in the interaction between steel and concrete, and should not be seen as relevant to the study.

4.2.1 Force-displacement comparison

The black line in Figure 4.15 represents the force-deformation curve derived from the hand calculation, while the green line corresponds to the final force-deformation curve obtained from the FE analysis. It can be observed that, while the curve from the FE analysis exhibits the same initial stiffness, it shows a higher cracking load. Additionally, the overall capacity beyond this point is higher, with the curve reaching a greater value until failure. The final force deformation curve from DIANA was obtained by using the material model that follows EC2 defined in the program, a user specified crack band width was calculated according to Appendix C, and set to 0.127 m and the reinforcement was modeled as embedded. In this final analysis all steps converged within 1-3 iterations, except for the step corre-

lating to where the concrete had its first crack and converged at the 15th iteration.

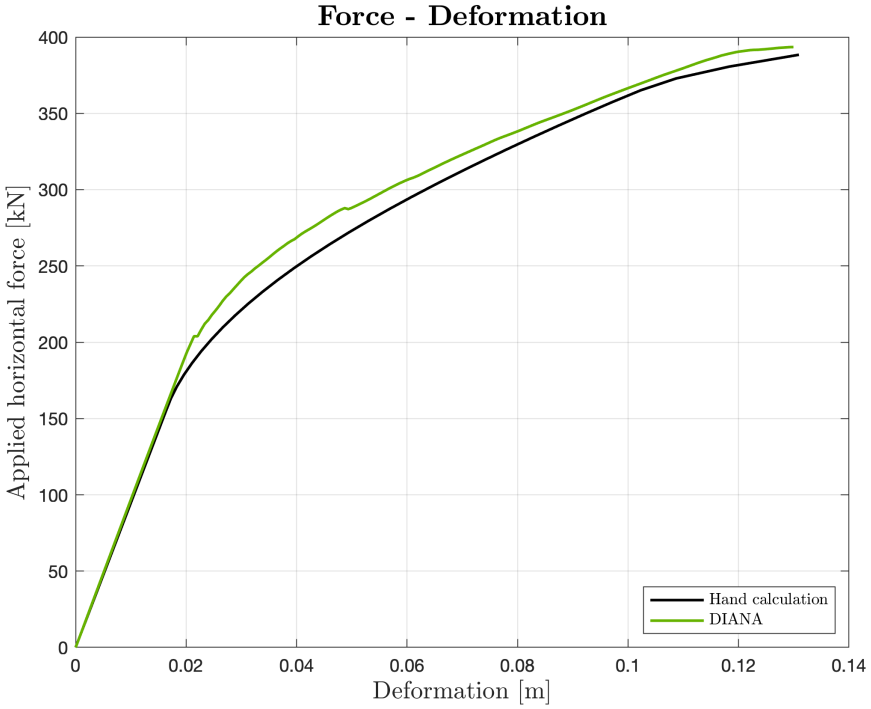

Figure 4.15: Force-displacement comparison.

4.2.2 Loading stages in DIANA

Figure 4.16 illustrates the progression of the column as it is loaded to its capacity. The surrounding images show the strain in the concrete and the corresponding stress in the reinforcement. When the first crack appears, a small plateau is visible on the curve, which then continues to rise with a reduced slope before plateauing again. The second plateau marks the point at which the reinforcement begins to yield, and shortly after, the capacity is reached and the concrete is crushed. The crack propagation pattern is very uniform in terms of formation, which is a consequence of modeling with embedded reinforcement. The second marker on the diagram indicates the onset of concrete cracking, but instead of appearing at the base of the column, the crack initiates roughly 20 cm above the support. To rule out a boundary-condition error, the model was extended with an added segment below the original support line, effectively lengthening the column while keeping its support in the same location. The crack still formed at the same 20 cm elevation, confirming that the unexpected crack position was not caused by incorrect boundary conditions.

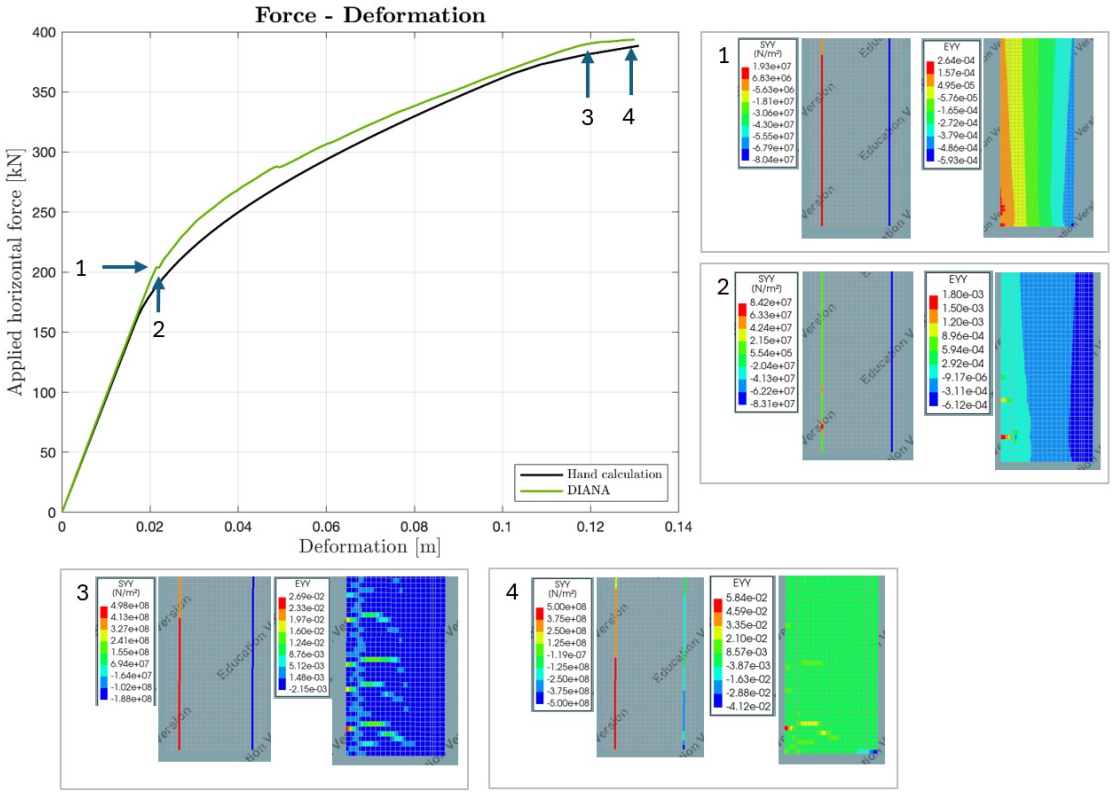

Figure 4.16: Loading stages in DIANA.

4.3 Results of parametric study

This section presents relevant results from calculations using different reinforcement contents, varying applied normal forces, and different concrete strengths. Specific results are selected to demonstrate the differences in moment-curvature and force-displacement diagrams when varying the reinforcement sizes and normal forces. Additionally, the results will highlight how the stiffness behavior change with different concrete strengths, represented by various percentiles. Finally, the section will show how the addition of an extra row of reinforcement influences the structural performance, providing a comprehensive view of the effect of reinforcement configuration on stiffness and deformation characteristics.

4.3.1 Moment-curvature

Figure 4.17 shows moment-curvature diagrams in ULS, with and without creep. The reinforcement content is $7\phi25$ and the axial force varies. The figure demonstrates that a higher applied axial force results in an increased moment capacity with reduced curvature. The magnitude of the curvature with the effect of creep remains proportional to the curvature without creep for all curves.

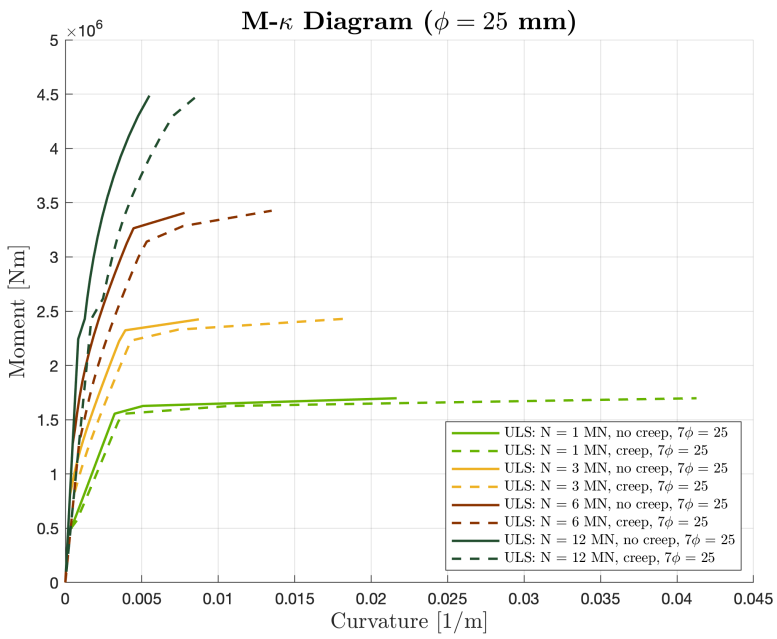

Figure 4.17: Moment-curvature diagram for varying axial force, $7\phi25$.

Figure 4.18 shows moment-curvature diagrams in ULS, with and without creep. The axial force is set to 6 MN, and the reinforcement content varies. The figure demonstrates an increase in moment capacity with higher reinforcement content, while the curvature remains constant. The curve with $9\phi32$ behaves differently from the others, as it features two layers of reinforcement. The two distinct bends in the curve correspond to the points where each layer of reinforcement yields.

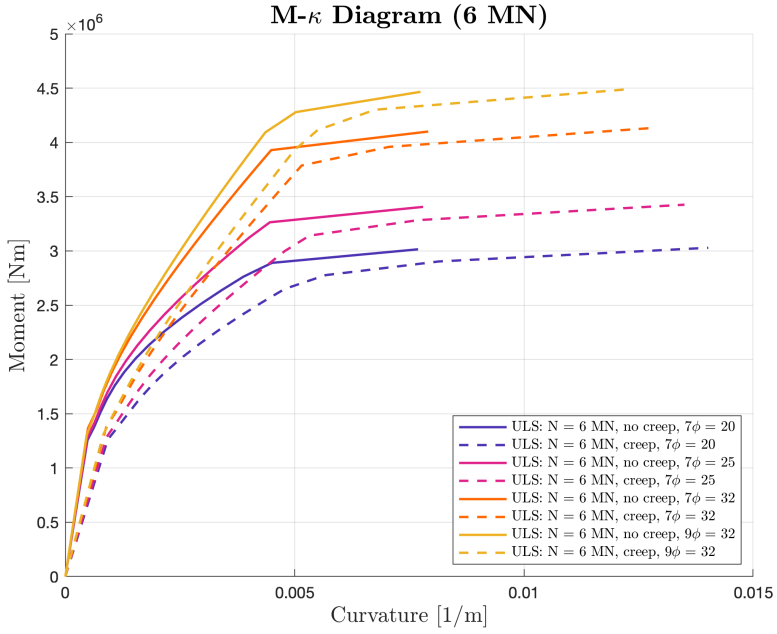

Figure 4.18: Moment-curvature diagram for varying reinforcement content, 6MN axial force.

Figure 4.19 shows the moment-curvature diagram for varying concrete strength. The curves differ proportionally to the difference in strength. The 5th percentile with partial factors has the lowest cracking moment while the 95th percentile has a slightly higher cracking moment than the 50th percentile. The 95th and 50th percentile have approximately the same capacity.

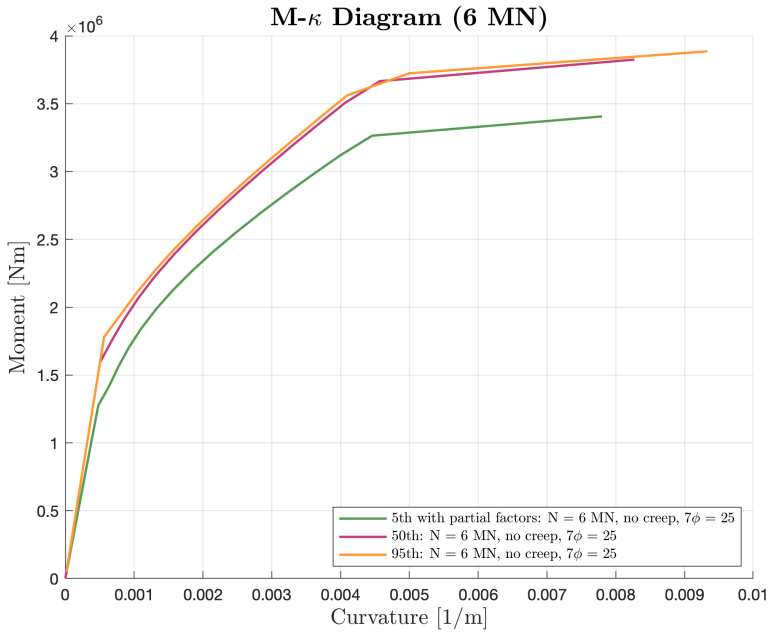

Figure 4.19: Moment-curvature diagram with 6 MN axial force and $7\phi25$, varying concrete strength.

4.3.2 Force-displacement

Figure 4.20 shows the force-displacement diagrams in ULS, with and without creep. The reinforcement content is $7\phi25$ and the axial force varies. The figure demonstrates that a higher applied axial force results in decreased deformation. The magnitude of the deformation with the effect of creep remains proportional to the deformation without creep for all curves.

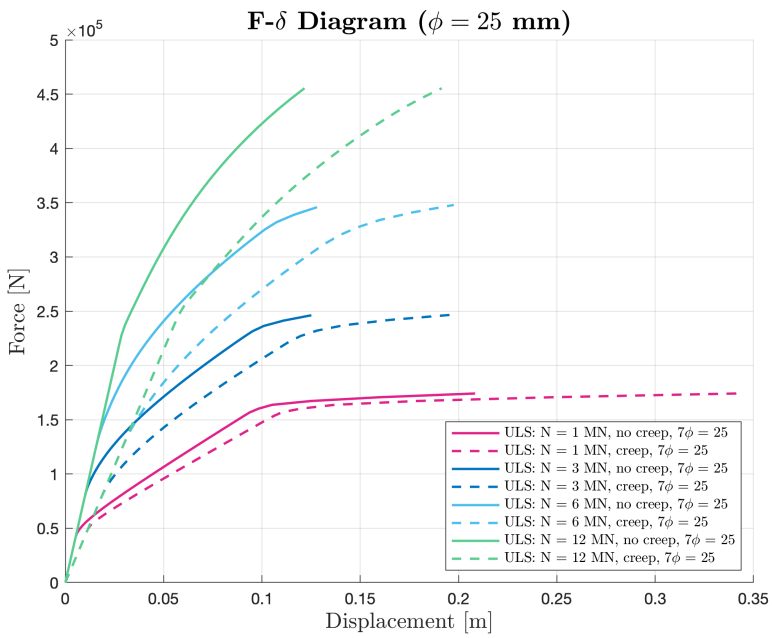

Figure 4.20: Force-Displacement diagram for varying axial force, 7ϕ25.

Figure 4.21 shows force-displacement diagrams in ULS, with and without creep. The axial force is set to 6 MN, and the reinforcement content varies. The figure demonstrates an increase in deformation with higher reinforcement content.

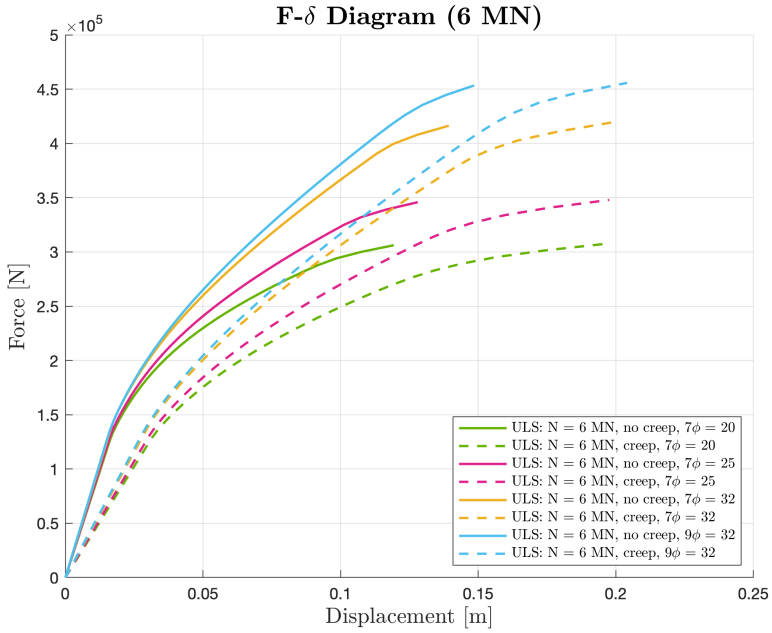

Figure 4.21: Force-Displacement diagram for varying reinforcement content, 6MN axial force.

Figure 4.22 shows the force-displacement diagram for varying concrete strength. The curves differ proportionally to the difference in strength. The applied horizontal force for the 95th percentile is the same as both that of the 50th- and 5th percentile with partial factors (ULS), as that is the largest load that will act on the structure in design.

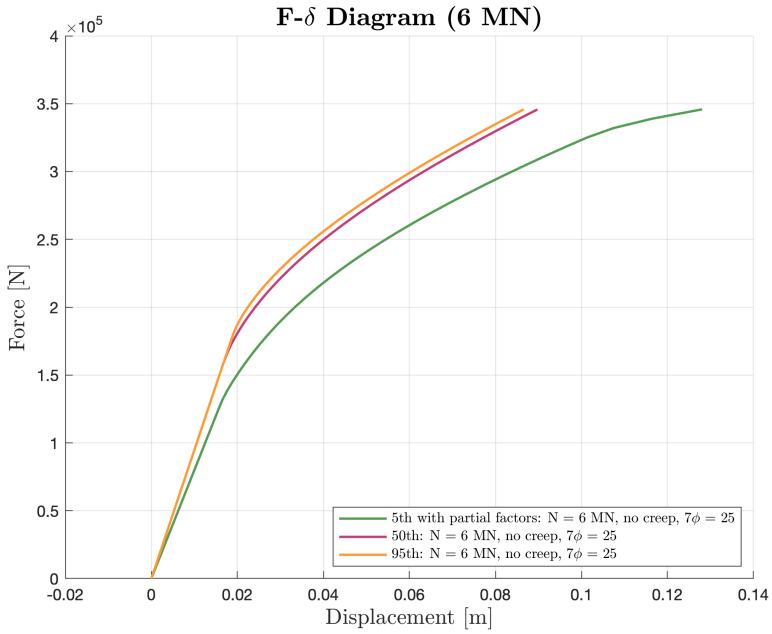

Figure 4.22: Force-Displacement diagram for $7\phi25$, varying concrete strength.

4.3.3 Stiffness for $9\phi32$ with 6MN

This section is included to illustrate the stiffness corresponding to where the first and last row of reinforcement yields, as only $9\phi32$ has multiple rows of reinforcement. To calculate the stiffness when the first and last reinforcement yields, the curvatures corresponding to yielding in the respective layers of reinforcement were determined. Figure 4.23 shows the curvatures at yielding. The moments corresponding to these curvatures were then used in Expression 2.52 from Section 3.2.8. Figure 4.24 shows every stiffness calculated for $9\phi32$, it can be observed that the stiffness where the first row of reinforcement yield correspond to the the yielding moment and the stiffness where the second row yields, correspond to ultimate capacity.

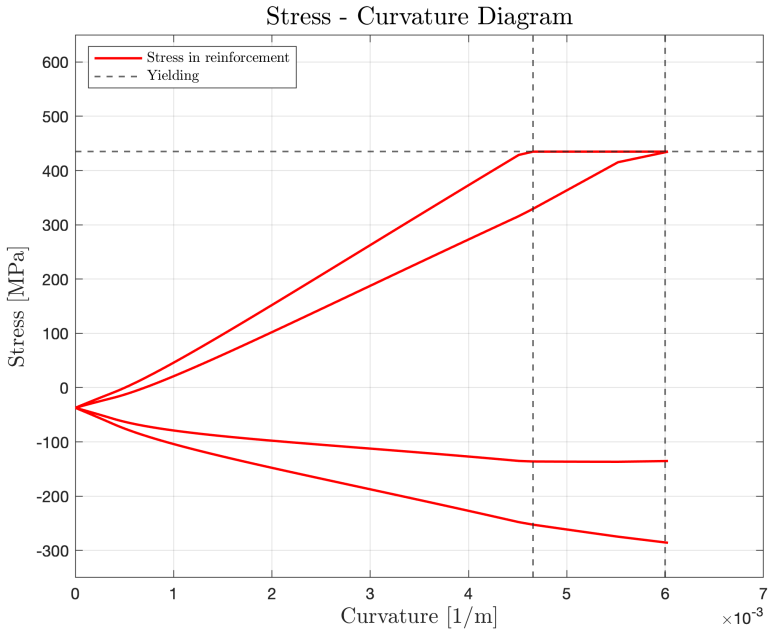

Figure 4.23: Stress-curvature diagram for 9ϕ32 in ULS, axial force 6MN.

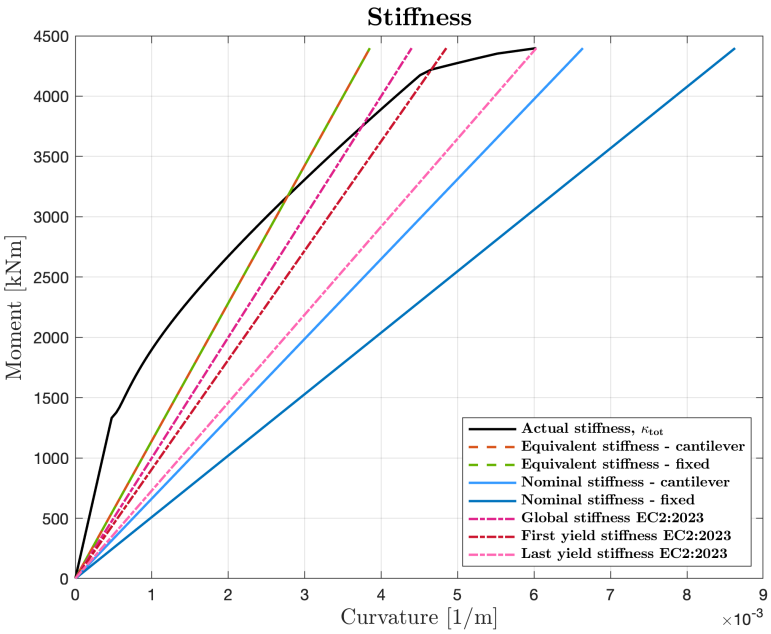

Figure 4.24: Every stiffness calculated for 9ϕ32 in ULS, axial force 6MN.

4.4 Results stiffness calculations across different percentiles and utilization ratios

This section presents the results of stiffness calculations based on percentiles of concrete strength and different utilization ratios. The results shows how stiffness varies with applied axial load and reinforcement amounts described in Table 3.2 in Section 3.1. All percentage values in Tables 4.3-4.6 and 4.10-4.13 indicates the fraction of the uncracked stage I stiffness that remains once non-linear effects are accounted for. It can be applied to scale linear bending-stiffness calculations accordingly.

4.4.1 Stiffness for different percentiles

This section presents both the equivalent and nominal stiffness values calculated according to EC2, along with the various stiffness methods specified in EC2:2023, evaluated across different percentiles.

Tables 4.3, 4.4, 4.5 and 4.6 shows all stiffness values for all percentiles and limit states. Entries highlighted in red are invalid because the calculated stiffness is at or near 100 % of the stage I value. This happens whenever the service-load moment in SLS is below the cracking moment, so the section remains uncracked and retains its full, theoretical stage I stiffness. This stems from the elevated tensile strength in the concrete in the 50th and 95 percentile. Similarly, the entries highlighted in green are also invalid, since they correspond to cases where the reinforcement has not yet yielded, they therefore do not represent the stiffness at the point when the steel begins to yield. nominal stiffness is only valid in ULS(5th(γ)), this is why entries are left blank under the other percentiles. The stiffness at first and last yield corresponds only to material strength and not limit state, the empty entries is SLS are the same as those for ULS and are only removed to simplify the display of results.

Table 4.3: Bending stiffness in MNm^2 for 7ϕ20, with and without creep.

7ϕ20		**Percentile**									
		ULS (0.05(γ)*)		ULS (0.50)		SLS (0.50)		ULS (0.95)		SLS (0.95)	
EC2	N[MN]	**Without creep**									
EI_{ekv}	1	295	10%	643	21%	3103	103%	966	32%	3103	103%
	3	732	24%	932	31%	1940	65%	1066	36%	3009	100%
	6	1024	34%	1408	47%	2103	70%	1486	50%	2300	77%
	12	1372	46%	2380	79%	2380	79%	2498	83%	2491	83%
EI_{nom}	1	175	6%	-	-	-	-	-	-	-	-
Cantilever	3	276	9%	-	-	-	-	-	-	-	-
	6	429	14%	-	-	-	-	-	-	-	-
	12	735	25%	-	-	-	-	-	-	-	-
EI_{nom}	1	149	5%	-	-	-	-	-	-	-	-
Fixed	3	200	7%	-	-	-	-	-	-	-	-
	6	276	9%	-	-	-	-	-	-	-	-
	12	429	14%	-	-	-	-	-	-	-	-
EC2:2023											
EI_{global}	–	1000	33%	1200	40%	-	-	-	-	-	-
$EI_{first.yield}$	1	292	10%	357	12%	-	-	224	7%	-	-
	3	474	16%	514	17%	-	-	368	12%	-	-
	6	662	22%	670	22%	-	-	731	24%	-	-
	12	765	25%	872	29%	-	-	740	25%	-	-
EC2		**With creep**									
EI_{ekv}	1	192	6%	545	18%	1613	54%	790	26%	1613	54%
	3	500	17%	696	23%	1378	46%	826	28%	1613	54%
	6	651	22%	905	30%	1345	45%	949	32%	1450	48%
	12	817	27%	1305	44%	1396	47%	1368	46%	1462	49%
EI_{nom}	1	149	5%	-	-	-	-	-	-	-	-
Cantilever	3	200	7%	-	-	-	-	-	-	-	-
	6	276	9%	-	-	-	-	-	-	-	-
	12	429	14%	-	-	-	-	-	-	-	-
EI_{nom}	1	136	5%	-	-	-	-	-	-	-	-
Fixed	3	162	5%	-	-	-	-	-	-	-	-
	6	200	7%	-	-	-	-	-	-	-	-
	12	276	9%	-	-	-	-	-	-	-	-
EC2:2023											
EI_{global}	–	500	17%	600	20%	-	-	-	-	-	-
$EI_{first.yield}$	1	316	11%	322	11%	-	-	276	9%	-	-
	3	407	14%	453	15%	-	-	434	14%	-	-
	6	505	17%	588	20%	-	-	553	18%	-	-
	12	469	16%	670	22%	-	-	711	24%	-	-

*with partial factors according to EC2 [2]

Table 4.4: Bending stiffness in MNm^2 for 7ϕ25, with and without creep.

7ϕ25		**Percentile**									
		ULS (0.05(γ)*)		ULS (0.50)		SLS (0.50)		ULS (0.95)		SLS (0.95)	
EC2	N[MN]	**Without creep**									
EI_{ekv}	1	488	16%	682	23%	3087	103%	808	27%	3157	105%
	3	800	27%	961	32%	1878	63%	1032	34%	2330	78%
	6	1053	35%	1121	37%	2113	70%	1435	48%	2251	75%
	12	1360	45%	2264	75%	2407	80%	2375	79%	2520	84%
EI_{nom}	1	244	8%	-	-	-	-	-	-	-	-
Cantilever	3	346	12%	-	-	-	-	-	-	-	-
	6	499	17%	-	-	-	-	-	-	-	-
	12	804	27%	-	-	-	-	-	-	-	-
EI_{nom}	1	219	7%	-	-	-	-	-	-	-	-
Fixed	3	270	9%	-	-	-	-	-	-	-	-
	6	346	12%	-	-	-	-	-	-	-	-
	12	499	17%	-	-	-	-	-	-	-	-
EC2:2023											
EI_{global}	–	1000	33%	1200	40%	-	-	-	-	-	-
$EI_{first.yield}$	1	349	12%	473	16%	-	-	330	11%	-	-
	3	614	20%	646	22%	-	-	487	16%	-	-
	6	725	24%	731	24%	-	-	743	25%	-	-
	12	816	27%	941	31%	-	-	825	28%	-	-
EC2		**With creep**									
EI_{ekv}	1	358	12%	594	20%	1676	56%	702	23%	1676	56%
	3	586	20%	746	25%	1339	45%	810	27%	1663	55%
	6	719	24%	943	31%	1386	46%	984	33%	1488	50%
	12	861	29%	1316	44%	1451	48%	1371	46%	1509	50%
EI_{nom}	1	219	7%	-	-	-	-	-	-	-	-
Cantilever	3	270	9%	-	-	-	-	-	-	-	-
	6	346	12%	-	-	-	-	-	-	-	-
	12	499	17%	-	-	-	-	-	-	-	-
EI_{nom}	1	206	7%	-	-	-	-	-	-	-	-
Fixed	3	231	8%	-	-	-	-	-	-	-	-
	6	270	9%	-	-	-	-	-	-	-	-
	12	346	12%	-	-	-	-	-	-	-	-
EC2:2023											
EI_{global}	–	500	17%	600	20%	-	-	-	-	-	-
$EI_{first.yield}$	1	420	14%	436	15%	-	-	327	11%	-	-
	3	521	17%	522	17%	-	-	376	13%	-	-
	6	605	20%	663	22%	-	-	587	20%	-	-
	12	520	17%	812	27%	-	-	812	27%	-	-

*with partial factors according to EC2 [2]

Table 4.5: Bending stiffness in MNm^2 for 7ϕ32, with and without creep.

7ϕ32		**Percentile**									
		ULS (0.05(γ)*)		ULS (0.50)		SLS (0.50)		ULS (0.95)		SLS (0.95)	
EC2	N[MN]	**Without creep**									
EI_{ekv}	1	715	24%	825	27%	1763	59%	886	30%	2684	90%
	3	925	31%	1071	36%	1839	61%	1118	37%	2141	71%
	6	1136	38%	1420	47%	2152	72%	1463	49%	2264	75%
	12	1394	46%	2153	72%	2484	83%	2249	75%	2587	86%
EI_{nom}	1	368	12%	-	-	-	-	-	-	-	-
Cantilever	3	469	16%	-	-	-	-	-	-	-	-
	6	622	21%	-	-	-	-	-	-	-	-
	12	928	31%	-	-	-	-	-	-	-	-
EI_{nom}	1	342	11%	-	-	-	-	-	-	-	-
Fixed	3	393	13%	-	-	-	-	-	-	-	-
	6	469	16%	-	-	-	-	-	-	-	-
	12	622	21%	-	-	-	-	-	-	-	-
EC2:2023											
EI_{global}	–	1000	33%	1200	40%	-	-	-	-	-	-
$EI_{first.yield}$	1	658	22%	690	23%	-	-	685	23%	-	-
	3	761	25%	790	26%	-	-	831	28%	-	-
	6	877	29%	984	33%	-	-	975	33%	-	-
	12	922	31%	1045	35%	-	-	987	33%	-	-
EC2		**With creep**									
EI_{ekv}	1	578	19%	714	24%	1397	47%	771	26%	1787	60%
	3	715	24%	861	29%	1356	45%	905	30%	1637	55%
	6	830	28%	1038	35%	1457	49%	1069	36%	1536	51%
	12	941	31%	1363	45%	1553	52%	1412	47%	1607	54%
EI_{nom}	1	342	11%	-	-	-	-	-	-	-	-
Cantilever	3	393	13%	-	-	-	-	-	-	-	-
	6	470	16%	-	-	-	-	-	-	-	-
	12	622	21%	-	-	-	-	-	-	-	-
EI_{nom}	1	330	11%	-	-	-	-	-	-	-	-
Fixed	3	355	13%	-	-	-	-	-	-	-	-
	6	393	13%	-	-	-	-	-	-	-	-
	12	470	16%	-	-	-	-	-	-	-	-
EC2:2023											
EI_{global}	–	500	17%	600	20%	-	-	-	-	-	-
$EI_{first.yield}$	1	506	17%	532	18%	-	-	480	16%	-	-
	3	595	20%	705	24%	-	-	652	22%	-	-
	6	652	22%	815	27%	-	-	803	27%	-	-
	12	616	21%	846	28%	-	-	968	32%	-	-

*with partial factors according to EC2 [2]

Table 4.6: Bending stiffness in MNm^2 for 9ϕ32, with and without creep.

9ϕ32		**Percentile**									
		ULS (0.05(γ)*)		ULS (0.50)		SLS (0.50)		ULS (0.95)		SLS (0.95)	
EC2	N[MN]	**Without creep**									
EI_{ekv}	1	731	24%	879	29%	1714	57%	925	31%	2415	81%
	3	943	31%	1103	37%	1842	61%	1141	38%	2072	69%
	6	1137	38%	1427	48%	2175	73%	1467	49%	2278	76%
	12	1394	46%	2116	71%	2504	84%	2212	74%	2612	87%
EI_{nom}	1	408	14%	-	-	-	-	-	-	-	-
Cantilever	3	509	17%	-	-	-	-	-	-	-	-
	6	662	22%	-	-	-	-	-	-	-	-
	12	968	32%	-	-	-	-	-	-	-	-
EI_{nom}	1	382	13%	-	-	-	-	-	-	-	-
Fixed	3	433	14%	-	-	-	-	-	-	-	-
	6	510	17%	-	-	-	-	-	-	-	-
	12	662	22%	-	-	-	-	-	-	-	-
EC2:2023											
EI_{global}	–	1000	33%	1200	40%	-	-	-	-	-	-
$EI_{first.yield}$	1	709	24%	719	24%	-	-	752	25%	-	-
	3	790	26%	823	27%	-	-	901	30%	-	-
	6	922	31%	1041	35%	-	-	1017	34%	-	-
	12	917	31%	1230	41%	-	-	1238	41%	-	-
$EI_{last.yield}$	1	505	17%	550	18%	-	-	464	15%	-	-
	3	549	18%	626	21%	-	-	525	18%	-	-
	6	596	20%	635	21%	-	-	876	29%	-	-
	12	917	31%	1079	36%	-	-	1073	36%	-	-
EC2		**With creep**									
EI_{ekv}	1	589	20%	757	25%	1347	45%	798	27%	1825	61%
	3	698	23%	884	29%	1370	46%	916	31%	1825	61%
	6	861	29%	1059	35%	1481	49%	1088	36%	1564	52%
	12	966	32%	1360	45%	1590	53%	1404	47%	1638	55%
EI_{nom}	1	382	13%	-	-	-	-	-	-	-	-
Cantilever	3	433	14%	-	-	-	-	-	-	-	-
	6	510	17%	-	-	-	-	-	-	-	-
	12	662	22%	-	-	-	-	-	-	-	-
EI_{nom}	1	370	12%	-	-	-	-	-	-	-	-
Fixed	3	395	13%	-	-	-	-	-	-	-	-
	6	433	14%	-	-	-	-	-	-	-	-
	12	510	17%	-	-	-	-	-	-	-	-
EC2:2023											
EI_{global}	–	500	17%	600	20%	-	-	-	-	-	-
$EI_{first.yield}$	1	631	21%	636	21%	-	-	560	19%	-	-
	3	704	23%	746	25%	-	-	688	23%	-	-
	6	762	25%	863	29%	-	-	848	28%	-	-
	12	817	27%	933	31%	-	-	951	32%	-	-
$EI_{last.yield}$	1	384	13%	504	17%	-	-	406	14%	-	-
	3	476	16%	571	19%	-	-	630	21%	-	-
	6	566	19%	627	21%	-	-	648	22%	-	-
	12	605	20%	646	22%	-	-	680	23%	-	-

*with partial factors according to EC2 [2]

Tables 4.7 and 4.8 show the percentage increase of stiffness from nominal to equivalent stiffness in the 5th(γ) percentile in ULS, with and without creep for all reinforcement contents. It can be observed that the percentages span from 29 to 150 for the cantilever column with the effect of creep, and from 41 to 226 for the fixed column with creep. These results are relevant in discussing how to increase capacity in calculation.

Cantilever	**Reinforcement content**			
Without creep	$7\phi20$	$7\phi25$	$7\phi32$	$9\phi32$
1 MN	69	100	95	79
3 MN	165	131	97	85
6 MN	138	111	83	72
12 MN	87	69	50	44
With creep				
1 MN	29	64	69	54
3 MN	150	117	82	61
6 MN	136	108	77	69
12 MN	90	73	51	46

Table 4.7: Percentage increase from nominal to equivalent stiffness, cantilever column.

Fixed	**Reinforcement content**			
Without creep	$7\phi20$	$7\phi25$	$7\phi32$	$9\phi32$
1 MN	98	123	109	91
3 MN	266	197	135	118
6 MN	270	204	142	123
12 MN	220	173	124	111
With creep				
1 MN	41	74	76	59
3 MN	209	153	101	77
6 MN	226	167	111	99
12 MN	196	149	100	89

Table 4.8: Percentage increase from nominal to equivalent stiffness, fixed column.

Table 4.9 shows the stiffness values in ULS for the 5th(γ) and 95th percentile. It shows that the equivalent stiffness increases with increasing normal force. The maximum equivalent stiffness values, for the reinforcement configurations studied, are 46% and 83% for the 5th(γ) and 95th percentile, respectively. This table highlights key results relevant in discussing how to reduce restraint forces.

Table 4.9: Bending stiffness in ULS for all reinforcement amounts, with and without creep.

		Percentile							
		ULS (0.05(γ)*)				**ULS (0.95)**			
EI_{ekv}	N[MN]	Without creep		With creep		Without creep		With creep	
7ϕ20	1	295	10%	192	6%	966	32%	790	26%
	3	732	24%	500	17%	1066	36%	826	28%
	6	1024	34%	651	22%	1486	50%	949	32%
	12	1372	46%	817	27%	2498	83%	1368	46%
7ϕ25	1	488	16%	358	12%	808	27%	702	23%
	3	800	27%	586	17 %	1032	34%	810	27%
	6	1053	35%	719	21%	1435	48%	984	33%
	12	1360	45%	861	25%	2375	79%	1376	46%
7ϕ32	1	715	24%	578	19%	886	30%	771	26%
	3	925	31%	715	24%	1118	37%	905	30%
	6	1136	38%	830	28%	1463	49%	1069	36%
	12	1394	46%	941	31%	2249	75%	1412	47%
9ϕ32	1	731	24%	589	20%	925	31%	798	27%
	3	943	31%	698	23%	1141	38%	916	31%
	6	1137	38%	861	29%	1467	49%	1088	36%
	12	1394	46%	966	32%	2212	74%	1404	47%
$EI_{global2023}$		1000	33%	500	17%	1200	40%	600	20%

*with partial factors according to EC2 [2]

Figure 4.25 graphically represents the data from Table 4.9, plotting relative equivalent stiffness in the ULS 5th-percentile with and without creep. All data points lie along an upward-sloping linear trend. At the lowest axial load (1 MN), the stiffness values are more widely dispersed, as the axial load increases, the points converge tightly for all reinforcement amounts, with and without creep. Notably, no stiffness value exceeds 46 %.

Figure 4.26 graphically represents the data from Table 4.9, plotting relative equivalent stiffness in the ULS 95th-percentile with and without creep. All results follow an upward-sloping linear trend. For axial loads of 1, 3, and 6 MN, the relative stiffness values across all reinforcement amounts align closely, whereas at 12 MN they exhibit a broader spread. It is also noteworthy that none of the stiffness values exceeds 83 %.

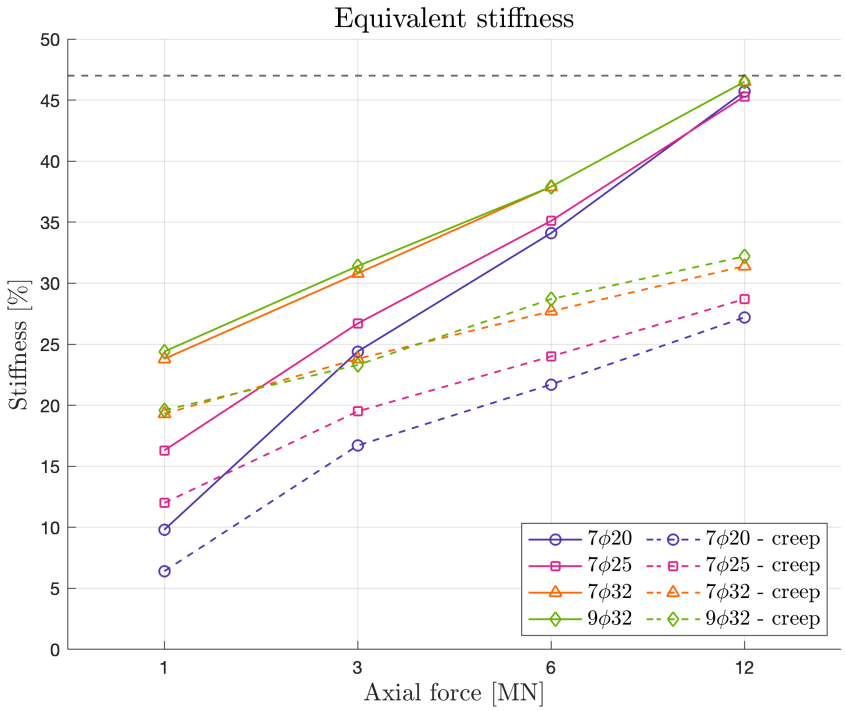

Figure 4.25: Equivalent stiffness with and without creep for different reinforcement configurations (7ϕ20, 7ϕ25, 7ϕ32, 9ϕ32) in ULS 5th(γ) percentile.

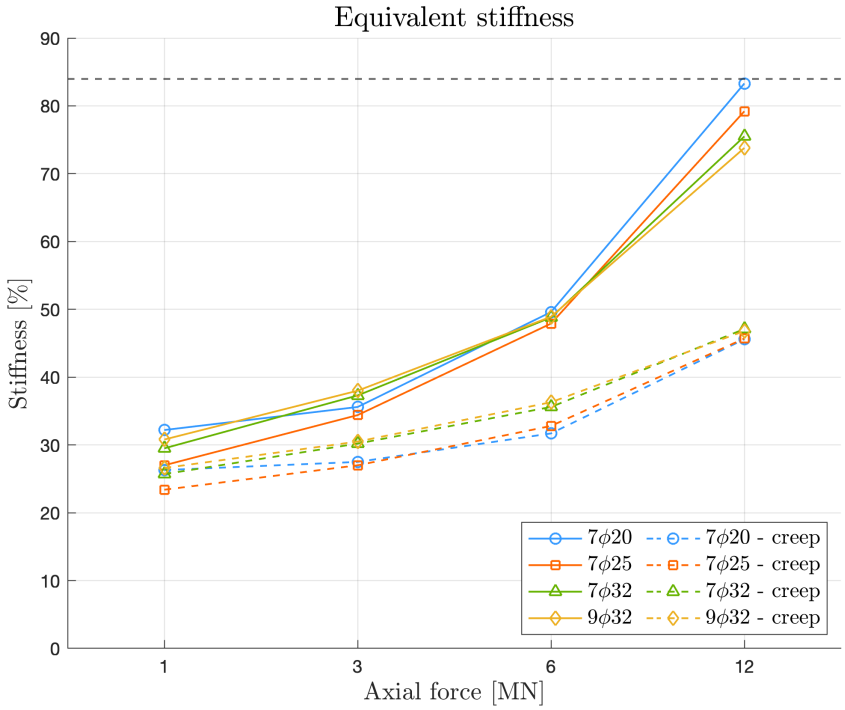

Figure 4.26: Equivalent stiffness with and without creep for different reinforcement configurations (7ϕ20, 7ϕ25, 7ϕ32, 9ϕ32) in ULS 95th percentile.

4.4.2 Stiffness for different utilization ratios

This section presents the equivalent stiffness calculated for various utilization ratios, compared to nominal stiffness for both columns. Tables 4.10, 4.11, 4.12 and 4.13 shows how the equivalent stiffness increase with increased normal force and decreased utilization ratio.

Table 4.10: Equivalent and nominal stiffness for 7ϕ20 in MNm^2, with creep.

7ϕ20	**With creep**											
	Equivalent stiffness								**nominal stiffness**			
N[MN]	99%		95%		80%		70%		Cantilever		Fixed	
1	112	4%	183	6%	405	13%	454	15%	149	5%	136	5%
3	350	12%	477	16%	639	21%	749	25%	200	7%	162	6%
6	524	17%	621	21%	805	27%	932	31%	276	9%	200	7%
12	725	24%	780	26%	968	32%	1104	37%	429	14%	276	9%

Table 4.11: Equivalent and nominal stiffness in MNm^2 for 7ϕ25, with creep.

7ϕ25	**With creep**											
	Equivalent stiffness								**nominal stiffness**			
N[MN]	99%		95%		80%		70%		Cantilever		Fixed	
1	184	6%	334	11%	471	16%	505	17%	219	7%	206	7%
3	421	14%	546	18%	663	22%	743	25%	270	9%	231	8%
6	574	19%	670	22%	817	27%	922	31%	346	12%	270	9%
12	753	25%	803	27%	974	32%	1094	36%	499	17%	346	12%

Table 4.12: Equivalent and nominal stiffness in MNm^2 for 7ϕ32, with creep.

7ϕ32	**With creep**											
	Equivalent stiffness								**nominal stiffness**			
N[MN]	99%		95%		80%		70%		Cantilever		Fixed	
1	387	13%	578	19%	643	21%	669	22%	342	11%	329	11%
3	585	20%	715	24%	806	27%	866	29%	393	13%	355	12%
6	728	24%	830	28%	953	32%	1041	35%	469	16%	393	13%
12	892	30%	941	31%	1105	37%	1212	40%	622	21%	469	16%

Table 4.13: Equivalent and nominal stiffness in MNm^2 for 9ϕ32, with creep.

9ϕ32	**With creep**											
	Equivalent stiffness								**nominal stiffness**			
N[MN]	99%		95%		80%		70%		Cantilever		Fixed	
1	396	13%	524	17%	615	21%	633	21%	382	13%	370	12%
3	478	16%	621	21%	734	24%	778	26%	433	14%	395	13%
6	686	23%	766	26%	862	29%	932	31%	510	17%	433	14%
12	812	27%	859	29%	1001	33%	1098	37%	662	22%	510	17%

Tables 4.14, 4.15, 4.16 and 4.17 show the the stiffness increase from nominal to equivalent stiffness. In nearly every case, the computed equivalent stiffness exceeds the nominal cantilever and fixed column stiffness, except for the case of 99% utilization ratio with 1 MN axial force for 7ϕ20 and 7ϕ25. These tables highlights key results relevant in discussing how to increase stiffness in capacity calculation.

7ϕ20		**Utilization ratio**			
	[MN]	99%	95%	80%	70%
Cantilever	1	-25	23	171	204
	3	75	138	220	274
	6	80	125	191	237
	12	69	82	125	157
Fixed	1	-18	34	197	233
	3	116	195	295	363
	6	162	211	302	366
	12	162	182	250	299

Table 4.14: Percentage increase from nominal to equivalent stiffness, 7ϕ20 with creep.

7ϕ25		**Utilization ratio**			
	[MN]	99%	95%	80%	70%
Cantilever	1	-16	53	115	131
	3	56	102	146	175
	6	66	94	136	166
	12	51	61	95	119
Fixed	1	-11	62	129	145
	3	82	136	186	221
	6	113	148	203	242
	12	118	132	181	216

Table 4.15: Percentage increase from nominal to equivalent stiffness, 7ϕ25 with creep.

7ϕ32		**Utilization ratio**			
	[MN]	99%	95%	80%	70%
Cantilever	1	13	69	88	96
	3	49	82	105	120
	6	55	77	103	122
	12	43	51	78	95
Fixed	1	18	76	95	103
	3	65	101	127	144
	6	85	111	142	165
	12	90	100	136	158

Table 4.16: Percentage increase from nominal to equivalent stiffness, 7ϕ32 with creep.

9ϕ32		**Utilization ratio**			
	[MN]	99%	95%	80%	70%
Cantilever	1	4	37	61	66
	3	10	43	69	80
	6	35	50	69	83
	12	23	30	51	66
Fixed	1	7	42	66	71
	3	21	57	86	97
	6	58	77	99	115
	12	59	69	96	115

Table 4.17: Percentage increase from nominal to equivalent stiffness, 9ϕ32 with creep.

5 Discussion

In the context of bridge design, this thesis aimed to demonstrate three specific outcomes. The first outcome is viewed from a capacity-control perspective: here, an increase in global stiffness is desirable to control deformations and maintain stability. The second perspective addresses restraint forces, by reducing the stiffness in a system model, the magnitude of restraint-induced forces and the amount of required reinforcement can be substantially lowered. Finally, in slender column and arch systems more precise calculations yield more accurate capacity estimates, resulting in a substantial increase in stiffness relative to nominal values and, consequently, higher buckling resistance. In this chapter, the thesis results are analyzed alongside the uncertainties identified and the discussion generated throughout the research.

5.1 Equivalent stiffness

In the current code, nominal stiffness is used to estimate capacity, and on average the calculated nominal stiffness in Table 4.3-4.6 is 12% of stage I stiffness for both cantilever and fixed-column configurations with creep. This can be considered as highly conservative, leading to potentially over-designed sections. By contrast, calculating an equivalent stiffness through non-linear analysis captures both concrete cracking and reinforcement post-yield behavior. Tables 4.7 and 4.8 shows that the equivalent stiffness exceeds nominal stiffness by at least 29 % for all cross-sections studied. However, since the 29 % stems from the $7\phi20$ section under only 1 MN of axial force, the cross-section can hardly be considered truly compressed, and nominal stiffness is intended for calculating stiffness in compression members. When excluding all configurations with low axial force, the equivalent stiffness exceeds the nominal stiffness by at least 44 %. The higher stiffness directly increases predicted buckling and moment capacities, enabling more efficient section sizing and reinforcement layouts without sacrificing safety. Adopting equivalent-stiffness estimates in early design not only yields more economical solutions but also aligns analytical predictions more closely with actual structural behavior.

The second perspective addresses restraint forces. By reducing the stiffness in a system model, the magnitude of restraint-induced forces and the required reinforcement amount can be reduced. Generally, 100 % of stage I stiffness is assumed in calculation, but this is not favorable as it leads to higher restraining forces. However, drawing on decades of industry experience, Norconsult typically applies a stiffness reduction factor of 0.80-0.85 in their projects. Based on the results from Table 4.9 it can be observed that none of the examined cross-section configurations has an equivalent stiffness that exceeds 83 % in the 95th percentile in ULS. This was also illustrated in Figure 4.26. Table 4.6 shows that the highest stiffness value is 87 % and comes from the analysis in the 95th percentile in SLS. These results indicate that, regardless of adjacent structural components, the stiffness can always be reduced to approximately 85 % of the stage I value without underestimating the stiffness of the entire system. This makes the reduction factor

adopted at Norconsult a reasonable and reliable design assumption. Based on the results from Table 4.9 it can be observed that none of the examined cross-section configurations has an equivalent stiffness that exceeds approximately 45 % in the 5th(γ) percentile in ULS. This was also illustrated in Figure 4.25. These results indicate that for single isolated columns it is possible to reduce the stiffness to 45%, which aligns with the global stiffness reduction mandated by the revised EC2:2023 standard, see Section 2.6. As presented in Table 4.9, the stiffness calculated in accordance with EC2:2023 amounts to 33 % of the stage I stiffness, which is of the same magnitude as the equivalent stiffness for 6MN for all reinforcement configurations. Luo et al [13] conducted studies to derive a stiffness reduction factor for rectangular cross-sections and found that, on average, the stiffness can be reduced by a factor of 0.3. When looking closer at their work, a better comparison can be made by looking at the correct axial compression ratio. When applying 6 MN on the cross-section studied in this thesis, the axial compression ratio is 0.2, in Luo et al's work, this would result in a stiffness reduction factor of 0.295. This value is lower but of the same magnitude as the stiffness corresponding to the 5th(γ) percentile in ULS. As their work combined numerical calculations with physical testing, the conclusion of this thesis, to always reduce the stiffness of isolated columns to approximately 45 % of stage I stiffness, is deemed reasonable and on the safe side, in order to decrease restraint forces.

The third perspective, and one of the primary motivations for this thesis, is the capacity assessment of existing structures, such as slender columns and arches in concrete bridges. When using nominal stiffness to assess the capacity of a slender member, the axial force magnitude often equals or exceeds the actual critical buckling load. This is especially applicable to reinforcement amounts of 7ϕ20 and 7ϕ25, which are reinforcement amounts likely to find in older structures that are sometimes insufficiently reinforced. Tables 4.10, 4.11, 4.12 and 4.13 show how the effective stiffness varies with axial load and utilization ratio. It can be observed that effective stiffness increases with higher axial force and lower utilization ratio. Tables 4.14-4.17 present the percentage increase from nominal to equivalent stiffness. For example, at a 70 % utilization ratio the effective stiffness can be from 66 % to 366 % higher than the nominal value, depending on the applied axial load and reinforcement content. Such an increase has a pronounced effect on buckling resistance. When this enhanced stiffness is used in capacity calculations the critical buckling load is significantly elevated. This makes it feasible to reassess and confirm the load-carrying capacity of existing slender members that might otherwise be deemed unsafe. In practice, incorporating the true stiffness can reveal substantial reserve capacity, enabling more economical retrofits or extending the service life of aging structures without costly strengthening measures.

5.2 Nominal, effective and global stiffness

From the results in this thesis, it is evident that the procedure for calculating nominal stiffness produces consistently low values. The formula for nominal stiffness is empirically derived and partly dependent on slenderness. Although the method is adaptable to different column types, the calculated stiffness remains

uniformly low across all cases. In the literature review, Bonet et al. [15] noted that nominal stiffness corresponded poorly with several tested specimens. Várdai & Bódi [16] also observed that nominal stiffness is generally very low compared to results from both non-linear and linear analyses. Andreatta & Kofler [12] state that nominal stiffness ensures accurate calculations for single columns but recommend non-linear analysis for complex cases. Westerberg [11], however, who conducted an extensive study on simplified stiffness calculation with comparison to over 900 test specimens from different sources, observed that nominal stiffness gives results with a high degree of agreement for most cases. In this context, the consistently low values and conflicting findings in earlier studies cast doubt on the formula's accuracy and practical applicability, which could be an explanation for its removal in the revised code.

In the theory chapter of this thesis, the method for calculating nominal curvature was presented. Due to time constraints, stiffness has not been determined using this approach but should be done in further studies to investigate how it compares to other methods of calculating stiffness. In EC2:2023, a minor modification was introduced concerning the assumption on the cross-section strains. This change results in a higher nominal curvature than that obtained with the current code.

In the revised code, EC2:2023, nominal stiffness has been replaced by a procedure that computes the effective stiffness at the moment when the reinforcement yields, deemed a conservative approach. However, the revised code does not clarify whether this yielding moment applies when more than one row of reinforcement is present. Tables 4.3–4.6 show that, with a single row of reinforcement, the stiffness at first yield is below the corresponding equivalent stiffness for all entries. When a second layer of reinforcement, consisting of just two additional bars is introduced, see Table 4.6, the stiffness at first-layer yielding becomes comparable to the equivalent value. In contrast, the stiffness at second-row yielding remains on the same order of magnitude as that for single-row sections. These results indicate that the new code should specify that stiffness be calculated at the point where the last row of reinforcement yields to maintain conservatism. Furthermore, the code does not specify whether stiffness should be determined from when the tensile or compressive reinforcement yield. Since compressive reinforcement yielding has small influence, stiffness was calculated based on the curvature at which the tensile reinforcement yields.

The revised code also introduces a simplified procedure for computing stiffness in global analysis, but its documentation is sparse and lacks critical detail. It does not specify whether, or how, E_{cd} should be modified by partial factors as in the current EC2 version. Here, it was assumed that $E_{cd} = E_{cm}/1.2$ in accordance with the current practice. Likewise, no guidance is given on incorporating creep. In this work, creep was treated by dividing E_{cd} by the effective creep coefficient, $(1+\varphi)$. Finally, the code does not clarify which moment of inertia to use (for example, whether I_I, or I_c is appropriate), leaving these choices undefined. An increase in global stiffness could be achieved, if state I moment of inertia was allowed to be used in the calculation. This method is very general and makes analysis of spe-

cific cases difficult, and given the number of assumptions involved, these results should be interpreted with caution. However, the global stiffness derived from the analysis corresponds to the results for equivalent stiffness, suggesting that the assumptions may be reasonable and accurate.

Both the retained and newly introduced stiffness calculation methods in EC2:2023 yield higher stiffness values than those of the existing code. This indicates that the Eurocode committee now places greater confidence in its stiffness models, as reflected by the elevated stiffness values achieved in the revised standard.

5.3 National differences in standards

The difference between the Swedish and Norwegian requirements for minimum reinforcement has important implications for Norconsult, as they are often involved in projects on the Norwegian market. Although both countries base their design codes on EC2, their national annexes diverge in their interpretation of minimum reinforcement ratios. In Sweden, the minimum reinforcement ratio is set at 0.2 %, in line with Eurocode's objective to optimize material use while maintaining safety. By contrast, the Norwegian annex mandates a much stricter 1 % minimum, which in this study renders only the $7\phi32$ and $9\phi32$ configurations sufficient under Norwegian regulations.

All recommendations and guidelines in this thesis (Section 5.1) assume a high utilization ratio of the cross-section. If the cross-section is designed for a lower utilization ratio or if minimum reinforcement results in a utilization ratio lower than 95 %, the recommendations and guidelines are no longer applicable. According to the Norwegian standard, sections reinforced with $7\phi20$ and $7\phi25$ would need additional reinforcement to meet the requirements, thereby reducing their utilization ratio.

5.4 Choosing material model

Before this work was initiated, Norconsult has previously used the simplified material model from EC2, presented in Figure 2.5 when using the calculation method presented in this thesis. However, during the literature study, it became clear that the material model for non-linear analysis, presented in Figure 2.4, should be used. When the two models were compared in this thesis, see Figure 3.5, it was observed that the non-linear material model exhibits a strain-softening behavior after peak strength. The simplified material model remains linear from its peak strength value to failure. For lower concrete classes, the non-linear material model exhibits a higher initial stiffness compared to the simplified material model. The curves for both material models across all concrete classes can be found in Appendix B. When integrating the non-linear material model a lower capacity is achieved compared to the simplified material model, since the area under the curve is smaller.

The issue arising from the use of two different material models is that the simpli-

fied curve is employed for cross-section design and capacity calculations, whereas the non-linear curve is used for structural analysis and stiffness determination. As a result, capacity and stiffness are derived from different material representations, potentially leading to inconsistencies when using the guidelines derived in this thesis. Figure 3.6 in Section 3.2.1 shows that the simplified design curve generates a capacity approximately 2 % higher than that of the non-linear material curve. This discrepancy is most pronounced under high axial loads, where the non-linear softening behavior reduces the effective stress level. Therefore, the recommendations and guidelines for adjusting stiffness presented in Section 5.1 should be fully applicable regardless of the material curve chosen, as the resulting difference in capacity is relatively small. Assuming that the capacity has been calculated at a high utilization ratio. This also allows for the conclusion that using the simplified curve, as previously adopted by Norconsult, is a reasonable choice.

5.5 Calculation process

During the calculation process in Mathcad, difficulties were encountered when replacing the simplified material model with the non-linear model. Because of the non-linear behavior of the model, the M–N interaction curve went outside of the first quadrant after integration, which prevented functions like 'linterp' from correctly determining the moment capacity at a given normal force. This issue was resolved by putting a reduction factor in the 'solveblock' functions, to let the solver skip the points on the curve going outside the quadrant.

There were also some initial problems when trying to integrate creep into the material model. Creep was inadvertently applied twice in different formulas, which led to it canceling itself out. In order to account for creep, the material model was modified by multiplying the strain value with the factor $1 + \varphi_{\text{ef}}$ in accordance with EC2. All other parameters in the material model remained unchanged. The revised code, EC2:2023, now explicitly states that the peak strain, ε_{c1}, is to be determined based on the concrete's mean cylinder strength f_{cm}, a clarification that was not clearly stated in the current code.

Additionally, calculation problems emerged for some cross-section configurations. When a high axial load was applied in combination with low reinforcement content, Mathcad encountered issues solving for the reinforcement stresses, resulting in large incorrect values appearing in the stress matrix. This computational error was resolved by slightly adjusting the initial strain values. No other entries in the stress matrix were affected by this modification. Another computational error arose under the same configurations in the moment–curvature analysis, where a large negative value appeared. This issue stemmed from the way reinforcement stress was evaluated once the concrete cracked and was corrected by imposing a lower bound of zero, preventing any negative values. Also, there were issues when integrating the curvature to get the deformation for the two different columns in Mathcad. To be able to integrate the curvature function made for the fixed column, the function 'sign' had to be integrated into the calculation to account for the sign change of the moment distribution.

Although the results are consistent, some inaccuracy may originate from the analysis procedure. Initially, only 25 evaluation points were used, producing less precise curves that appeared jagged because the program interpolates linearly between the sparse points. Raising the count to 35 improved both smoothness and accuracy without taking extensive time for the program to solve, but did not change the overall result. For greater precision and a smoother response, future studies should employ a finer discretization, on the order of 100 points or more, to minimize interpolation distortions.

Moreover, conducting a parametric study across multiple Mathcad files proved time-consuming, ultimately resulting in around 130 separate calculation files for the project. During the process, numerous errors were uncovered and several faulty documents had to be corrected. Combining these sheets into fewer files would have been highly beneficial, but doing so would have demanded deeper Mathcad expertise and greater computational capacity. Such improvements could have saved a substantial amount of time, which could then have been devoted to exploring additional cross-sections and column types. Utilizing tools such as MATLAB or Python could have been advantageous. Future studies could apply this to examine how different cross-sectional shapes and a broader range of parameters influence stiffness.

5.6 FE-analysis

Initially, the FE analysis was conducted in the software ATENA instead of DIANA. The two programs are quite similar in functionality, but the force-displacement curve obtained from ATENA did not correspond the hand calculations in an expected way. The initial stiffness was incorrect, the cracking load was higher, and the curve intersected the hand calculations before settling on a much lower final capacity, an unexpected result. There were uncertainties regarding how ATENA performed its calculations and which input data that was actually used. For example, it was possible to define both bond-slip and embedded reinforcement simultaneously in the same model, which led to confusion and uncertainty about which option the software used in the analysis, since both cannot be utilized at the same time. ATENA also required more input data than DIANA and demanded knowledge of additional parameters. Due to these uncertainties, DIANA was used instead, as it has more features that are automatically linked to EC2, which made it more suitable for the purposes in this thesis.

Initial challenges arose in selecting the appropriate concrete strength within DIANA. Depending on the chosen model, the concrete strength had to be entered manually, adding complexity to the setup. After thorough testing, it was determined that mean values should be used when applying the EC2 model available directly in DIANA. However, this choice introduced its own difficulties. Substantial time was required to master the program's functionality and to grasp how different parameters affected the results. The interface and material-property management

were not always intuitive, and it was necessary to learn how minor input variations could significantly alter the analysis. This learning curve was essential to ensure that DIANA's outputs were reliable and consistent with expected behavior.

Since the hand calculation method was based on full interaction between concrete and reinforcement, the reinforcement was modeled as embedded. However, bond-slip was also tested, even though it is primarily intended for examining crack formation and propagation in reinforced concrete structures. The bond-slip model simulates the interaction between the reinforcing steel and the surrounding concrete, considering the non-linear behavior at the interface. This model is particularly useful for analyzing how cracks develop and propagate under loading conditions, as it accounts for the gradual loss of bond between the steel and concrete due to slip, leading to localized stresses. By incorporating bond-slip behavior, DIANA provides a more accurate representation of crack formation, allowing for a better understanding of how reinforcement and concrete interact under real-world conditions. This is essential for predicting failure mechanisms, particularly in structures subjected to complex loading or degradation over time. Further studies should explore how crack formation behaves under these conditions, as it was outside the scope of this thesis.

Creep has not been considered in the analysis conducted in DIANA, as there was no simplified way to include it that would have matched the way it was incorporated in the hand calculations. While it is possible to create a custom material curve with creep, this would require performing a verification with a time-dependent analysis in DIANA, which is time-consuming and outside the scope of this thesis. Additionally, assumptions about the time of loading and unloading would need to be made to carry out the analysis. The more factors that need to be assumed, the more challenging it becomes to interpret the results accurately. Further studies should be undertaken to examine how time-dependent effects influence stiffness in FE analysis.

The comparison between the hand-calculated and FE-derived force–deformation curves reveals several important observations. Both approaches exhibit the same initial stiffness, confirming that they are based on consistent material and geometric assumptions. However, the FE model predicts a noticeably higher cracking load. When cracking starts in the FE-model, the first crack appears approximately 20 cm above the bottom of the column, this means that the lever arm of the applied deformation becomes shorter, which could be a reason for the increased cracking load. In State II, when concrete undergoes cracking, tension stiffening provides additional capacity. In the hand calculations, however, its contribution is minimal because the section is predominantly in compression, and EC2 [2] prescribes tension stiffening mainly for bending-dominated members. This difference could help explain why DIANA predicts a higher capacity, the hand-calculated model may underestimate capacity when the section is mainly in compression. Once the response enters State III, the effect of tension stiffening disappears and the two curves converge. Also the integration schemes used can affect the result slightly, since the analysis in DIANA is performed over 300 steps in total, while the in-

tegration in the analytical solution is made with only 50, the outcomes can vary slightly. Most load increments converged rapidly, but the increment at first crack required 15 iterations, underscoring the numerical complexity of crack initiation. Overall, these results highlight the importance of advanced material modeling and crack-band calibration for achieving realistic predictions of structural response. The fact that the FE model predicts a slightly higher capacity is advantageous, as it confirms that the hand-calculated results remain conservative and provide a built-in safety margin.

5.7 Environmental aspects

In addition to structural performance, environmental considerations are increasingly important in bridge design. Optimizing stiffness through more accurate analyses, rather than conservatively over-reinforcing, directly reduces material consumption and embodied carbon. For example, adopting equivalent-stiffness methods can allow slimmer sections or lower reinforcement ratios while still meeting safety requirements, cutting concrete and steel volumes. This not only decreases CO_2 emissions associated with production and transport but also minimizes resource extraction and waste. Furthermore, refined stiffness estimates can extend service life by preventing premature cracking and degradation, reducing the need for repairs or replacement.Additionally, applying a reduced utilization ratio when refurbishing existing bridges permits the use of higher stiffness values in calculations than nominal values, thereby enabling more effective upgrades. Future work should therefore integrate life-cycle assessment tools with stiffness optimization workflows to quantify carbon savings and support greener design decisions.

6 Concluding remarks

In this thesis, a parametric study using non-linear analysis has been conducted to evaluate the stiffness of reinforced concrete columns. The aim has been to provide a more realistic depiction of their behavior compared to the linear assumptions in Eurocode 2, and to develope guidelines and recommendations for adjusting stiffness in calculation. This chapter includes the conclusions from this analysis as well as directions for future studies.

6.1 Conclusions

Three key perspectives emerged throughout the study. First, from a capacity control perspective, the use of equivalent stiffness calculated through non-linear analysis that accounts for cracking, reinforcement yielding, and concrete non-linearity, results in a more realistic representation of the true structural behavior. As observed in this thesis, detailed calculations of stiffness are considerably higher than the nominal stiffness provided by EC2, with equivalent stiffness being at least 44 % greater for all studied cross-sections. This aligns with the findings from hand calculations and non-linear FE analysis, which confirm that nominal stiffness underestimates actual behavior. The method of calculating nominal stiffness has been removed in EC2:2023, where both retained and new methods now yield higher stiffness values, reflecting an increased confidence in stiffness estimation by the Eurocode committee.

Second, regarding restraint forces, the results support a reduction of stiffness in global system models in order to avoid overestimation of restraint effects and excessive reinforcement. The analyses indicate that an assumed stiffness of approximately 85 % of the uncracked value is sufficiently conservative for most practical cases, in agreement with Norconsult's standard design practices. For isolated members, a further reduction down to approximately 45 % was found to be reasonable, which aligns closely with the global stiffness reduction introduced in EC2:2023. These insights validate the revised code's direction and provide practical recommendations for implementation in real projects.

Third, in the context of structural assessment, especially of slender existing members with low reinforcement content, this thesis has shown that stiffness increases significantly when realistic behavior is accounted for. In some cases, the stiffness can be increased up to three times higher than the nominal value, enabling a substantial increase in calculated buckling loads. This result emphasizes the potential for more accurate and cost-efficient evaluations of existing infrastructure, potentially avoiding unnecessary strengthening measures.

Previous Norconsult projects have employed both simplified and non-linear models for concrete compressive strength. As this thesis adopts the non-linear curve, a comparative analysis was conducted to evaluate differences between the two approaches. When integrated, the non-linear model produces only about a 2 % lower

capacity than the simplified model. Although using simplified curves for design and non-linear curves for stiffness analysis can introduce minor inconsistencies, this deviation is small and the simplified model remains a reasonable choice, and it is concluded that the stiffness-adjustment guidelines from this thesis can be applied regardless of the material model chosen.

In conclusion, this thesis demonstrates that adopting equivalent stiffness based on non-linear behavior provides a more realistic and efficient design and assessment method for reinforced concrete columns. The results have practical implications for both new design and reassessment of existing structures, and support a transition toward both structurally and environmentally optimized bridge engineering.

6.2 Future studies

Future studies should investigate other cross-sectional shapes, particularly circular cross-sections, as they are frequently used in bridge design. It would also be of interest of exploring a wider collection of parameters as well as increasing the number of parametric scenarios considered. The nominal curvature method should also be studied further. Since it has been retained, and updated, in the revised code, it would be valuable to investigate how the method compares to other stiffness approaches.

Research should also explore the inclusion of time-dependent effects such as creep and shrinkage in finite-element analyses, potentially via a parametric workflow, to more accurately predict long-term structural performance. Bond-slip models of concrete-reinforcement interaction should be used to study crack formation and propagation in concrete columns.

Finally, integrating life-cycle analysis with stiffness optimization would quantify carbon dioxide savings and support more sustainable bridge designs by evaluating the environmental impact of design configurations early in the design process.

References

[1] Boverket, Växthusgaser – miljöindikatorer, Accessed: April 16, 2025, 2022. [Online]. Available: https://www.boverket.se/sv/byggande/hallbart-byggande-och-forvaltning/miljoindikatorer---aktuell-status/vaxthusgaser/.

[2] "Eurocode 2: Design of concrete structures - part 1-1: General rules and rules for buildings," European Committee for Standardization (CEN), Brussels, Belgium, Tech. Rep. EN 1992-1-1:2005, 2004.

[3] European Concrete Platform ASBL, Eurocode 2 Commentary (rev A 31-03-2017), Jean-Pierre Jacobs, Ed. Brussels, Belgium: European Concrete Platform ASBL, 2008, Revised by J.F. Denoël (FEBELCEM) in 2017.

[4] J. Hellesland, N. Challamel, C. Casandjian, and C. Lanos, Reinforced Concrete Beams, Columns and Frames: Section and Slender Member Analysis. John Wiley & Sons, Incorporated, Mar. 2013, ISBN: 9781118619787.

[5] M. Al-Emrani, B. Engström, M. Johansson, and P. Johansson, Bärande konstruktioner, Part 2. Gothenburg, Sweden: Chalmers University of Technology, 2011, Department of Civil and Environmental Engineering, Division of Structural Engineering.

[6] B. Engström, "Design and analysis of continuous beams and columns," Gothenburg, Sweden, Tech. Rep., 2015.

[7] M. Al-Emrani, B. Engström, M. Johansson, and P. Johansson, "Bärande konstruktioner, part 1," Gothenburg, Sweden, Tech. Rep., 2013, Department of Civil and Environmental Engineering, Division of Structural Engineering.

[8] Norwegian Standard, Next generation eurocodes, Accessed: 2025-05-12, 2025. [Online]. Available: https://standard.no/en/sectors/eurokoder/next-generation-eurocodes-second-generation/.

[9] MPA The Concrete Centre, 2nd generation eurocode 2, [Accessed: 07-Feb-2025], 2024. [Online]. Available: https://www.concretecentre.com/Structural-design/Eurocode-2-concrete/2nd-generation-Eurocode-2.aspx.

[10] "Eurocode 2: Design of concrete structures – part 1-1: General rules and rules for buildings, bridges, and civil engineering structures," European Committee for Standardization (CEN), Brussels, Belgium, Tech. Rep. EN 1992-1-1:2023, 2023.

[11] B. Westerberg, "Time-dependent effects in the analysis and design of slender concrete compression members," Ph.D. dissertation, KTH, Division of Concrete Structures, Stockholm, Sweden, 2008.

[12] M. Kofler and A. Andreatta, Tragfähigkeit von Einzelstützen nach Eurocode 2 mit besonderem Bezug auf das Verfahren mit Nennsteifigkeiten. Ernst & Sohn Verlag, 2009, vol. 104, pp. 218–225. DOI: 10.1002/best.200900666.

[13] P. Luo, D. Shen, H. Mi, X. Kong, and J. Wang, "Stiffness reduction factor of reinforced concrete bridge pier considering characters of nonlinear," in *ICCTP 2009: Critical Issues in Transportation Systems Planning, Development, and Management*, ASCE, 2009, pp. 2482–2490.

[14] C. Zhang, Z. Yao, P. Luo, D. Shen, and J. Wang, "Flexural stiffness reduction factor of reinforced concrete bridge pier with circular section," in *ICCTP 2010: Integrated Transportation Systems — Green Intelligent Reliable*, ASCE, 2010, pp. 3410–3416.

[15] J. L. Bonet, M. L. Romero, and P. F. Miguel, "Effective flexural stiffness of slender reinforced concrete columns under axial forces and biaxial bending," *Engineering structures*, vol. 33, no. 3, pp. 881–893, 2011.

[16] A. Várdai and I. Bódi, "Reinforced concrete column design according to the nominal stiffness method," in *Proceedings of the 10th fib International PhD Symposium in Civil Engineering*, Budapest, Hungary: Budapest University of Technology and Economics, 2023.

[17] D. Gebauer, M. Stümpel, C. von der Haar, and S. Marx, "Criteria and influencing parameters for the design of piers of semi-integral bridges," *Structural Concrete*, vol. 19, no. 4, pp. 625–634, 2018. DOI: 10.1002/suco.201700087.

[18] D. Gebauer, M. Stümpel, C. von der Haar C, and S. Marx, "Design criteria for piers of semi-integral bridges: Investigations on normal force and reinforcement ratio," in *High Tech Concrete: Where Technology and Engineering Meet*, D. Hordijk and M. Luković, Eds., Cham: Springer International Publishing, 2018, pp. 1421–1428. DOI: 10.1007/978-3-319-59471-2_142.

[19] S. Das, I. Mansouri, S. Choudhury, A. H. Gandomi, and J. W. Hu, "A prediction model for the calculation of effective stiffness ratios of reinforced concrete columns," *Materials*, vol. 14, no. 7, p. 1792, 2021. DOI: 10.3390/ma14071792.

[20] DIANA FEA BV, Finite element analysis software, Accessed: April 2, 2025, 2025. [Online]. Available: https://dianafea.com.

[21] FIB - Fédération Internationale du Béton / International Federation for Structural Concrete, FIB Model Code for Concrete Structures 2010, First. Berlin: Ernst & Sohn GmbH & Co. KG, 2013, © 2013 FIB – Fédération Internationale du Béton / International Federation for Structural Concrete.

[22] Comité Euro-International du Béton, Recommendations based on research and best current practice. Trowbridge, Wiltshire: Redwood Books, 1993, Typeset in Great Britain by Alden Multimedia. Printed in Great Britain by Redwood Books., ISBN: 0-7277-1696-4.

[23] M. Plos, M. Johansson, K. Zandi, and J. Shu, "Recommendations for assessment of reinforced concrete slabs: Enhanced structural analysis with the finite element method," Chalmers University of Technology, Department of Architecture and Civil Engineering, Division of Structural Engineering, Concrete Structures, Gothenburg, Sweden, Tech. Rep. Report ACE 2021:3, 2021. [Online]. Available: `https://www.chalmers.se`.

A Appendix: General calculations

General calculation method

Innehållsförteckning

1 INDATA

1.1 Geometri

Höjd balk $h := 1000 \cdot mm$ (knäckning kring styv axel)

Bredd liv $b := 1000 \cdot mm$

Yttre linje av tvärsnitt för plottning $p_{yz} := \begin{bmatrix} 0 & b & b & 0 & 0 \\ 0 & 0 & h & h & 0 \end{bmatrix}^T$

1.2 Geometri armering

Vald armerings diameter $\phi := 25$

Indata för armering ges i matriser. Denna del döljs.

Koordinater för armering

$$A_{s.kord} := \begin{bmatrix} 125 & 250 & 375 & 500 & 625 & 750 & 875 & 125 & 250 & 375 & 500 & 625 & 750 & 875 \\ 125 & 125 & 125 & 125 & 125 & 125 & 125 & 875 & 875 & 875 & 875 & 875 & 875 & 875 \end{bmatrix} \cdot mm$$

$$A_{s.kord} := stack\left(\left(\left(A_{s.kord}^{\ T}\right)^{\langle 0 \rangle}\right)^T, \left(\left(A_{s.kord}^{\ T}\right)^{\langle 1 \rangle}\right)^T\right) = \begin{bmatrix} 0.13 & 0.25 & 0.38 & \\ 0.13 & 0.13 & 0.13 & \dots \end{bmatrix} m$$

Diametrar för armeringsjärn

$$\phi_{s.i} := [\phi \ \phi \ \phi \ \phi \ \phi \ \phi \ \phi \ \phi \ \phi \ \phi \ \phi \ \phi \ \phi \ \phi] \cdot mm$$

Area för enskilda armeringsstänger $A_{s.i} := \frac{\overrightarrow{\phi_{s.i}^{\ 2}} \cdot \pi}{4}$

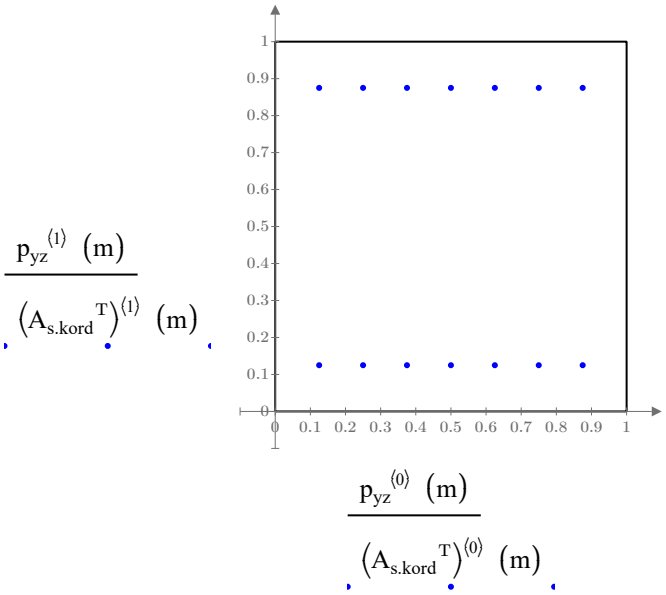

$$A_{s.kord}^{\ T} = \begin{bmatrix} 125 & 125 \\ 250 & 125 \\ 375 & 125 \\ 500 & 125 \\ 625 & 125 \\ 750 & 125 \\ 875 & 125 \\ 125 & 875 \\ 250 & 875 \\ 375 & 875 \\ 500 & 875 \\ 625 & 875 \\ 750 & 875 \\ 875 & 875 \end{bmatrix} mm \qquad \phi_{s.i}^{\ T} = \begin{bmatrix} 25 \\ 25 \\ 25 \\ 25 \\ 25 \\ 25 \\ 25 \\ 25 \\ 25 \\ 25 \\ 25 \\ 25 \\ 25 \\ 25 \end{bmatrix} mm$$

1.3 Laster

Beräkningarna i detta ark utförs baserat på en verkande normalkraft. Denna anges positiv i tryck.

Dimensionerande normalkraft $N_{Ed} := 6 \cdot MN$

1.4 Långtidseffekter

Kryptal $\phi_c := 2$

Andel långtidslast $andel := 50\%$

Effektivt kryptal $\phi_{ef} := \phi_c \cdot andel = 1.00$

1.5 Material Betong

Elasticitetsmodul $E_{cm} := 36 \cdot GPa$

Partialkoefficient för betongens elasticitetsmodul $\gamma_{cE} := 1.2$ för design 1.2

Karakteristisk tryckhållfasthet $f_{ck} := 45 \cdot MPa$

Medeldraghållfasthet $f_{ctm} := 0.30 \cdot \left(\frac{f_{ck}}{MPa}\right)^{\frac{2}{3}} \cdot MPa = 3.8\ MPa$

Karakteristisk draghållfasthet $f_{ctk} := 0.7 \cdot f_{ctm} = 2.66\ MPa$

Medeltryckhållfasthet $f_{cm} := f_{ck} + 8 \cdot MPa$

Partialfaktor hållfasthet $\gamma_c := 1.5$ för design 1.5

Partialfaktor hållfasthet $\alpha_c := 1.0$

För betong av klass C12/15 till C50/60 anger EC2 följande materialparametrar för att beräkna töjning-spänningsambandet i betongen. Om högre betongklass är aktuell så måste värdena nedan justeras.

Brottstukning $\varepsilon_{cu} := 3.5 \cdot 10^{-3} \left(1 + \phi_{ef}\right) = 0.01$

Koefficient som används i formel för arbetskurva $n. := 2$

Töjningsvärde nyttjat i arbteskurva enligt 3.1.5.
Ska ej moddas för krypnig $\varepsilon_{c1} := 0.7 \cdot \left(\frac{f_{cm}}{MPa}\right)^{0.31} \cdot 10^{-3} = 0$

1.6 Armering

Elasticitetsmodul $E_s := 200 \cdot GPa$

Karakteristisk flytgräns längsgående armering $f_{yk} := 500 \cdot MPa$

Partialfaktor $\gamma_s := 1.15$ för design 1.15

1.7 Betong mellan sprickor

Interpolation mellan osprucken och sprucken krökning utförs enligt EN1992-1-1 avsnitt 7.4.3. Denna interpolation beror av följande koefficient som sätts till 0.5 vid långtidslast och 1.0 vid korttidslast.

Koefficient för lastens varaktighet $\beta := 0.5$

2 GENERELLA BERÄKNINGAR

Alla generella beräkningar är dolda.

2.1 Dim. materialegenskaper

Dimensionerande materialegenskaper beräknas enligt EN1992-1-1.

Dimensionerande tryckhållfasthet betong $f_{cd} := \frac{\alpha_c \cdot f_{ck}}{\gamma_c} = 30\ \text{MPa}$

Dimensionerande draghållfasthet betong $f_{ctd} := \frac{\alpha_c \cdot f_{ctk}}{\gamma_c} = 1.77\ \text{MPa}$

Dimensionerande flytgräns armering $f_{yd} := \frac{f_{yk}}{\gamma_s} = 434.78\ \text{MPa}$

Elasticitetsmodul betong $E_{cd} := \frac{E_{cm}}{\gamma_{cE}} = 30\ \text{GPa}$

2.2 Tvärsnittsegenskaper

Tröghetsmoment för betongtvärsnittet $I_c := \frac{b \cdot h^3}{12} = 0.08\ \text{m}^4$

Betongens area $A_c := b \cdot h = 1\ \text{m}^2$

Tröghetsradie för betongtvärsnittet $i_c := \sqrt{\frac{I_c}{A_c}} = 0.29\ \text{m}$

Tröghetsmoment armering

$$j := 0 .. \text{length}\left(A_{s.i}{}^{T}\right) - 1$$

$$I_s := \sum_j \left(\left(A_{s.i}{}^{T}\right)_j \cdot \left(A_{s.kord_{1,j}} - \frac{h}{2} \right)^2 \right) = 0\ \text{m}^4$$

Armeringens area $A_s := \sum A_{s.i} = 6872.23\ \text{mm}^2$

Tröghetsradie för armering $i_{s.y} := \sqrt{\frac{I_s}{A_s}} = 0.38\ \text{m}$

3 MOMENTKAPACITET (M-N KURVA) KRING STYV AXEL

3.1 Funktion för materialkurva

Betongens arbetskurva som funktion av töjning enligt SS-EN 1992-1-1:2005, avsnitt 3.1.5.

$$k_c := \frac{1.05 \cdot E_{cd} \cdot |\varepsilon_{c1}|}{f_{cd}} = 2.52$$

$$\eta(\varepsilon) := \frac{\varepsilon}{\varepsilon_{c1} \cdot (1 + \phi_{ef})}$$

$$\sigma_{cd.315}(\varepsilon) := \left\| \begin{array}{l} 0 \cdot MPa \\ \text{if } \varepsilon < 0 \\ \quad \left\| \left(\frac{k_c \cdot \eta(-\varepsilon) - \eta(-\varepsilon)^2}{1 + (k_c - 2) \cdot \eta(-\varepsilon)} \cdot -f_{cd} \right) \right\| \end{array} \right\|$$

Parameter för plottning

$$\varepsilon_{plot} := 0, \frac{\varepsilon_{cu}}{45} .. \varepsilon_{cu}$$

3.2 Materialkurva

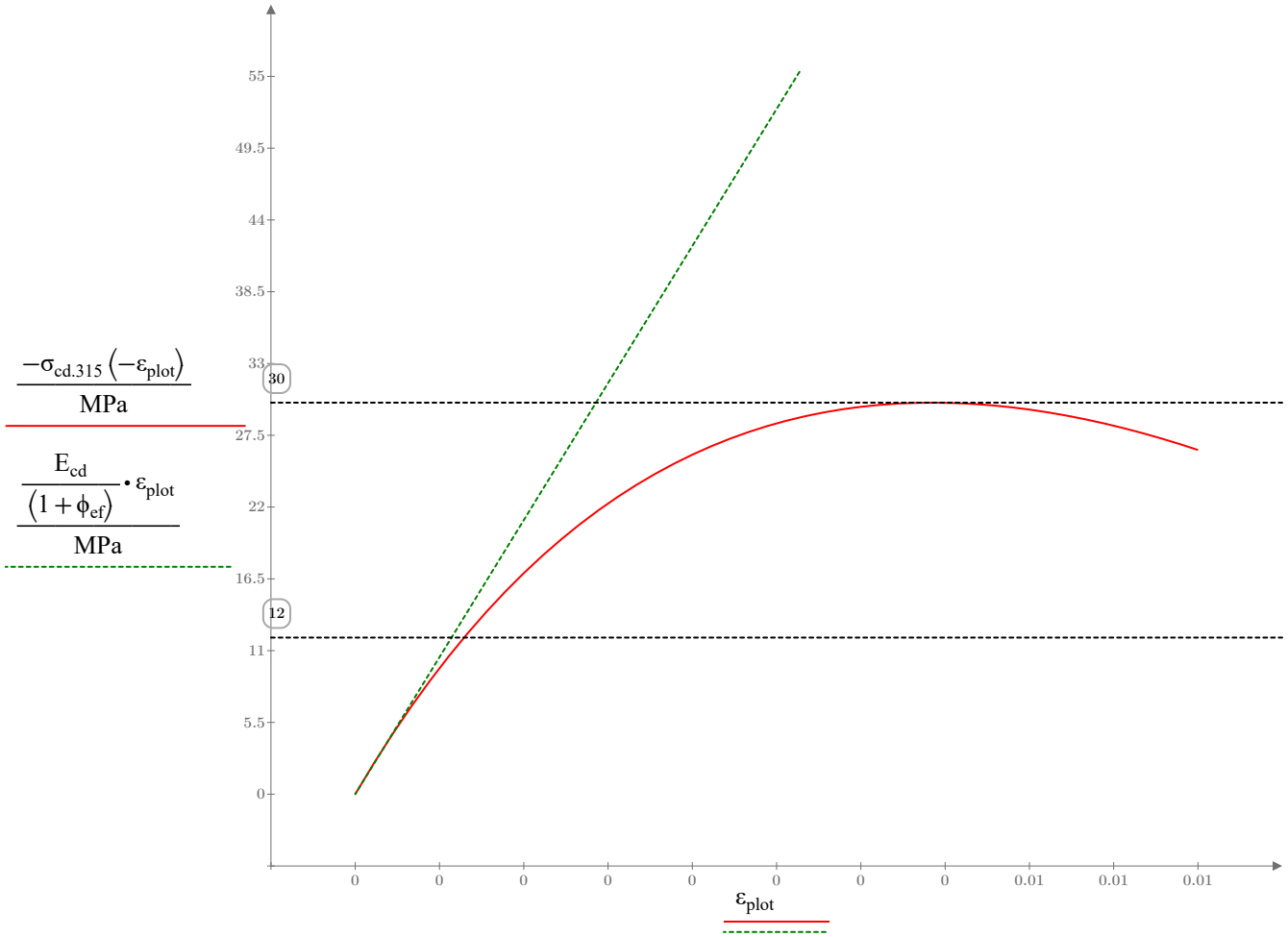

3.3 Vald materialkurva

Arbetskurva för bärverksanalys (3.1.5).

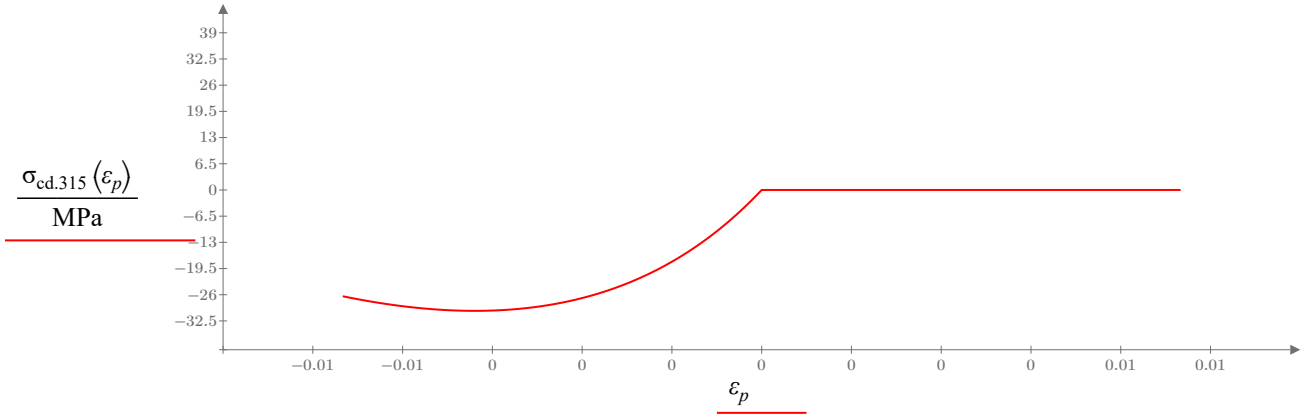

Armeringens arbetskurva som funktion av töjning

$$\sigma_s(\varepsilon) := \left\| \begin{array}{l} \text{if } \varepsilon \geq 0 \\ \quad \left\| \min\left(E_s \cdot \varepsilon, f_{yd}\right) \right. \\ \text{else} \\ \quad \left\| \max\left(E_s \cdot \varepsilon, -f_{yd}\right) \right. \end{array} \right.$$

Töjning i stålet vid plasticering

$$\varepsilon_{yd} := \frac{f_{yd}}{E_s} = 0$$

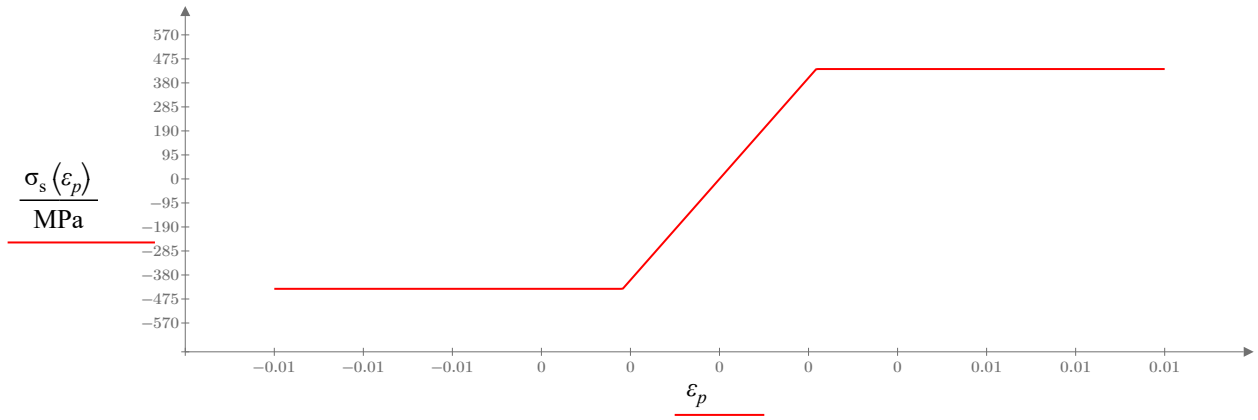

3.4 Beräkning av M-N kurvor

M-N kurvor skapas genom att stegvis ange töjning i ytterkanter och för varje spänningsfördelning integrera vilken normalkraft och moment som verkar på tvärsnittet tillsammans. Beräkningarna är dolda.

Bredd av betong som funktion av x

$$b_c(x) := b$$

Töjning i tvärsnittet som funktion av x och töjning i ytterkanter

$$\varepsilon(x, \varepsilon_1, \varepsilon_2) := \varepsilon_1 + (\varepsilon_2 - \varepsilon_1) \cdot \frac{x}{h}$$

Funktion för M-N kurva för hela samverkanstvärsnittet.

Variabel

$$j := 0 .. \text{length}\left(\left(A_{s.kord}{}^{T}\right)^{\langle 0 \rangle}\right) - 1$$

Koordinat för enskilda armeringsjärn mht tryckt kant

$$x_{s.i_j} := h - A_{s.kord_{1,j}}$$

Normalkraft som funktion av töjning i ytterkanter

$$N_{Rd.315}(\varepsilon_1, \varepsilon_2) := -\left(\int_0^h b_c(x) \cdot \sigma_{cd.315}(\varepsilon(x, \varepsilon_1, \varepsilon_2))\, dx + \sum_j \left(\left(A_{s.i}{}^{T}\right)_j \cdot \sigma_s\left(\varepsilon\left(x_{s.i_j}, \varepsilon_1, \varepsilon_2\right)\right)\right)\right)$$

Momentkapacitet som funktion av töjning i ytterkanter

$$M_{Rd.315}(\varepsilon_1, \varepsilon_2) := \int_0^h x \cdot b_c(x) \cdot \sigma_{cd.315}(\varepsilon(x, \varepsilon_1, \varepsilon_2))\, dx + \sum_j \left(x_{s.i_j} \cdot \left(A_{s.i}{}^{T}\right)_j \cdot \sigma_s\left(\varepsilon\left(x_{s.i_j}, \varepsilon_1, \varepsilon_2\right)\right)\right) \hookleftarrow$$
$$+ N_{Rd.315}(\varepsilon_1, \varepsilon_2) \cdot \frac{h}{2}$$

3.5 M-N kurvor

Plastisk M-N kurva skapas genom att anta töjningar vid kanter. Vid plastisk kurva ansätts betongens brottöjning vid ena kanten och töjning på andra sidan itereras från betongens brottöjning till en hög dragtöjning. Beräkningarna är dolda.

Töjning i första ytterkant vid plastisk respons

$$\varepsilon_1 := -\varepsilon_{cu} = -0.01$$

Töjning i andra ytterkant vid plastisk respons

$$\varepsilon_2 := -\varepsilon_{cu}, -\varepsilon_{cu} + \frac{\varepsilon_{cu}}{10} .. 10 \cdot \varepsilon_{cu}$$

Envelop för momentkapacitet som funktion av verkande normalkraft

$$tol := 0.0000001 \cdot kN$$

$$N_{Rd} := \left\| \begin{array}{l} \text{for } i \in 0 .. 100 \\ \quad \left\| \begin{array}{l} \varepsilon_1 \leftarrow -\varepsilon_{cu} \\ \varepsilon_2 \leftarrow -\varepsilon_{cu} \cdot \left(1 - \frac{i}{10}\right) 0.53 \\ N_i \leftarrow N_{Rd.315}(\varepsilon_1, \varepsilon_2) - tol \cdot i \end{array} \right. \\ N \end{array} \right.$$

$$M_{Rd} := \left\| \begin{array}{l} \text{for } i \in 0 .. 100 \\ \quad \left\| \begin{array}{l} \varepsilon_1 \leftarrow -\varepsilon_{cu} \\ \varepsilon_2 \leftarrow -\varepsilon_{cu} \cdot \left(1 - \frac{i}{10}\right) 0.53 \\ M_i \leftarrow M_{Rd.315}(\varepsilon_1, \varepsilon_2) \end{array} \right. \\ M \end{array} \right.$$

$M_{Rd.ULS}(N) := \text{linterp}(-N_{Rd}, M_{Rd}, -N)$ $M_{Rd.ULS}(N_{Ed}) = 3478.98\ kN \cdot m$

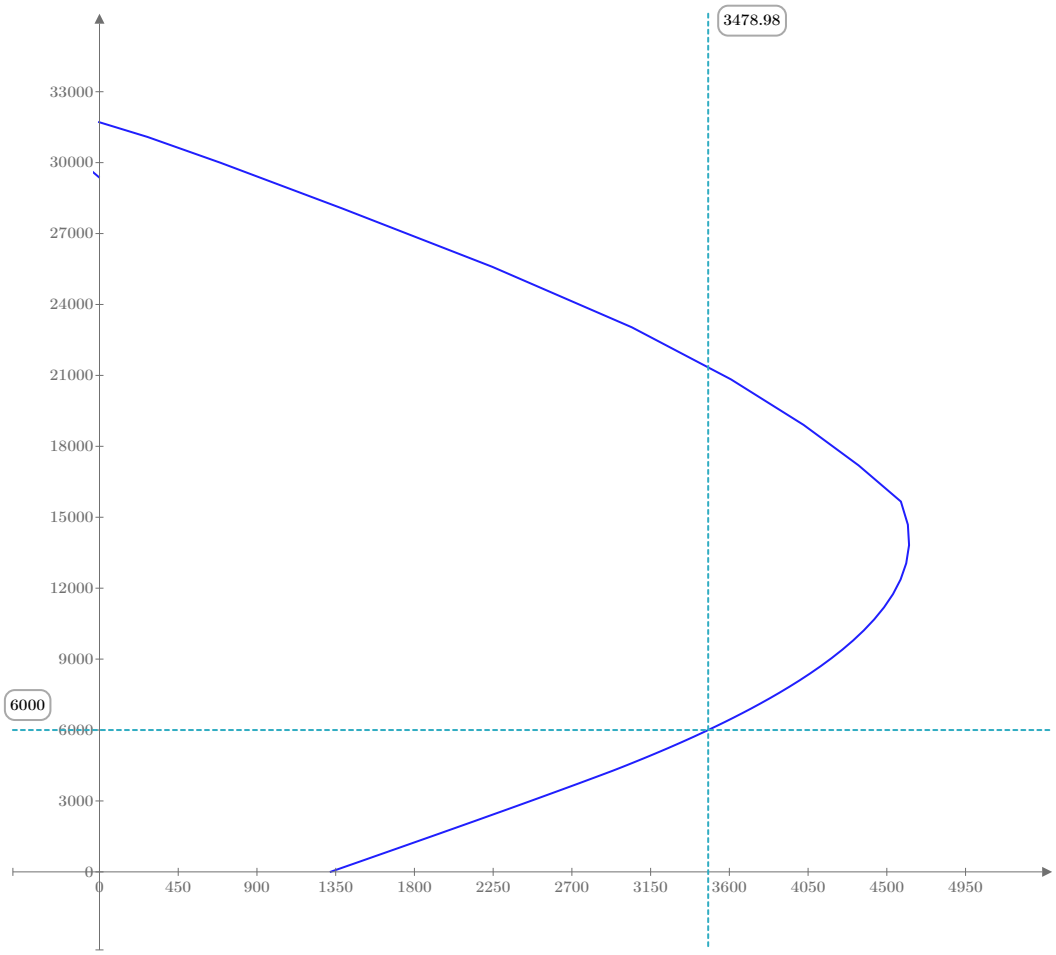

$\frac{N_{Rd.315}(\varepsilon_1, \varepsilon_2)}{kN}$

$\frac{M_{Rd.315}(\varepsilon_1, \varepsilon_2)}{kN \cdot m}$

3.6 Beräkning av exakt respons i ULS

Det är av intresse att beräkna den exakta töjningsresponsen för varje uppsättning av normalkraft och moment. Detta utförs genom följande solve block. Beräkningarna är dolda.

Solve block för lösning av töjning i ytterkanter för given NEd och MEd

$k_{avdrag} := M_{Rd.ULS}(N_{Ed}) \cdot 0.08 = 278.32\ kN \cdot m$

$M_{ex} := M_{Rd.ULS}(N_{Ed}) - k_{avdrag} = 3200.66\ kN \cdot m$

$\varepsilon_1 := -2 \cdot 10^{-3}$

$\varepsilon_2 := 2 \cdot 10^{-3}$

Given

$N_{Rd.315}(\varepsilon_1, \varepsilon_2) = N_d$

$M_{Rd.315}(\varepsilon_1, \varepsilon_2) = M_d$

Solver

$solve_\varepsilon(N_d, M_d) := \mathbf{Find}(\varepsilon_1, \varepsilon_2)$

Exempel med delvis plasticering (snittkrafter väljs mellan elastisk och full plastisk kurva)

$\varepsilon_{ex} := solve_\varepsilon(N_{Ed}, M_{ex}) = \begin{bmatrix} 0 \\ 0 \end{bmatrix}$

$x_{plot} := 0, \frac{h}{100} .. h$

Spänningsfördelningar

$\frac{\sigma_{cd.315}(\varepsilon(x_{plot}, \varepsilon_{ex_0}, \varepsilon_{ex_1}))}{MPa}$

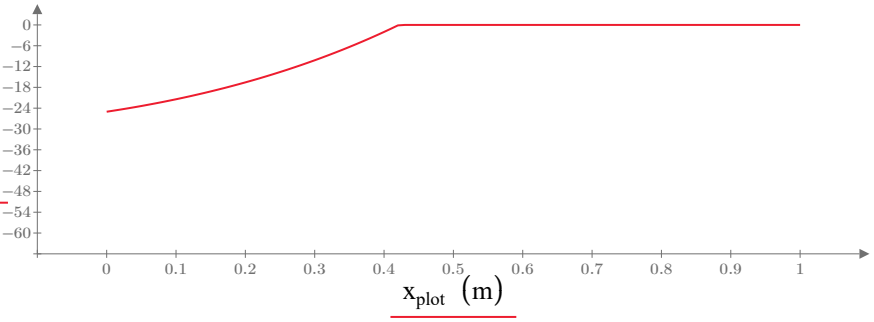

Moment för utvärdering av böjstyvhet beräknas utifrån maximalt tillåtet moment vid angiven dimensionerande normalkraft.

Momentkapacitet för definierad normalkraft $M_{Ed} := M_{Rd.ULS}(N_{Ed}) = 3478.98\ kN \cdot m$

Antal punkter för beräkning av kurva $n := 35$

$i := 0 .. (n - 1)$

Avrundade värden på moment anges nedan. Högsta värdet sänkas för att undvika konvergensproblem. Lägsta värdet justeras från 0 för att erhålla bättre grafiskt resultat.

Vektor med analyserade moment

$$M_{Ed.i_i} := \text{floor}\left(\frac{\left(M_{Ed} - k_{avdrag}\right) \cdot \frac{i}{n-1}}{kN \cdot m}\right) \cdot kN \cdot m$$

$$M_{Ed.i_0} := 1 \cdot kN \cdot m$$

Vektor med normalkraft

$$N_{Ed.i_i} := N_{Ed}$$

Funktion för beräkning av töjningar i ytterkanter baserat på vektor med N och M

$$\varepsilon_v\left(N_d, M_d, n\right) := \left\| \begin{array}{l} \varepsilon_{ULS_{n-1,1}} \leftarrow 0 \\ \text{for } i \in 0..n-1 \\ \quad \left\| \begin{array}{l} \varepsilon_i \leftarrow \text{solve}_\varepsilon\left(N_{d_i}, M_{d_i}\right) \\ \varepsilon_{ULS_{i,0}} \leftarrow \varepsilon_{i_0} \\ \varepsilon_{ULS_{i,1}} \leftarrow \varepsilon_{i_1} \end{array} \right. \\ \varepsilon_{ULS} \end{array} \right.$$

Töjningar i ytterkant av tvärsnittet i ULS

$$\varepsilon_{ULS} := \varepsilon_v\left(N_{Ed.i}, M_{Ed.i}, n\right)$$

Töjning vid respektive kant i kontrollsnitt

$$\varepsilon_{1.1} := \varepsilon_{ULS}^{\langle 0 \rangle} \qquad \varepsilon_{1.2} := \varepsilon_{ULS}^{\langle 1 \rangle}$$

Kurvatur

$$\kappa_{II} := -\frac{\varepsilon_{1.1} - \varepsilon_{1.2}}{h}$$

Beräkning av spänning i armering

$$\varepsilon_{s.ULS_{i,j}} := \varepsilon\left(x_{s.i_j}, \varepsilon_{1.1_i}, \varepsilon_{1.2_i}\right)$$

$$\sigma_{s.ULS_{i,j}} := \sigma_s\left(\varepsilon\left(x_{s.i_j}, \varepsilon_{1.1_i}, \varepsilon_{1.2_i}\right)\right)$$

$$\sigma_{s.max_i} := \max\left(\left(\sigma_{s.ULS}{}^{T}\right)^{\langle i \rangle}\right)$$

$$\varepsilon_{s.max_i} := \max\left(\left(\varepsilon_{s.ULS}{}^{T}\right)^{\langle i \rangle}\right)$$

3.7 Moment-krökningsdiagram

Nedan visas en sammanställning av resultat.

$$\frac{\varepsilon_{1.1}}{10^{-3}} = \begin{bmatrix} -0.37 \\ \vdots \end{bmatrix} \quad \frac{\varepsilon_{1.2}}{10^{-3}} = \begin{bmatrix} -0.37 \\ \vdots \end{bmatrix} \quad \frac{\kappa_{II}}{10^{-3}} = \begin{bmatrix} 0.00 \\ \vdots \end{bmatrix} \frac{1}{m} \quad \sigma_{s.max} = \begin{bmatrix} -74.73 \\ \vdots \end{bmatrix} MPa \quad \frac{\varepsilon_{s.max}}{10^{-3}} = \begin{bmatrix} -0.37 \\ \vdots \end{bmatrix}$$

Spänningsbegränsning för SLS (sprickviddsbegränsning)

$$\sigma_w := 150\ MPa$$

Justering av linterp

$$\sigma_{s.max32} := \sigma_{s.max_{32}} + 0.0000001\ MPa$$

$$\sigma_{s.max_{33}} := \sigma_{s.max_{33}} + 0.000001\ MPa$$

$$\sigma_{s.max_{34}} := \sigma_{s.max_{34}} + 0.00001\ MPa$$

Funktion för kurvatur beroende på stålspänning

$$\kappa_{s.w}(\sigma) := linterp(\sigma_{s.max}, \kappa_{II}, \sigma)$$

Max krökning i SLS

$$\kappa_{SLS} := \kappa_{s.w}(\sigma_w)$$

Funktion för moment

$$M_{Rd.\kappa}(\kappa) := linterp(\kappa_{II}, M_{Ed.i}, \kappa)$$

Max moment SLS

$$M_{Rd.SLS} := M_{Rd.\kappa}(\kappa_{SLS}) = 2187.38\ kN \cdot m$$

Krökning vid yield

$$\kappa_y := \kappa_{s.w}(f_{yd} - 2\ MPa) = 0.01\ \frac{1}{m}$$

Moment vid yield

$$M_{Rd.y} := M_{Rd.\kappa}(\kappa_y) = 3175.8\ kN \cdot m$$

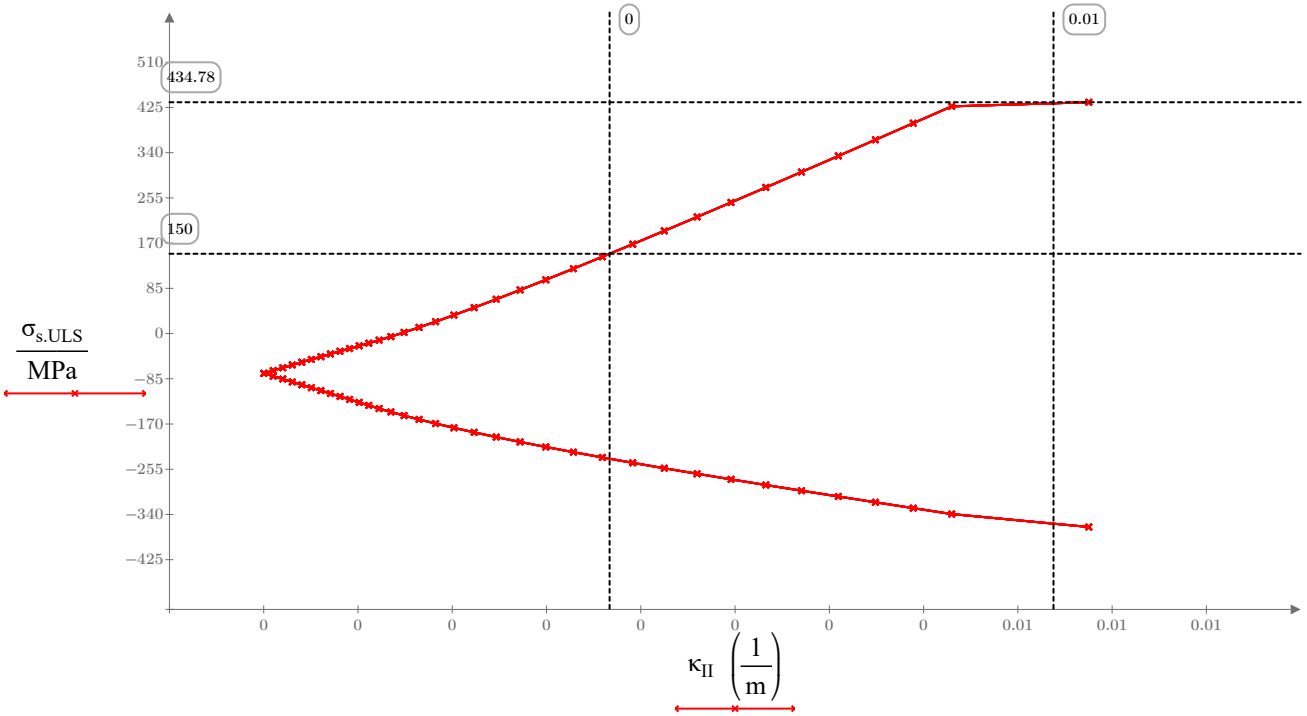

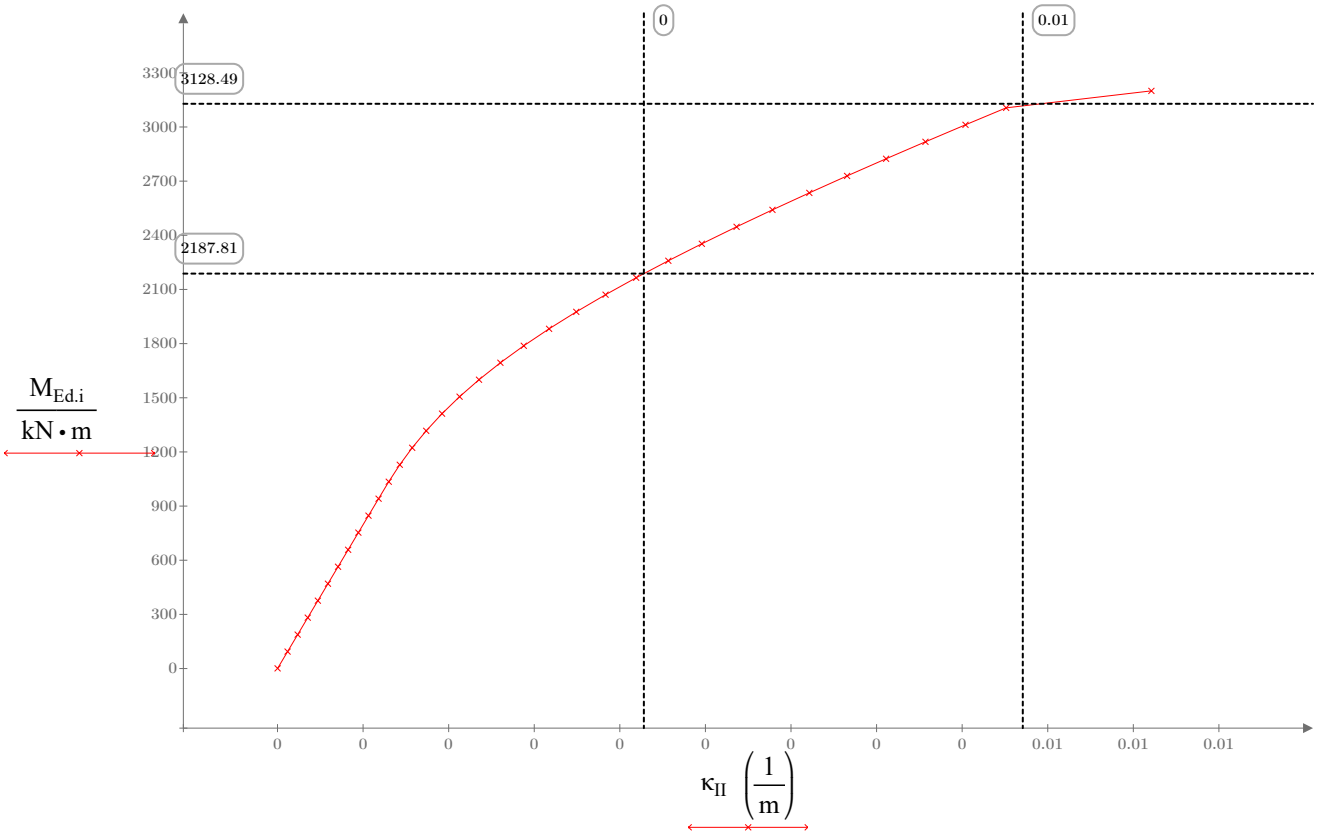

3.8 Inverkan av betong mellan sprickor

Beräkning enligt metodiken som beskrivs i SS-EN 1992-1-1, avsnitt 7.4.3. Uppstyvning tillåts i enlighet med avsnitt 5.8.6 (5). Beräkningarna är dolda.

Tröghetsmoment för stadie I inklusive armering

$$I_I := I_c + I_s \cdot \left(\frac{E_s}{\frac{E_{cd}}{(1+\phi_{ef})}} - 1 \right) = 0.1 \ m^4$$

Sprickmoment

$$M_{cr} := \left(f_{ctd} + \frac{N_{Ed}}{A_c + A_s \cdot \left(\frac{E_s}{\frac{E_{cd}}{(1+\phi_{ef})}} - 1 \right)} \right) \cdot \frac{I_I}{\left(\frac{h}{2}\right)}$$

Töjning i ytterkanter vid sprickmoment

$$\varepsilon_{cr} := \text{solve}_{\varepsilon}\left(N_{Ed}, M_{cr}\right) = \begin{bmatrix} 0 \\ \vdots \end{bmatrix}$$

Spänning i armering vid sprickmoment

$$\sigma_{cr_j} := \sigma_s\left(\varepsilon\left(x_{s.i_j}, \varepsilon_{cr_0}, \varepsilon_{cr_1}\right)\right)$$

Maximal spänning i armering vid sprickmoment

$$\sigma_{cr.max} := \max\left(\sigma_{cr}\right) = 9.42\ \text{MPa}$$

Kvot mellan sprickspänning och verkande spänning

$$k_\sigma := \frac{\sigma_{cr.max}}{\sigma_{s.max}}$$

Osprucken krökning

$$\kappa_I := \frac{M_{Ed.i}}{\frac{E_{cd}}{\left(1+\phi_{ef}\right)} \cdot I_I}$$

Fördelningskoefficient

$$\zeta_i := \begin{cases} \text{if } M_{Ed.i_i} < M_{cr} \\ \quad 0 \\ \text{else} \\ \quad \left(1-\beta\cdot\left(k_{\sigma_i}\right)^2\right) \end{cases}$$

Krökning inklusive uppstyvning från betong mellan sprickor

$$\kappa_{tot_i} := \zeta_i \cdot \kappa_{II_i} + \left(1-\zeta_i\right)\cdot \kappa_{I_i}$$

$$k_\sigma = \begin{bmatrix} -0.13 \\ \vdots \end{bmatrix} \quad \zeta = \begin{bmatrix} 0 \\ \vdots \end{bmatrix} \quad \frac{\kappa_I}{10^{-3}} = \begin{bmatrix} 0.00 \\ \vdots \end{bmatrix} \frac{1}{m} \quad \frac{\kappa_{II}}{10^{-3}} = \begin{bmatrix} 0.00 \\ \vdots \end{bmatrix} \frac{1}{m} \quad \frac{\kappa_{tot}}{10^{-3}} = \begin{bmatrix} 0.00 \\ \vdots \end{bmatrix} \frac{1}{m}$$

3.9 Moment-krökningsdiagram med inverkan från betong mellan sprickor

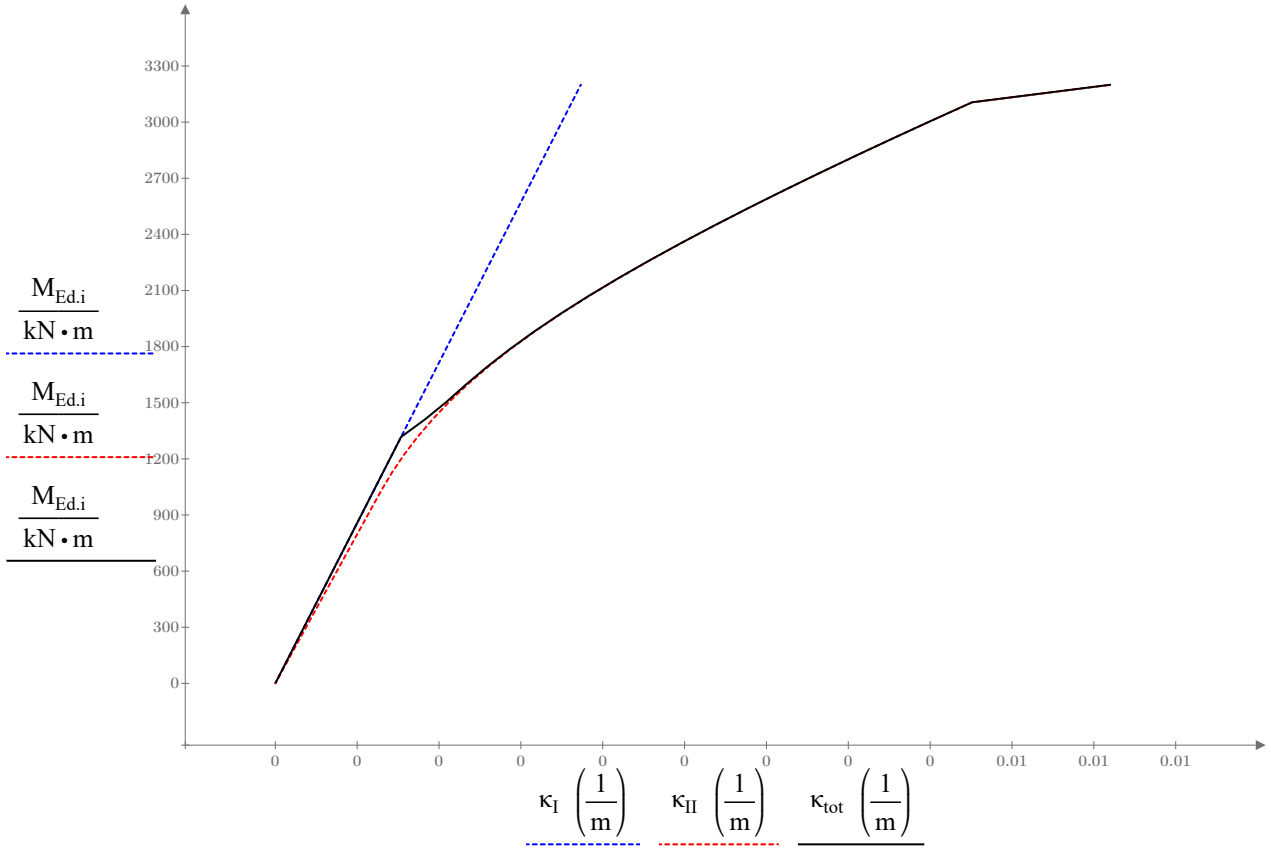

4 Deformation

4.1 Deformation elementarfall

Längd pelare

$l_0 := 10\ m$

Ansatt horisontalkraft

$H_0 := 300\ kN$

Funktion för momentvariation längs pelare

$M(x) := H_0 \cdot (l_0 - x)$

Test med elementarfall

$$\delta_{elem} := -\frac{H_0 \cdot {l_0}^3}{3 \cdot E_{cd} \cdot I_I} = -34.99\ mm$$

4.2 Faktisk deformation

Kurvatur som funktion av moment

$\kappa_f(M) := \text{linterp}(M_{Ed.i}, \kappa_{tot}, M)$

Deformation av konsol

$$\delta(x) := -\int_0^x \int_0^x \kappa_f(M(x))\, dx\, dx$$

$x_{plot} := 0\ m, 0.5\ m .. 10\ m$

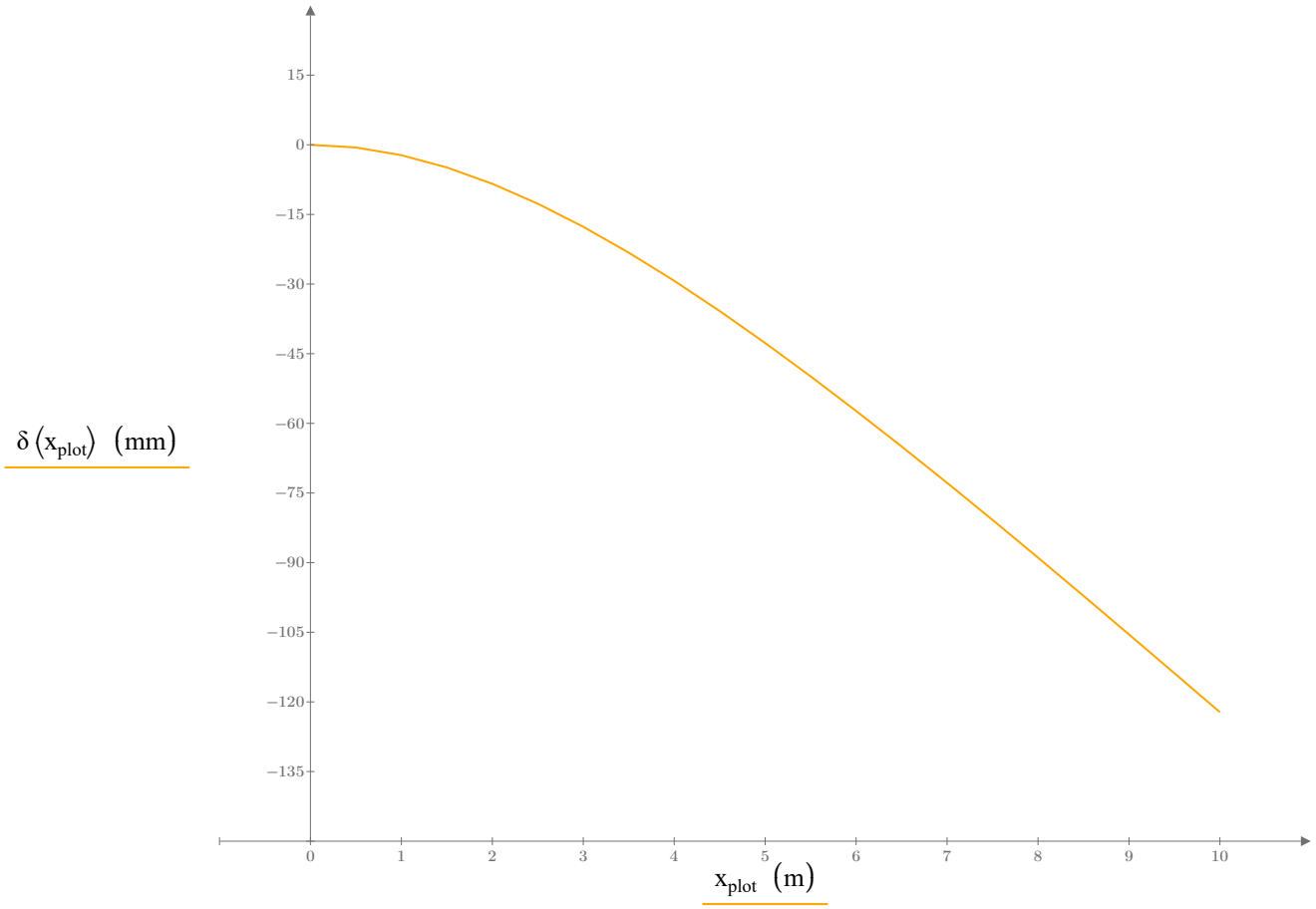

4.3 Kraft-deformationskurva konsolpelare

Max tillåten horisontalkraft

$$H_{Ed} := \frac{M_{Ed}}{l_0} = 347.9\ \text{kN}$$

$$n_\delta := 50$$

$$i_\delta := 0, 1 .. n_\delta$$

Vektor med stigande horisontalkraft

$$H_{v_{i_\delta}} := H_{Ed} \cdot \frac{i_\delta}{n_\delta}$$

Moment som funktion av horisontalkraft och position längs pelaren

$$M(H, x) := H \cdot (l_0 - x)$$

Deformation av pelare beroende på horisontalkraft och position längs pelaren

$$\delta_{max}(H, x) := -\int_0^x \int_0^x \kappa_f(M(H, x))\, dx\, dx$$

Deformation för stigande värden på horisontalkraft

$$\delta_{max_{i_\delta}} := \delta_{max}\left(H_{v_{i_\delta}}, l_0\right)$$

Maxdeformation

$$\delta_{max}(50) = -176.81\ \text{mm}$$

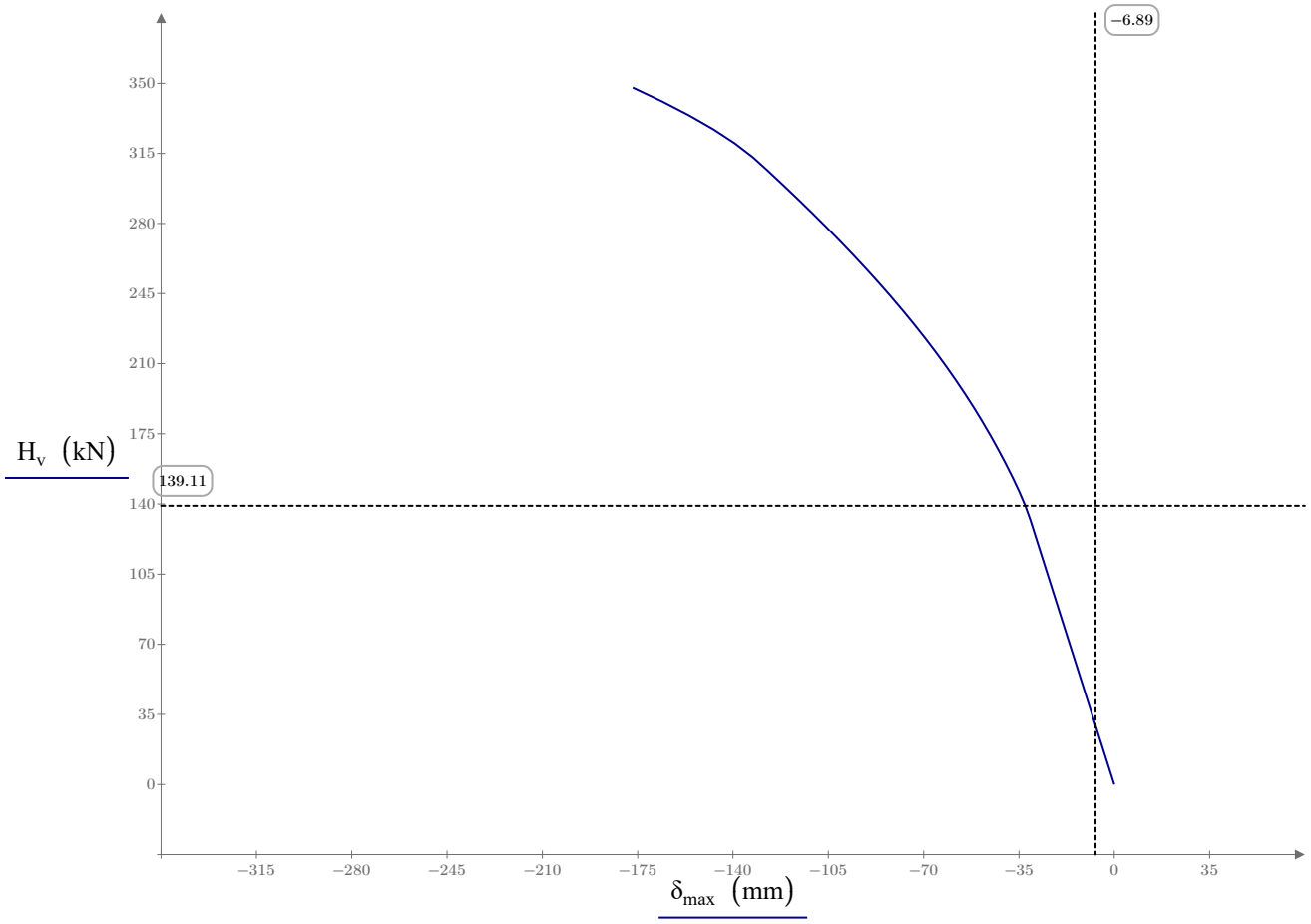

5 Tvångskrafter

5.1 Konsolpelare

Moment som funktion av horisontalkraft och position längs pelaren

$$M(H, x) := H \cdot (l_0 - x)$$

Utnyttjandegrad av maxmoment

$$UR := 0.95$$

Deformation av pelare beroende på horisontalkraft och position längs pelaren

$$\delta_1(H, x) := -\int_0^x \int_0^x \kappa_f(M(H, x))\, dx\, dx$$

5.1.1 ULS konsolpelare

Max tillåten horisontalkraft

$$H_{Ed.ULS} := \frac{M_{Ed} \cdot UR}{l_0} = 330.5 \text{ kN}$$

Vektor med stigande horisontalkraft

$$H_{v.ULS_{i_\delta}} := H_{Ed.ULS} \cdot \frac{i_\delta}{n_\delta}$$

Deformation för stigande värden på horisontalkraft

$$\delta_{max.ULS_{i_\delta}} := \delta_1\left(H_{v.ULS_{i_\delta}}, l_0\right)$$

Maxdeformation

$$\delta_{max.ULS}(50) = -151.55 \text{ mm}$$

5.1.2 SLS konsolpelare

Max tillåten horisontalkraft

$$H_{Ed.SLS} := \frac{M_{Rd.SLS}}{l_0} = 218.74 \text{ kN}$$

Vektor med stigande horisontalkraft

$$H_{v.SLS_{i_\delta}} := H_{Ed.SLS} \cdot \frac{i_\delta}{n_\delta}$$

Deformation för stigande värden på horisontalkraft

$$\delta_{max.SLS_{i_\delta}} := \delta_1\left(H_{v.SLS_{i_\delta}}, l_0\right)$$

Maxdeformation

$$\delta_{max.SLS}(50) = -67.22 \text{ mm}$$

5.2 Fast inspänd pelare

Moment som funktion av horisontalkraft och position längs pelaren

$$M_2(H, x) := H \cdot \left(\frac{l_0}{2} - x\right)$$

Deformation av pelare beroende på horisontalkraft och position längs pelaren

$$\delta_2(H, x) := -\int_0^x \int_0^x \text{sign}\left(M_2(H, x)\right) \cdot \kappa_f\left(\left|M_2(H, x)\right|\right) dx\, dx$$

5.2.1 ULS fast inspänning

Max tillåten horisontalkraft

$$H_{Ed2.ULS} := \frac{2 \cdot M_{Ed} \cdot UR}{l_0}$$

Vektor med stigande horisontalkraft

$$H_{v.ULS2_{i_\delta}} := H_{Ed2.ULS} \cdot \frac{i_\delta}{n_\delta}$$

Deformation för stigande värden på horisontalkraft

$$\delta_{max.2.ULS_{i_\delta}} := \delta_2\left(H_{v.ULS2_{i_\delta}}, l_0\right)$$

Maxdeformation

$$\delta_{max.2.ULS}(50) = -75.77\ mm$$

5.2.2 SLS fast inspänning

Max tillåten horisontalkraft

$$H_{Ed2.SLS} := \frac{2 \cdot M_{Rd.SLS}}{l_0}$$

Vektor med stigande horisontalkraft

$$H_{v.SLS2_{i_\delta}} := H_{Ed2.SLS} \cdot \frac{i_\delta}{n_\delta}$$

Deformation för stigande värden på horisontalkraft

$$\delta_{max.2.SLS_{i_\delta}} := \delta_2\left(H_{v.SLS2_{i_\delta}}, l_0\right)$$

Maxdeformation

$$\delta_{max.2.SLS}(50) = -33.61\ mm$$

6 Ekvivalenta styvheter

6.1 Konsolpelare

Ekvivalent styvhet ULS

$$E_{ekv.ULS} := -\frac{H_{Ed.ULS} \cdot {l_0}^3}{3 \cdot \delta_{max.ULS}(50) \cdot I_I} = 7.63\ GPa$$

Ekvivalent kurvatur

$$\kappa_{ekv.ULS} := \frac{M_{Ed.i}}{E_{ekv.ULS} \cdot I_I}$$

Kvot

$$\frac{E_{ekv.ULS}}{E_{cm}} = 0.21$$

$$\kappa_{ekv1.ULS}(M) := \text{linterp}\left(M_{Ed.i}, \kappa_{ekv.ULS}, M\right)$$

$$\delta_{ekv.ULS}(H, x) := -\int_0^x \int_0^x \kappa_{ekv1.ULS}(M(H, x))\, dx\, dx$$

Ekvivalent styvhet SLS

$$E_{ekv.SLS} := -\frac{H_{Ed.SLS} \cdot {l_0}^3}{3 \cdot \delta_{max.SLS}(50) \cdot I_I} = 11.39\ GPa$$

Ekvivalent kurvatur

$$\kappa_{ekv.SLS} := \frac{M_{Ed.i}}{E_{ekv.SLS} \cdot I_I}$$

Kvot

$$\frac{E_{ekv.SLS}}{E_{cm}} = 0.32$$

$$\kappa_{ekv1.SLS}(M) := \text{linterp}\left(M_{Ed.i}, \kappa_{ekv.SLS}, M\right)$$

$$\delta_{ekv.SLS}(H, x) := -\int_0^x \int_0^x \kappa_{ekv1.SLS}(M(H, x))\, dx\, dx$$

6.2 Fast inspänning

Ekvivalent styvhet ULS

$$E_{ekv2.ULS} := -\frac{H_{Ed2.ULS} \cdot (l_0)^3}{12 \cdot \delta_{max.2.ULS}(50) \cdot I_I} = 7.63\ GPa$$

Ekvivalent kurvatur

$$\kappa_{ekv2.ULS} := \frac{M_{Ed.i}}{E_{ekv2.ULS} \cdot I_I}$$

Kvot

$$\frac{E_{ekv2.ULS}}{E_{cm}} = 0.21$$

$$\kappa_{ekv.2.ULS}(M) := \text{linterp}\left(M_{Ed.i}, \kappa_{ekv2.ULS}, M\right)$$

$$\delta_{ekv.2.ULS}(H, x) := -\int_0^x \int_0^x \kappa_{ekv.2.ULS}\left(M_2(H, x)\right) dx\, dx$$

Ekvivalent styvhet SLS

$$E_{ekv2.SLS} := -\frac{H_{Ed2.SLS} \cdot (I_0)^3}{12 \cdot \delta_{max.2.SLS}(50) \cdot I_I} = 11.39 \text{ GPa}$$

Ekvivalent kurvatur

$$\kappa_{ekv2.SLS} := \frac{M_{Ed.i}}{E_{ekv2.SLS} \cdot I_I}$$

Kvot

$$\frac{E_{ekv2.SLS}}{E_{cm}} = 0.32$$

$$\kappa_{ekv.2.SLS}(M) := \text{linterp}\left(M_{Ed.i}, \kappa_{ekv2.SLS}, M\right)$$

$$\delta_{ekv.2.SLS}(H, x) := -\int_0^x \int_0^x \kappa_{ekv.2.SLS}\left(M_2(H, x)\right) dx\, dx$$

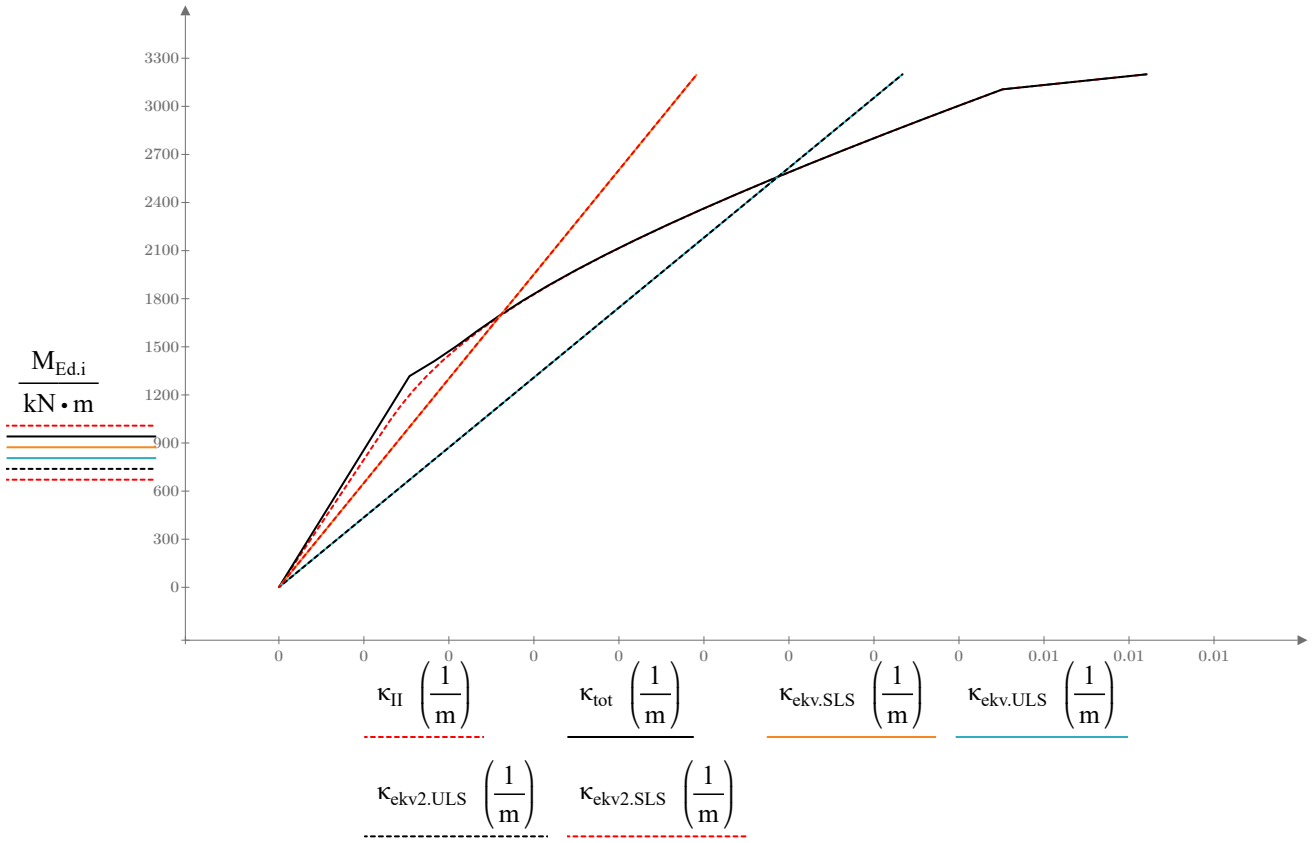

$\delta_1\left(H_{Ed.ULS}, x_{plot}\right)\ (mm)$

$\delta_{ekv.ULS}\left(H_{Ed.ULS}, x_{plot}\right)\ (mm)$

$\delta_1\left(H_{Ed.SLS}, x_{plot}\right)\ (mm)$

$\delta_{ekv.SLS}\left(H_{Ed.SLS}, x_{plot}\right)\ (mm)$

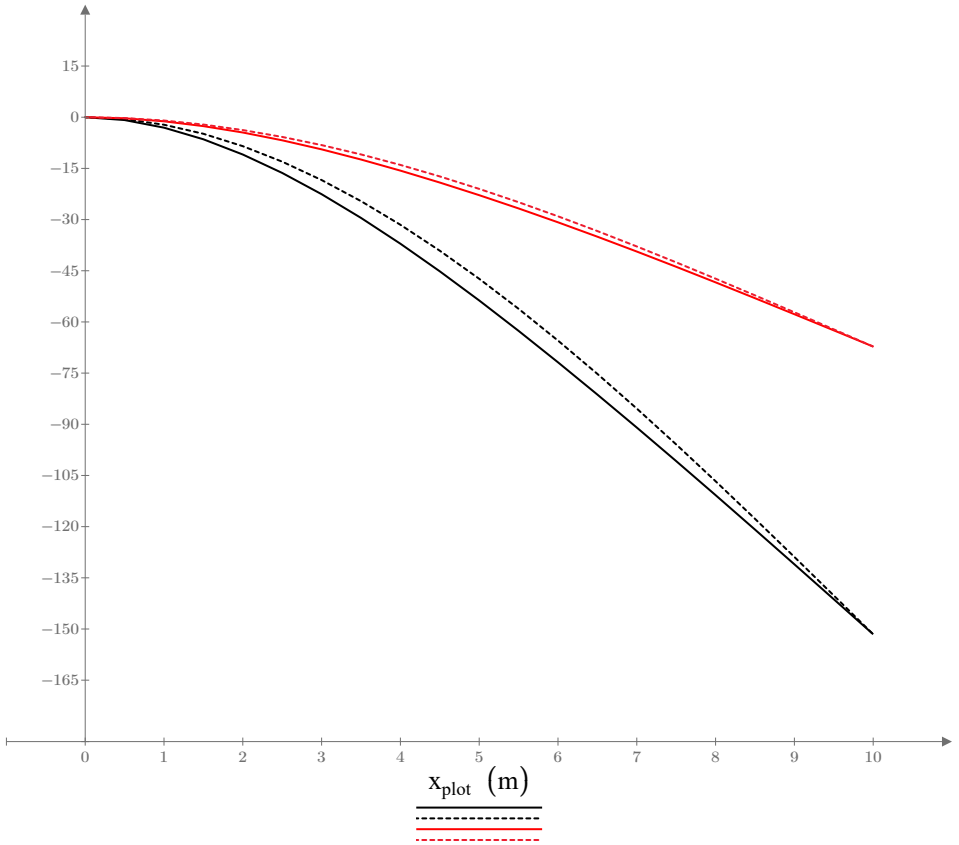

$\delta_2\left(H_{Ed2.ULS}, x_{plot}\right)\ (mm)$

$\delta_{ekv.2.ULS}\left(H_{Ed2.ULS}, x_{plot}\right)\ (mm)$

$\delta_2\left(H_{Ed2.SLS}, x_{plot}\right)\ (mm)$

$\delta_{ekv.2.SLS}\left(H_{Ed2.SLS}, x_{plot}\right)\ (mm)$

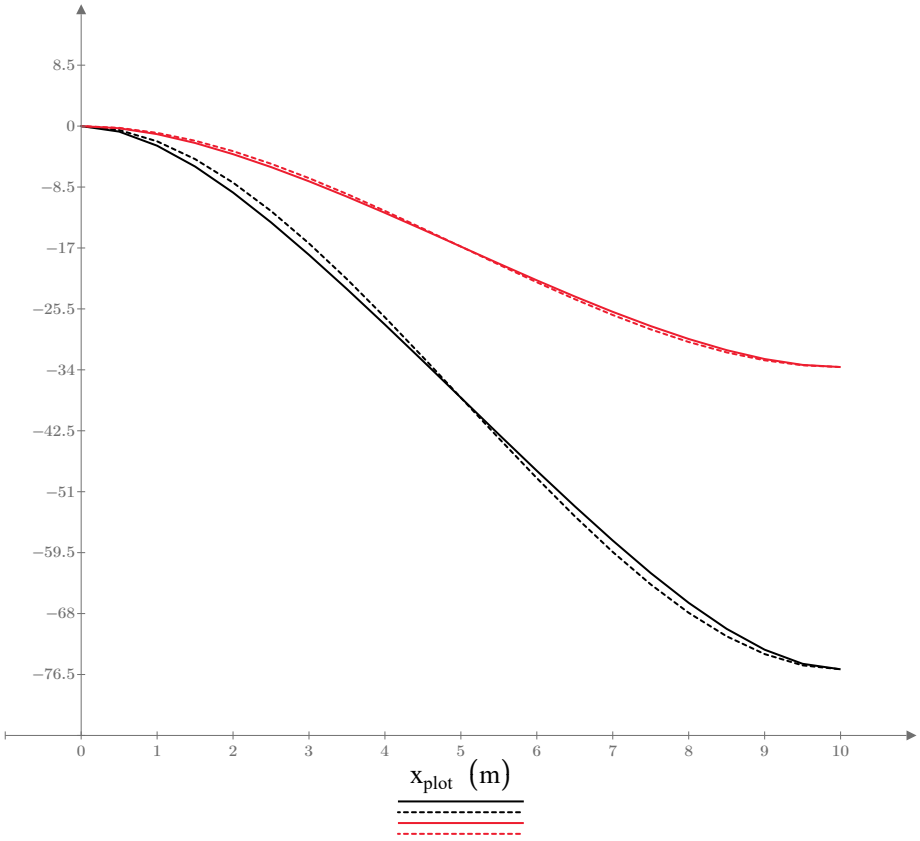

7 Metod baserad på nominell styvhet

7.1 Nominell styvhet konsolpelare

Beräkning enligt EN 1992-1-1 avsnitt 5.8.7.

Relativ normalkraft

$$n_n := \frac{|N_{Ed}|}{A_c \cdot f_{cd}} = 0.2$$

Beräkningen förutsätter att elementet är tryckbelastat.

Slankhetstalet

$$\lambda := \frac{2\ l_0}{i_c} = 69.28$$

Faktor som beaktar normalkraft och slankhet

$$k_{2.c} := n_n \cdot \frac{\lambda}{170} = 0.08$$

Faktor som beaktar betongens hållfasthetsklass

$$k_{1.c} := \sqrt{\frac{f_{ck}}{20 \cdot MPa}} = 1.5$$

Följande faktorer får användas om ρ > 0.002.

Armeringskvot

$$\rho := \frac{A_s}{A_c} = 0.01$$

Faktor som beaktar inverkan av sprickbildning och krypning (ekv 5.22)

$$K_c := \frac{k_{1.c} \cdot k_{2.c}}{1 + \phi_{ef}} = 0.06$$

Faktor för armeringens bidrag (ekv 5.22)

$$K_s := 1$$

Beräkningen förutsätter att p > 0.002.

Nominell böjstyvhet kring vald axel

$$EI_{nom} := K_c \cdot E_{cd} \cdot I_c + K_s \cdot E_s \cdot I_s = 346.11\ MN \cdot m^2$$

$$E_{nom} := \frac{EI_{nom}}{I_c} = 4.15\ GPa$$

Krökning erhållen från nominell styvhet

$$\kappa_{nom} := \frac{M_{Ed.i}}{EI_{nom}}$$

7.2 Nominell styvhet inspänd pelare

Slankhetstalet

$$\lambda_2 := \frac{l_0}{i_c} = 34.64$$

Faktor som beaktar normalkraft och slankhet

$$k_{2.c.2} := n_n \cdot \frac{\lambda_2}{170} = 0.04$$

Faktor som beaktar inverkan av sprickbildning och krypning (ekv 5.22)

$$K_{c2} := \frac{k_{1.c} \cdot k_{2.c.2}}{1 + \phi_{ef}} = 0.03$$

Faktor för armeringens bidrag (ekv 5.22)

Nominell böjstyvhet kring vald axel

$$EI_{nom.2} := K_{c2} \cdot E_{cd} \cdot I_c + K_s \cdot E_s \cdot I_s = 269.7\ MN \cdot m^2$$

$$E_{nom.2} := \frac{EI_{nom.2}}{I_c} = 3.24\ GPa$$

Krökning erhållen från nominell styvhet

$$\kappa_{nom.2} := \frac{M_{Ed.i}}{EI_{nom.2}}$$

7.3 Nominell styvhet enligt EN 1992-1-1:2023

Beräkning enligt EN 1992-1-1:2023 annex O.8.1.

Styvhet för vägg och pelare

$$EI_{nom.2023.1} := 0.4 \cdot E_{cd} \cdot I_c = 1000\ MN \cdot m^2$$

$$E_{nom.2023.1} := \frac{EI_{nom.2023.1}}{I_c} = 12\ GPa$$

Krökning erhållen från nominell styvhet

$$\kappa_{nom.23} := \frac{M_{Ed.i}}{EI_{nom.2023.1}}$$

Styvhet från yield

$$EI_y := \frac{M_{Rd.y}}{\kappa_y} = 541.53\ MN \cdot m^2$$

$$E_y := \frac{EI_y}{I_c} = 6.5\ GPa$$

$$\kappa_{nom.y.23} := \frac{M_{Ed.i}}{EI_y}$$

Med den nya metoden för nominell styvhet (eller andra ordningens styvhet som nya koden kallar det) kan man inte längre anpassa beräkingen efter vilken betongklass eller slankhet somstrukturen har.

8 Jämförelse av beräknad styvhet mot nominell styvhet

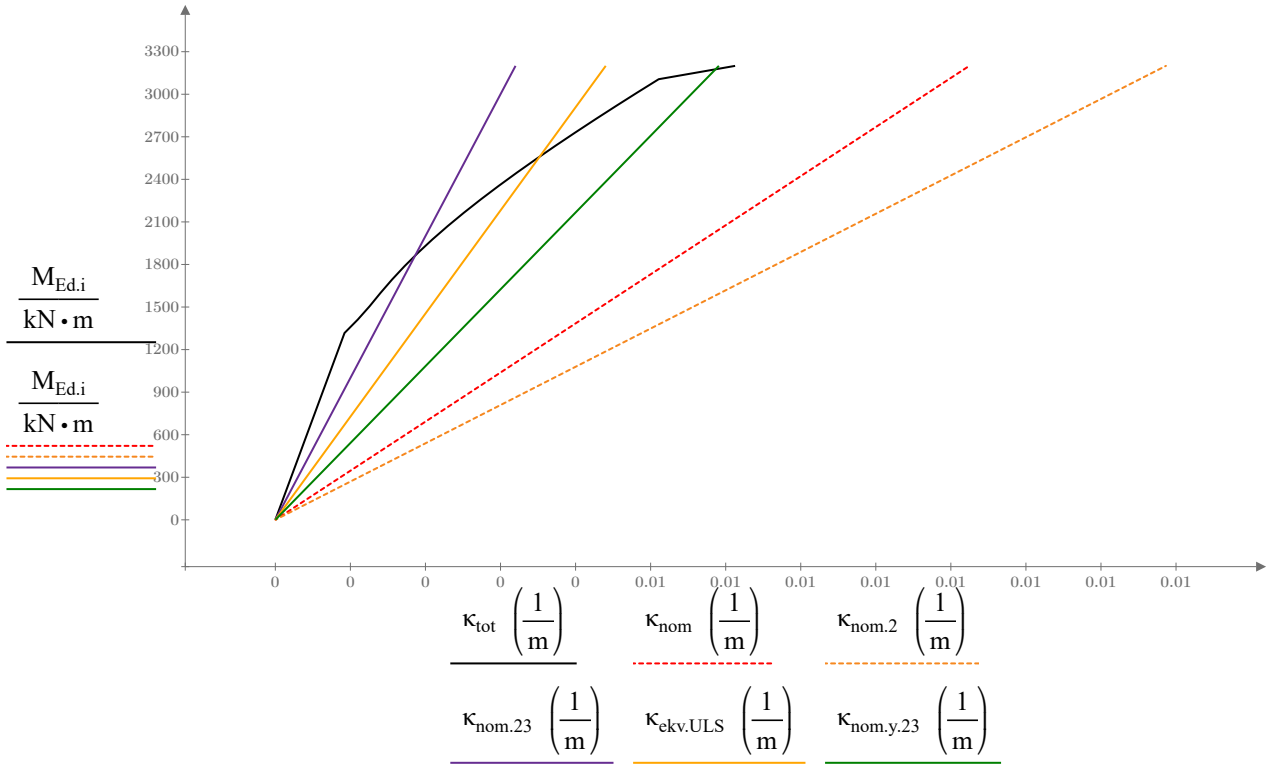

B Appendix: Material Model curves

Betongklasser

Innehållsförteckning

1 INDATA

1.1 Partialfaktorer

Alla partialfaktorer sätts till 0 för att erhålla karaktäristiska värden

Partialfaktor hållfasthet $\gamma_c := 1.5$

Partialfaktor hållfasthet $\alpha_c := 1.0$

Partialkoefficient för betongens elasticitetsmodul $\gamma_{cE} := 1.2$

1.2 Material Betong

Elasticitetsmodul

$E_{cm.12} := 27\ GPa$ $E_{cm.45} := 36\ GPa$
$E_{cm.16} := 29\ GPa$ $E_{cm.50} := 37\ GPa$
$E_{cm.20} := 30\ GPa$ $E_{cm.55} := 38\ GPa$
$E_{cm.25} := 31\ GPa$ $E_{cm.60} := 39\ GPa$
$E_{cm.30} := 33\ GPa$ $E_{cm.70} := 41\ GPa$
$E_{cm.35} := 34\ GPa$ $E_{cm.80} := 42\ GPa$
$E_{cm.40} := 35\ GPa$ $E_{cm.90} := 44\ GPa$

Karakteristisk tryckhållfasthet

$f_{ck.12} := 12 \cdot MPa$ $f_{ck.45} := 45 \cdot MPa$
$f_{ck.16} := 16 \cdot MPa$ $f_{ck.50} := 50 \cdot MPa$
$f_{ck.20} := 20 \cdot MPa$ $f_{ck.55} := 55 \cdot MPa$
$f_{ck.25} := 25 \cdot MPa$ $f_{ck.60} := 60 \cdot MPa$
$f_{ck.30} := 30 \cdot MPa$ $f_{ck.70} := 70 \cdot MPa$
$f_{ck.35} := 35 \cdot MPa$ $f_{ck.80} := 80 \cdot MPa$
$f_{ck.40} := 40 \cdot MPa$ $f_{ck.90} := 90 \cdot MPa$

Medeltryckhållfasthet

$f_{cm.12} := f_{ck.12} + 8 \cdot MPa$ $f_{cm.45} := f_{ck.45} + 8 \cdot MPa$
$f_{cm.16} := f_{ck.16} + 8 \cdot MPa$ $f_{cm.50} := f_{ck.50} + 8 \cdot MPa$
$f_{cm.20} := f_{ck.20} + 8 \cdot MPa$ $f_{cm.55} := f_{ck.55} + 8 \cdot MPa$
$f_{cm.25} := f_{ck.25} + 8 \cdot MPa$ $f_{cm.60} := f_{ck.60} + 8 \cdot MPa$
$f_{cm.30} := f_{ck.30} + 8 \cdot MPa$ $f_{cm.70} := f_{ck.70} + 8 \cdot MPa$
$f_{cm.35} := f_{ck.35} + 8 \cdot MPa$ $f_{cm.80} := f_{ck.80} + 8 \cdot MPa$
$f_{cm.40} := f_{ck.40} + 8 \cdot MPa$ $f_{cm.90} := f_{ck.90} + 8 \cdot MPa$

Brottstukning

$$\varepsilon_{cu2.12\_50} := 3.5 \cdot 10^{-3}$$

$$\varepsilon_{cu2.55} := \left(2.6 + 35 \cdot \left(\frac{\left(90 - \frac{f_{ck.55}}{MPa}\right)}{100}\right)^4\right) \cdot 10^{-3} = 3.1 \cdot 10^{-3}$$

$$\varepsilon_{cu2.60} := \left(2.6 + 35 \cdot \left(\frac{\left(90 - \frac{f_{ck.60}}{MPa}\right)}{100}\right)^4\right) \cdot 10^{-3} = 2.9 \cdot 10^{-3}$$

$$\varepsilon_{cu2.70} := \left(2.6 + 35 \cdot \left(\frac{\left(90 - \frac{f_{ck.70}}{MPa}\right)}{100}\right)^4\right) \cdot 10^{-3} = 2.7 \cdot 10^{-3}$$

$$\varepsilon_{cu2.80} := \left(2.6 + 35 \cdot \left(\frac{\left(90 - \frac{f_{ck.80}}{MPa}\right)}{100}\right)^4\right) \cdot 10^{-3} = 2.6 \cdot 10^{-3}$$

$$\varepsilon_{cu2.90} := \left(2.6 + 35 \cdot \left(\frac{\left(90 - \frac{f_{ck.90}}{MPa}\right)}{100}\right)^4\right) \cdot 10^{-3} = 2.6 \cdot 10^{-3}$$

Töjning då arbetskurvan blir horisontell (arbteskurva enligt 3.1.7)

$$\varepsilon_{c2.12\_50} := 2 \cdot 10^{-3}$$

$$\varepsilon_{c2.55} := \left(2.0 + 0.085 \cdot \left(\frac{f_{ck.55}}{MPa} - 50\right)^{0.53}\right) \cdot 10^{-3} = 2.2 \cdot 10^{-3}$$

$$\varepsilon_{c2.60} := \left(2.0 + 0.085 \cdot \left(\frac{f_{ck.60}}{MPa} - 50\right)^{0.53}\right) \cdot 10^{-3} = 2.3 \cdot 10^{-3}$$

$$\varepsilon_{c2.70} := \left(2.0 + 0.085 \cdot \left(\frac{f_{ck.70}}{MPa} - 50\right)^{0.53}\right) \cdot 10^{-3} = 2.4 \cdot 10^{-3}$$

$$\varepsilon_{c2.80} := \left(2.0 + 0.085 \cdot \left(\frac{f_{ck.80}}{MPa} - 50\right)^{0.53}\right) \cdot 10^{-3} = 2.5 \cdot 10^{-3}$$

$$\varepsilon_{c2.90} := \left(2.0 + 0.085 \cdot \left(\frac{f_{ck.90}}{MPa} - 50\right)^{0.53}\right) \cdot 10^{-3} = 2.6 \cdot 10^{-3}$$

Koefficient som används i formel för arbetskurva

$$n. := 2$$

Brottstukning kurva 3.1.5

$$\varepsilon_{cu1.12\_50} := 3.5 \cdot 10^{-3}$$

$$\varepsilon_{cu1.55} := 3.2 \cdot 10^{-3}$$

$$\varepsilon_{cu1.60} := 3.0 \cdot 10^{-3}$$

$$\varepsilon_{cu1.70} := 2.8 \cdot 10^{-3}$$

$$\varepsilon_{cu1.80} := 2.8 \cdot 10^{-3}$$

$$\varepsilon_{cu1.90} := 2.8 \cdot 10^{-3}$$

Töjningsvärde nyttjat i arbteskurva enligt 3.1.5.

$$\varepsilon_{c1.12} := 0.7 \cdot \left(\frac{f_{cm.12}}{MPa}\right)^{0.31} \cdot 10^{-3} = 1.77 \cdot 10^{-3}$$

$$\varepsilon_{c1.16} := 0.7 \cdot \left(\frac{f_{cm.16}}{MPa}\right)^{0.31} \cdot 10^{-3} = 1.87 \cdot 10^{-3}$$

$$\varepsilon_{c1.20} := 0.7 \cdot \left(\frac{f_{cm.20}}{MPa}\right)^{0.31} \cdot 10^{-3} = 1.97 \cdot 10^{-3}$$

$$\varepsilon_{c1.25} := 0.7 \cdot \left(\frac{f_{cm.25}}{MPa}\right)^{0.31} \cdot 10^{-3} = 2.07 \cdot 10^{-3}$$

$$\varepsilon_{c1.30} := 0.7 \cdot \left(\frac{f_{cm.30}}{MPa}\right)^{0.31} \cdot 10^{-3} = 2.16 \cdot 10^{-3}$$

$$\varepsilon_{c1.35} := 0.7 \cdot \left(\frac{f_{cm.35}}{MPa}\right)^{0.31} \cdot 10^{-3} = 2.25 \cdot 10^{-3}$$
$$\varepsilon_{c1.40} := 0.7 \cdot \left(\frac{f_{cm.40}}{MPa}\right)^{0.31} \cdot 10^{-3} = 2.32 \cdot 10^{-3}$$
$$\varepsilon_{c1.45} := 0.7 \cdot \left(\frac{f_{cm.45}}{MPa}\right)^{0.31} \cdot 10^{-3} = 2.4 \cdot 10^{-3}$$
$$\varepsilon_{c1.50} := 0.7 \cdot \left(\frac{f_{cm.50}}{MPa}\right)^{0.31} \cdot 10^{-3} = 2.46 \cdot 10^{-3}$$
$$\varepsilon_{c1.55} := 0.7 \cdot \left(\frac{f_{cm.55}}{MPa}\right)^{0.31} \cdot 10^{-3} = 2.53 \cdot 10^{-3}$$
$$\varepsilon_{c1.60} := 0.7 \cdot \left(\frac{f_{cm.60}}{MPa}\right)^{0.31} \cdot 10^{-3} = 2.59 \cdot 10^{-3}$$
$$\varepsilon_{c1.70} := 0.7 \cdot \left(\frac{f_{cm.70}}{MPa}\right)^{0.31} \cdot 10^{-3} = 2.7 \cdot 10^{-3}$$
$$\varepsilon_{c1.80} := 2.8 \cdot 10^{-3}$$
$$\varepsilon_{c1.90} := 2.8 \cdot 10^{-3}$$

Dimensionerande tryckhållfasthet betong

$$f_{cd.12} := \frac{\alpha_c \cdot f_{ck.12}}{\gamma_c} = 8\ MPa \qquad f_{cd.45} := \frac{\alpha_c \cdot f_{ck.45}}{\gamma_c} = 30\ MPa$$
$$f_{cd.16} := \frac{\alpha_c \cdot f_{ck.16}}{\gamma_c} = 10.7\ MPa \qquad f_{cd.50} := \frac{\alpha_c \cdot f_{ck.50}}{\gamma_c} = 33.3\ MPa$$
$$f_{cd.20} := \frac{\alpha_c \cdot f_{ck.20}}{\gamma_c} = 13.3\ MPa \qquad f_{cd.55} := \frac{\alpha_c \cdot f_{ck.55}}{\gamma_c} = 36.7\ MPa$$
$$f_{cd.25} := \frac{\alpha_c \cdot f_{ck.25}}{\gamma_c} = 16.7\ MPa \qquad f_{cd.60} := \frac{\alpha_c \cdot f_{ck.60}}{\gamma_c} = 40\ MPa$$
$$f_{cd.30} := \frac{\alpha_c \cdot f_{ck.30}}{\gamma_c} = 20\ MPa \qquad f_{cd.70} := \frac{\alpha_c \cdot f_{ck.70}}{\gamma_c} = 46.7\ MPa$$
$$f_{cd.35} := \frac{\alpha_c \cdot f_{ck.35}}{\gamma_c} = 23.3\ MPa \qquad f_{cd.80} := \frac{\alpha_c \cdot f_{ck.80}}{\gamma_c} = 53.3\ MPa$$
$$f_{cd.40} := \frac{\alpha_c \cdot f_{ck.40}}{\gamma_c} = 26.7\ MPa \qquad f_{cd.90} := \frac{\alpha_c \cdot f_{ck.90}}{\gamma_c} = 60\ MPa$$

Dimensionerande elasticitetsmodul betong

$$E_{cd.12} := \frac{E_{cm.12}}{\gamma_{cE}} = 22.5\ GPa \qquad E_{cd.45} := \frac{E_{cm.45}}{\gamma_{cE}} = 30\ GPa$$
$$E_{cd.16} := \frac{E_{cm.16}}{\gamma_{cE}} = 24.2\ GPa \qquad E_{cd.50} := \frac{E_{cm.50}}{\gamma_{cE}} = 30.8\ GPa$$
$$E_{cd.20} := \frac{E_{cm.20}}{\gamma_{cE}} = 25\ GPa \qquad E_{cd.55} := \frac{E_{cm.55}}{\gamma_{cE}} = 31.7\ GPa$$
$$E_{cd.25} := \frac{E_{cm.25}}{\gamma_{cE}} = 25.8\ GPa \qquad E_{cd.60} := \frac{E_{cm.60}}{\gamma_{cE}} = 32.5\ GPa$$
$$E_{cd.30} := \frac{E_{cm.30}}{\gamma_{cE}} = 27.5\ GPa \qquad E_{cd.70} := \frac{E_{cm.70}}{\gamma_{cE}} = 34.2\ GPa$$
$$E_{cd.35} := \frac{E_{cm.35}}{\gamma_{cE}} = 28.3\ GPa \qquad E_{cd.80} := \frac{E_{cm.80}}{\gamma_{cE}} = 35\ GPa$$
$$E_{cd.40} := \frac{E_{cm.40}}{\gamma_{cE}} = 29.2\ GPa \qquad E_{cd.90} := \frac{E_{cm.90}}{\gamma_{cE}} = 36.7\ GPa$$

2 Funktioner för materialkurvor

Nedan jämförs olika materialkurvor för betong enligt EN1992-1-1 3.15 och 3.1.7. Båda kurvorna presenteras både med och utan modifiering av töjning mht krypning.

Betongens arbetskurva som funktion av töjning enligt SS-EN 1992-1-1:2005, avsnitt 3.1.5.

$$k_{12} := \frac{1.05 \cdot E_{cd.12} \cdot |\varepsilon_{c1.12}|}{f_{cd.12}} = 5.2$$

$$k_{16} := \frac{1.05 \cdot E_{cd.16} \cdot |\varepsilon_{c1.16}|}{f_{cd.16}} = 4.5$$

$$k_{20} := \frac{1.05 \cdot E_{cd.20} \cdot |\varepsilon_{c1.20}|}{f_{cd.20}} = 3.9$$

$$k_{25} := \frac{1.05 \cdot E_{cd.25} \cdot |\varepsilon_{c1.25}|}{f_{cd.25}} = 3.4$$

$$k_{30} := \frac{1.05 \cdot E_{cd.30} \cdot |\varepsilon_{c1.30}|}{f_{cd.30}} = 3.1$$

$$k_{35} := \frac{1.05 \cdot E_{cd.35} \cdot |\varepsilon_{c1.35}|}{f_{cd.35}} = 2.9$$

$$k_{40} := \frac{1.05 \cdot E_{cd.40} \cdot |\varepsilon_{c1.40}|}{f_{cd.40}} = 2.7$$

$$k_{45} := \frac{1.05 \cdot E_{cd.45} \cdot |\varepsilon_{c1.45}|}{f_{cd.45}} = 2.5$$

$$k_{50} := \frac{1.05 \cdot E_{cd.50} \cdot |\varepsilon_{c1.50}|}{f_{cd.50}} = 2.4$$

$$k_{55} := \frac{1.05 \cdot E_{cd.55} \cdot |\varepsilon_{c1.55}|}{f_{cd.55}} = 2.3$$

$$k_{60} := \frac{1.05 \cdot E_{cd.60} \cdot |\varepsilon_{c1.60}|}{f_{cd.60}} = 2.2$$

$$k_{70} := \frac{1.05 \cdot E_{cd.70} \cdot |\varepsilon_{c1.70}|}{f_{cd.70}} = 2.1$$

$$k_{80} := \frac{1.05 \cdot E_{cd.80} \cdot |\varepsilon_{c1.80}|}{f_{cd.80}} = 1.9$$

$$k_{90} := \frac{1.05 \cdot E_{cd.90} \cdot |\varepsilon_{c1.90}|}{f_{cd.90}} = 1.8$$

$$\eta_{12}(\varepsilon) := \frac{\varepsilon}{\varepsilon_{c1.12}}$$

$$\eta_{16}(\varepsilon) := \frac{\varepsilon}{\varepsilon_{c1.16}}$$

$$\eta_{20}(\varepsilon) := \frac{\varepsilon}{\varepsilon_{c1.20}}$$

$$\eta_{25}(\varepsilon) := \frac{\varepsilon}{\varepsilon_{c1.25}}$$

$$\eta_{30}(\varepsilon) := \frac{\varepsilon}{\varepsilon_{c1.30}}$$

$$\eta_{35}(\varepsilon) := \frac{\varepsilon}{\varepsilon_{c1.35}}$$

$$\eta_{40}(\varepsilon) := \frac{\varepsilon}{\varepsilon_{c1.40}}$$

$$\eta_{45}(\varepsilon) := \frac{\varepsilon}{\varepsilon_{c1.45}}$$

$$\eta_{50}(\varepsilon) := \frac{\varepsilon}{\varepsilon_{c1.50}}$$

$$\eta_{55}(\varepsilon) := \frac{\varepsilon}{\varepsilon_{c1.55}}$$

$$\eta_{60}(\varepsilon) := \frac{\varepsilon}{\varepsilon_{c1.60}}$$

$$\eta_{70}(\varepsilon) := \frac{\varepsilon}{\varepsilon_{c1.70}}$$

$$\eta_{80}(\varepsilon) := \frac{\varepsilon}{\varepsilon_{c1.80}}$$

$$\eta_{90}(\varepsilon) := \frac{\varepsilon}{\varepsilon_{c1.90}}$$

$$\sigma_{c.315.12}(\varepsilon) := \left\| \begin{array}{l} 0 \cdot \mathrm{MPa} \\ \text{if } \varepsilon < 0 \\ \quad \left\| \left(\frac{k_{12} \cdot \eta_{12} \langle -\varepsilon \rangle - \eta_{12} \langle -\varepsilon \rangle^2}{1 + (k_{12} - 2) \cdot \eta_{12} \langle -\varepsilon \rangle} \cdot -f_{cd.12} \right) \right\| \end{array} \right\|$$

$$\sigma_{c.315.45}(\varepsilon) := \left\| \begin{array}{l} 0 \cdot \mathrm{MPa} \\ \text{if } \varepsilon < 0 \\ \quad \left\| \left(\frac{k_{45} \cdot \eta_{45} \langle -\varepsilon \rangle - \eta_{45} \langle -\varepsilon \rangle^2}{1 + (k_{45} - 2) \cdot \eta_{45} \langle -\varepsilon \rangle} \cdot -f_{cd.45} \right) \right\| \end{array} \right\|$$

$$\sigma_{c.315.16}(\varepsilon) := \left\| \begin{array}{l} 0 \cdot \mathrm{MPa} \\ \text{if } \varepsilon < 0 \\ \quad \left\| \left(\frac{k_{16} \cdot \eta_{16} \langle -\varepsilon \rangle - \eta_{16} \langle -\varepsilon \rangle^2}{1 + (k_{16} - 2) \cdot \eta_{16} \langle -\varepsilon \rangle} \cdot -f_{cd.16} \right) \right\| \end{array} \right\|$$

$$\sigma_{c.315.50}(\varepsilon) := \left\| \begin{array}{l} 0 \cdot \mathrm{MPa} \\ \text{if } \varepsilon < 0 \\ \quad \left\| \left(\frac{k_{50} \cdot \eta_{50} \langle -\varepsilon \rangle - \eta_{50} \langle -\varepsilon \rangle^2}{1 + (k_{50} - 2) \cdot \eta_{50} \langle -\varepsilon \rangle} \cdot -f_{cd.50} \right) \right\| \end{array} \right\|$$

$$\sigma_{c.315.20}(\varepsilon) := \left\| \begin{array}{l} 0 \cdot \mathrm{MPa} \\ \text{if } \varepsilon < 0 \\ \quad \left\| \left(\frac{k_{20} \cdot \eta_{20} \langle -\varepsilon \rangle - \eta_{20} \langle -\varepsilon \rangle^2}{1 + (k_{20} - 2) \cdot \eta_{20} \langle -\varepsilon \rangle} \cdot -f_{cd.20} \right) \right\| \end{array} \right\|$$

$$\sigma_{c.315.55}(\varepsilon) := \left\| \begin{array}{l} 0 \cdot \mathrm{MPa} \\ \text{if } \varepsilon < 0 \\ \quad \left\| \left(\frac{k_{55} \cdot \eta_{55} \langle -\varepsilon \rangle - \eta_{55} \langle -\varepsilon \rangle^2}{1 + (k_{55} - 2) \cdot \eta_{55} \langle -\varepsilon \rangle} \cdot -f_{cd.55} \right) \right\| \end{array} \right\|$$

$$\sigma_{c.315.25}(\varepsilon) := \left\| \begin{array}{l} 0 \cdot \mathrm{MPa} \\ \text{if } \varepsilon < 0 \\ \quad \left\| \left(\frac{k_{25} \cdot \eta_{25} \langle -\varepsilon \rangle - \eta_{25} \langle -\varepsilon \rangle^2}{1 + (k_{25} - 2) \cdot \eta_{25} \langle -\varepsilon \rangle} \cdot -f_{cd.25} \right) \right\| \end{array} \right\|$$

$$\sigma_{c.315.60}(\varepsilon) := \left\| \begin{array}{l} 0 \cdot \mathrm{MPa} \\ \text{if } \varepsilon < 0 \\ \quad \left\| \left(\frac{k_{60} \cdot \eta_{60} \langle -\varepsilon \rangle - \eta_{60} \langle -\varepsilon \rangle^2}{1 + (k_{60} - 2) \cdot \eta_{60} \langle -\varepsilon \rangle} \cdot -f_{cd.60} \right) \right\| \end{array} \right\|$$

$$\sigma_{c.315.30}(\varepsilon) := \left\| \begin{array}{l} 0 \cdot \mathrm{MPa} \\ \text{if } \varepsilon < 0 \\ \quad \left\| \left(\frac{k_{30} \cdot \eta_{30} \langle -\varepsilon \rangle - \eta_{30} \langle -\varepsilon \rangle^2}{1 + (k_{30} - 2) \cdot \eta_{30} \langle -\varepsilon \rangle} \cdot -f_{cd.30} \right) \right\| \end{array} \right\|$$

$$\sigma_{c.315.70}(\varepsilon) := \left\| \begin{array}{l} 0 \cdot \mathrm{MPa} \\ \text{if } \varepsilon < 0 \\ \quad \left\| \left(\frac{k_{70} \cdot \eta_{70} \langle -\varepsilon \rangle - \eta_{70} \langle -\varepsilon \rangle^2}{1 + (k_{70} - 2) \cdot \eta_{70} \langle -\varepsilon \rangle} \cdot -f_{cd.70} \right) \right\| \end{array} \right\|$$

$$\sigma_{c.315.35}(\varepsilon) := \left\| \begin{array}{l} 0 \cdot \mathrm{MPa} \\ \text{if } \varepsilon < 0 \\ \quad \left\| \left(\frac{k_{35} \cdot \eta_{35} \langle -\varepsilon \rangle - \eta_{35} \langle -\varepsilon \rangle^2}{1 + (k_{35} - 2) \cdot \eta_{35} \langle -\varepsilon \rangle} \cdot -f_{cd.35} \right) \right\| \end{array} \right\|$$

$$\sigma_{c.315.80}(\varepsilon) := \left\| \begin{array}{l} 0 \cdot \mathrm{MPa} \\ \text{if } \varepsilon < 0 \\ \quad \left\| \left(\frac{k_{80} \cdot \eta_{80} \langle -\varepsilon \rangle - \eta_{80} \langle -\varepsilon \rangle^2}{1 + (k_{80} - 2) \cdot \eta_{80} \langle -\varepsilon \rangle} \cdot -f_{cd.80} \right) \right\| \end{array} \right\|$$

$$\sigma_{c.315.40}(\varepsilon) := \left\| \begin{array}{l} 0 \cdot \mathrm{MPa} \\ \text{if } \varepsilon < 0 \\ \quad \left\| \left(\frac{k_{40} \cdot \eta_{40} \langle -\varepsilon \rangle - \eta_{40} \langle -\varepsilon \rangle^2}{1 + (k_{40} - 2) \cdot \eta_{40} \langle -\varepsilon \rangle} \cdot -f_{cd.40} \right) \right\| \end{array} \right\|$$

$$\sigma_{c.315.90}(\varepsilon) := \left\| \begin{array}{l} 0 \cdot \mathrm{MPa} \\ \text{if } \varepsilon < 0 \\ \quad \left\| \left(\frac{k_{90} \cdot \eta_{90} \langle -\varepsilon \rangle - \eta_{90} \langle -\varepsilon \rangle^2}{1 + (k_{90} - 2) \cdot \eta_{90} \langle -\varepsilon \rangle} \cdot -f_{cd.90} \right) \right\| \end{array} \right\|$$

Betongens arbetskurva som funktion av töjning enligt SS-EN 1992-1-1:2005, avsnitt 3.1.7.

$$\sigma_{c.317.12}(\varepsilon) := \left\| \begin{array}{l} \text{if } \varepsilon > 0 \\ \quad \left\| (0 \cdot \text{MPa}) \right. \\ \text{if } 0 \geq \varepsilon > -\varepsilon_{c2.12\_50} \\ \quad \left\| \left(-f_{cd.12} \cdot \left(1 - \left(1 - \frac{-\varepsilon}{\varepsilon_{c2.12\_50}} \right)^{n.} \right) \right) \right. \\ \text{if } -\varepsilon_{c2.12\_50} \geq \varepsilon \\ \quad \left\| -f_{cd.12} \right. \end{array} \right.$$

$$\sigma_{c.317.45}(\varepsilon) := \left\| \begin{array}{l} \text{if } \varepsilon > 0 \\ \quad \left\| (0 \cdot \text{MPa}) \right. \\ \text{if } 0 \geq \varepsilon > -\varepsilon_{c2.12\_50} \\ \quad \left\| \left(-f_{cd.45} \cdot \left(1 - \left(1 - \frac{-\varepsilon}{\varepsilon_{c2.12\_50}} \right)^{n.} \right) \right) \right. \\ \text{if } -\varepsilon_{c2.12\_50} \geq \varepsilon \\ \quad \left\| -f_{cd.45} \right. \end{array} \right.$$

$$\sigma_{c.317.16}(\varepsilon) := \left\| \begin{array}{l} \text{if } \varepsilon > 0 \\ \quad \left\| (0 \cdot \text{MPa}) \right. \\ \text{if } 0 \geq \varepsilon > -\varepsilon_{c2.12\_50} \\ \quad \left\| \left(-f_{cd.16} \cdot \left(1 - \left(1 - \frac{-\varepsilon}{\varepsilon_{c2.12\_50}} \right)^{n.} \right) \right) \right. \\ \text{if } -\varepsilon_{c2.12\_50} \geq \varepsilon \\ \quad \left\| -f_{cd.16} \right. \end{array} \right.$$

$$\sigma_{c.317.50}(\varepsilon) := \left\| \begin{array}{l} \text{if } \varepsilon > 0 \\ \quad \left\| (0 \cdot \text{MPa}) \right. \\ \text{if } 0 \geq \varepsilon > -\varepsilon_{c2.12\_50} \\ \quad \left\| \left(-f_{cd.50} \cdot \left(1 - \left(1 - \frac{-\varepsilon}{\varepsilon_{c2.12\_50}} \right)^{n.} \right) \right) \right. \\ \text{if } -\varepsilon_{c2.12\_50} \geq \varepsilon \\ \quad \left\| -f_{cd.50} \right. \end{array} \right.$$

$$\sigma_{c.317.20}(\varepsilon) := \left\| \begin{array}{l} \text{if } \varepsilon > 0 \\ \quad \left\| (0 \cdot \text{MPa}) \right. \\ \text{if } 0 \geq \varepsilon > -\varepsilon_{c2.12\_50} \\ \quad \left\| \left(-f_{cd.20} \cdot \left(1 - \left(1 - \frac{-\varepsilon}{\varepsilon_{c2.12\_50}} \right)^{n.} \right) \right) \right. \\ \text{if } -\varepsilon_{c2.12\_50} \geq \varepsilon \\ \quad \left\| -f_{cd.20} \right. \end{array} \right.$$

$$\sigma_{c.317.55}(\varepsilon) := \left\| \begin{array}{l} \text{if } \varepsilon > 0 \\ \quad \left\| (0 \cdot \text{MPa}) \right. \\ \text{if } 0 \geq \varepsilon > -\varepsilon_{c2.55} \\ \quad \left\| \left(-f_{cd.55} \cdot \left(1 - \left(1 - \frac{-\varepsilon}{\varepsilon_{c2.55}} \right)^{n.} \right) \right) \right. \\ \text{if } -\varepsilon_{c2.55} \geq \varepsilon \\ \quad \left\| -f_{cd.55} \right. \end{array} \right.$$

$$\sigma_{c.317.25}(\varepsilon) := \left\| \begin{array}{l} \text{if } \varepsilon > 0 \\ \quad \left\| (0 \cdot \text{MPa}) \right. \\ \text{if } 0 \geq \varepsilon > -\varepsilon_{c2.12\_50} \\ \quad \left\| \left(-f_{cd.25} \cdot \left(1 - \left(1 - \frac{-\varepsilon}{\varepsilon_{c2.12\_50}} \right)^{n.} \right) \right) \right. \\ \text{if } -\varepsilon_{c2.12\_50} \geq \varepsilon \\ \quad \left\| -f_{cd.25} \right. \end{array} \right.$$

$$\sigma_{c.317.60}(\varepsilon) := \left\| \begin{array}{l} \text{if } \varepsilon > 0 \\ \quad \left\| (0 \cdot \text{MPa}) \right. \\ \text{if } 0 \geq \varepsilon > -\varepsilon_{c2.60} \\ \quad \left\| \left(-f_{cd.60} \cdot \left(1 - \left(1 - \frac{-\varepsilon}{\varepsilon_{c2.60}} \right)^{n.} \right) \right) \right. \\ \text{if } -\varepsilon_{c2.60} \geq \varepsilon \\ \quad \left\| -f_{cd.60} \right. \end{array} \right.$$

$$\sigma_{c.317.30}(\varepsilon) := \left\| \begin{array}{l} \text{if } \varepsilon > 0 \\ \quad \left\| (0 \cdot \text{MPa}) \right. \\ \text{if } 0 \geq \varepsilon > -\varepsilon_{c2.12\_50} \\ \quad \left\| \left(-f_{cd.30} \cdot \left(1 - \left(1 - \frac{-\varepsilon}{\varepsilon_{c2.12\_50}} \right)^{n.} \right) \right) \right. \\ \text{if } -\varepsilon_{c2.12\_50} \geq \varepsilon \\ \quad \left\| -f_{cd.30} \right. \end{array} \right.$$

$$\sigma_{c.317.70}(\varepsilon) := \left\| \begin{array}{l} \text{if } \varepsilon > 0 \\ \quad \left\| (0 \cdot \text{MPa}) \right. \\ \text{if } 0 \geq \varepsilon > -\varepsilon_{c2.70} \\ \quad \left\| \left(-f_{cd.70} \cdot \left(1 - \left(1 - \frac{-\varepsilon}{\varepsilon_{c2.70}} \right)^{n.} \right) \right) \right. \\ \text{if } -\varepsilon_{c2.70} \geq \varepsilon \\ \quad \left\| -f_{cd.70} \right. \end{array} \right.$$

$$\sigma_{c.317.35}(\varepsilon) := \left\| \begin{array}{l} \text{if } \varepsilon > 0 \\ \quad \left\| (0 \cdot \text{MPa}) \right. \\ \text{if } 0 \geq \varepsilon > -\varepsilon_{c2.12\_50} \\ \quad \left\| \left(-f_{cd.35} \cdot \left(1 - \left(1 - \frac{-\varepsilon}{\varepsilon_{c2.12\_50}} \right)^{n.} \right) \right) \right. \\ \text{if } -\varepsilon_{c2.12\_50} \geq \varepsilon \\ \quad \left\| -f_{cd.35} \right. \end{array} \right.$$

$$\sigma_{c.317.80}(\varepsilon) := \left\| \begin{array}{l} \text{if } \varepsilon > 0 \\ \quad \left\| (0 \cdot \text{MPa}) \right. \\ \text{if } 0 \geq \varepsilon > -\varepsilon_{c2.80} \\ \quad \left\| \left(-f_{cd.80} \cdot \left(1 - \left(1 - \frac{-\varepsilon}{\varepsilon_{c2.80}} \right)^{n.} \right) \right) \right. \\ \text{if } -\varepsilon_{c2.80} \geq \varepsilon \\ \quad \left\| -f_{cd.80} \right. \end{array} \right.$$

$$\sigma_{c.317.40}(\varepsilon) := \left\| \begin{array}{l} \text{if } \varepsilon > 0 \\ \quad \left\| (0 \cdot \text{MPa}) \right. \\ \text{if } 0 \geq \varepsilon > -\varepsilon_{c2.12\_50} \\ \quad \left\| \left(-f_{cd.40} \cdot \left(1 - \left(1 - \frac{-\varepsilon}{\varepsilon_{c2.12\_50}} \right)^{n.} \right) \right) \right. \\ \text{if } -\varepsilon_{c2.12\_50} \geq \varepsilon \\ \quad \left\| -f_{cd.40} \right. \end{array} \right.$$

$$\sigma_{c.317.90}(\varepsilon) := \left\| \begin{array}{l} \text{if } \varepsilon > 0 \\ \quad \left\| (0 \cdot \text{MPa}) \right. \\ \text{if } 0 \geq \varepsilon > -\varepsilon_{c2.90} \\ \quad \left\| \left(-f_{cd.90} \cdot \left(1 - \left(1 - \frac{-\varepsilon}{\varepsilon_{c2.90}} \right)^{n.} \right) \right) \right. \\ \text{if } -\varepsilon_{c2.90} \geq \varepsilon \\ \quad \left\| -f_{cd.90} \right. \end{array} \right.$$

Parametrar för plottning

$$\varepsilon_{plot.12\_50} := 0, \frac{\varepsilon_{cu1.12\_50}}{20} .. \varepsilon_{cu1.12\_50} \qquad \varepsilon_{plot2.12\_50} := 0, \frac{\varepsilon_{cu2.12\_50}}{20} .. \varepsilon_{cu2.12\_50}$$

$$\varepsilon_{plot.55} := 0, \frac{\varepsilon_{cu1.55}}{20} .. \varepsilon_{cu1.55} \qquad \varepsilon_{plot2.55} := 0, \frac{\varepsilon_{cu2.55}}{20} .. \varepsilon_{cu2.55}$$

$$\varepsilon_{plot.60} := 0, \frac{\varepsilon_{cu1.60}}{20} .. \varepsilon_{cu1.60} \qquad \varepsilon_{plot2.60} := 0, \frac{\varepsilon_{cu2.60}}{20} .. \varepsilon_{cu2.60}$$

$$\varepsilon_{plot.70} := 0, \frac{\varepsilon_{cu1.70}}{20} .. \varepsilon_{cu1.70} \qquad \varepsilon_{plot2.70} := 0, \frac{\varepsilon_{cu2.70}}{20} .. \varepsilon_{cu2.70}$$

$$\varepsilon_{plot.80} := 0, \frac{\varepsilon_{cu1.80}}{20} .. \varepsilon_{cu1.80} \qquad \varepsilon_{plot2.80} := 0, \frac{\varepsilon_{cu2.80}}{20} .. \varepsilon_{cu2.80}$$

$$\varepsilon_{plot.90} := 0, \frac{\varepsilon_{cu1.90}}{20} .. \varepsilon_{cu1.90} \qquad \varepsilon_{plot2.90} := 0, \frac{\varepsilon_{cu2.90}}{20} .. \varepsilon_{cu2.90}$$

3 MATERIALKURVOR

3.1 Kurva 3.1.5 alla betongklasser

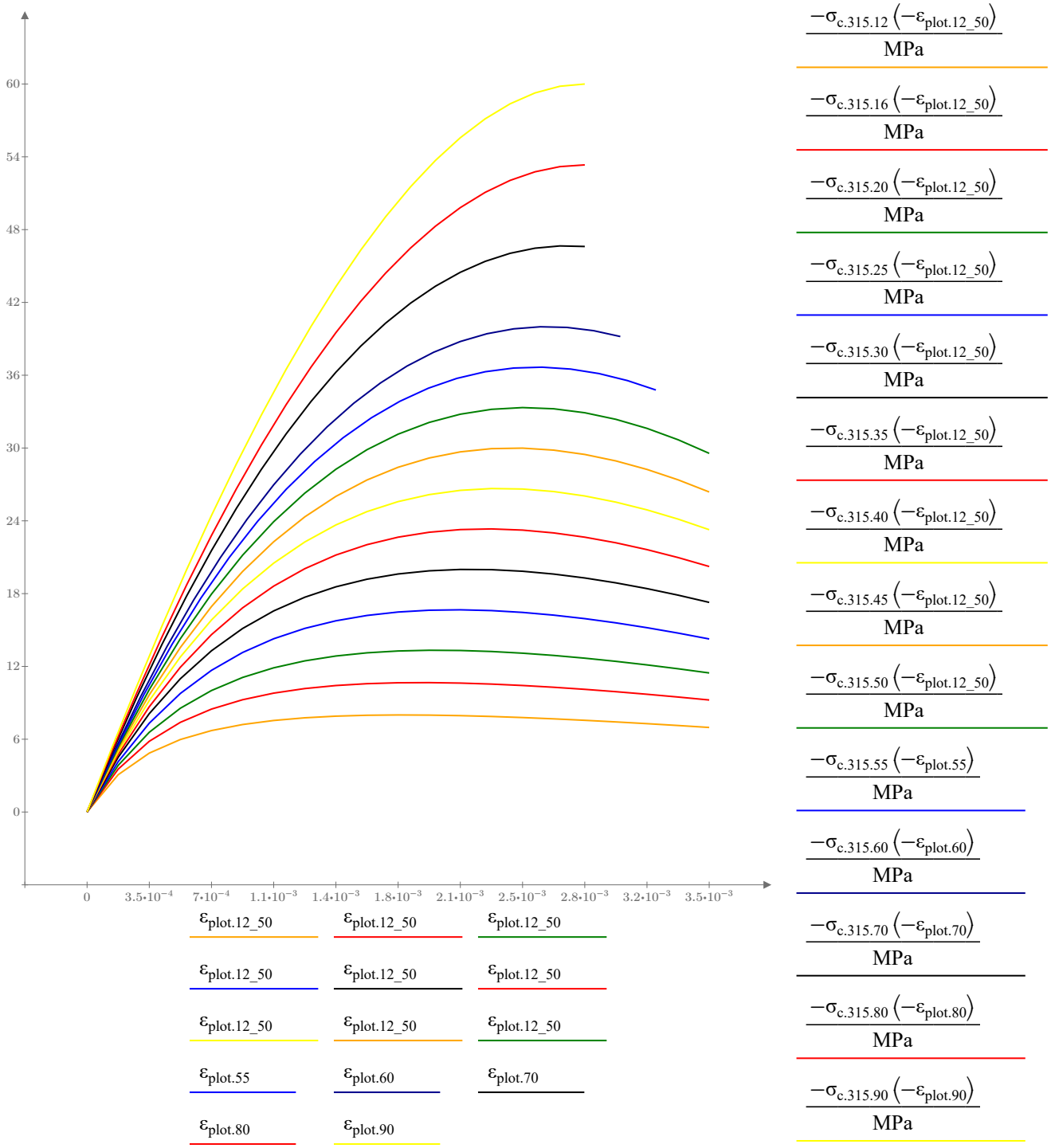

3.2 Kurva 3.1.7 alla betongklasser

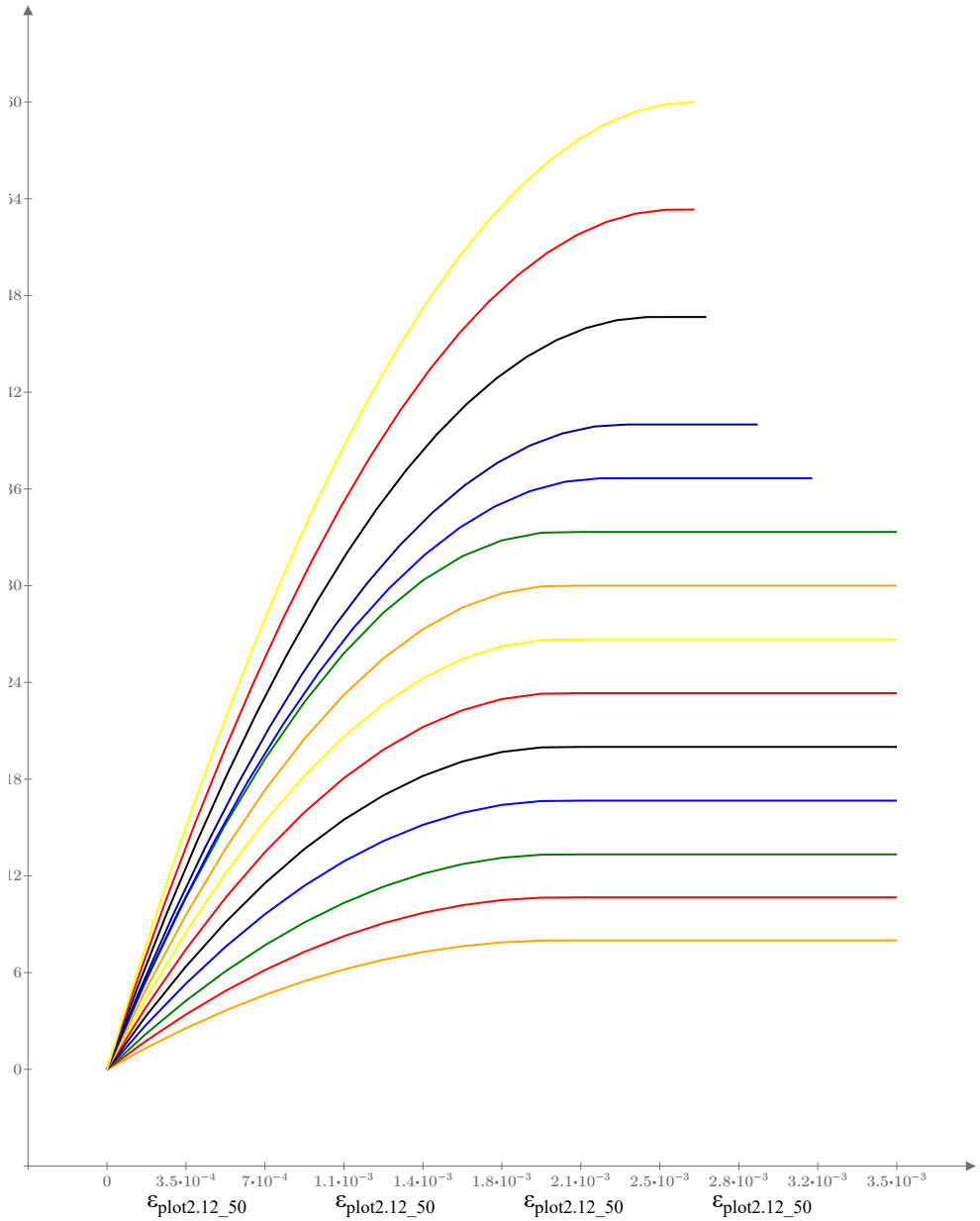

$$\frac{-\sigma_{c.317.12}\left(-\varepsilon_{plot2.12\_50}\right)}{MPa}$$

$$\frac{-\sigma_{c.317.16}\left(-\varepsilon_{plot2.12\_50}\right)}{MPa}$$

$$\frac{-\sigma_{c.317.20}\left(-\varepsilon_{plot2.12\_50}\right)}{MPa}$$

$$\frac{-\sigma_{c.317.25}\left(-\varepsilon_{plot2.12\_50}\right)}{MPa}$$

$$\frac{-\sigma_{c.317.30}\left(-\varepsilon_{plot2.12\_50}\right)}{MPa}$$

$$\frac{-\sigma_{c.317.35}\left(-\varepsilon_{plot2.12\_50}\right)}{MPa}$$

$$\frac{-\sigma_{c.317.40}\left(-\varepsilon_{plot2.12\_50}\right)}{MPa}$$

$$\frac{-\sigma_{c.317.45}\left(-\varepsilon_{plot2.12\_50}\right)}{MPa}$$

$$\frac{-\sigma_{c.317.50}\left(-\varepsilon_{plot2.12\_50}\right)}{MPa}$$

$$\frac{-\sigma_{c.317.55}\left(-\varepsilon_{plot2.55}\right)}{MPa}$$

$$\frac{-\sigma_{c.317.60}\left(-\varepsilon_{plot2.60}\right)}{MPa}$$

$$\frac{-\sigma_{c.317.70}\left(-\varepsilon_{plot2.70}\right)}{MPa}$$

$$\frac{-\sigma_{c.317.80}\left(-\varepsilon_{plot2.80}\right)}{MPa}$$

$$\frac{-\sigma_{c.317.90}\left(-\varepsilon_{plot2.90}\right)}{MPa}$$

3.3 Båda kurvor klasser 30, 35 och 40

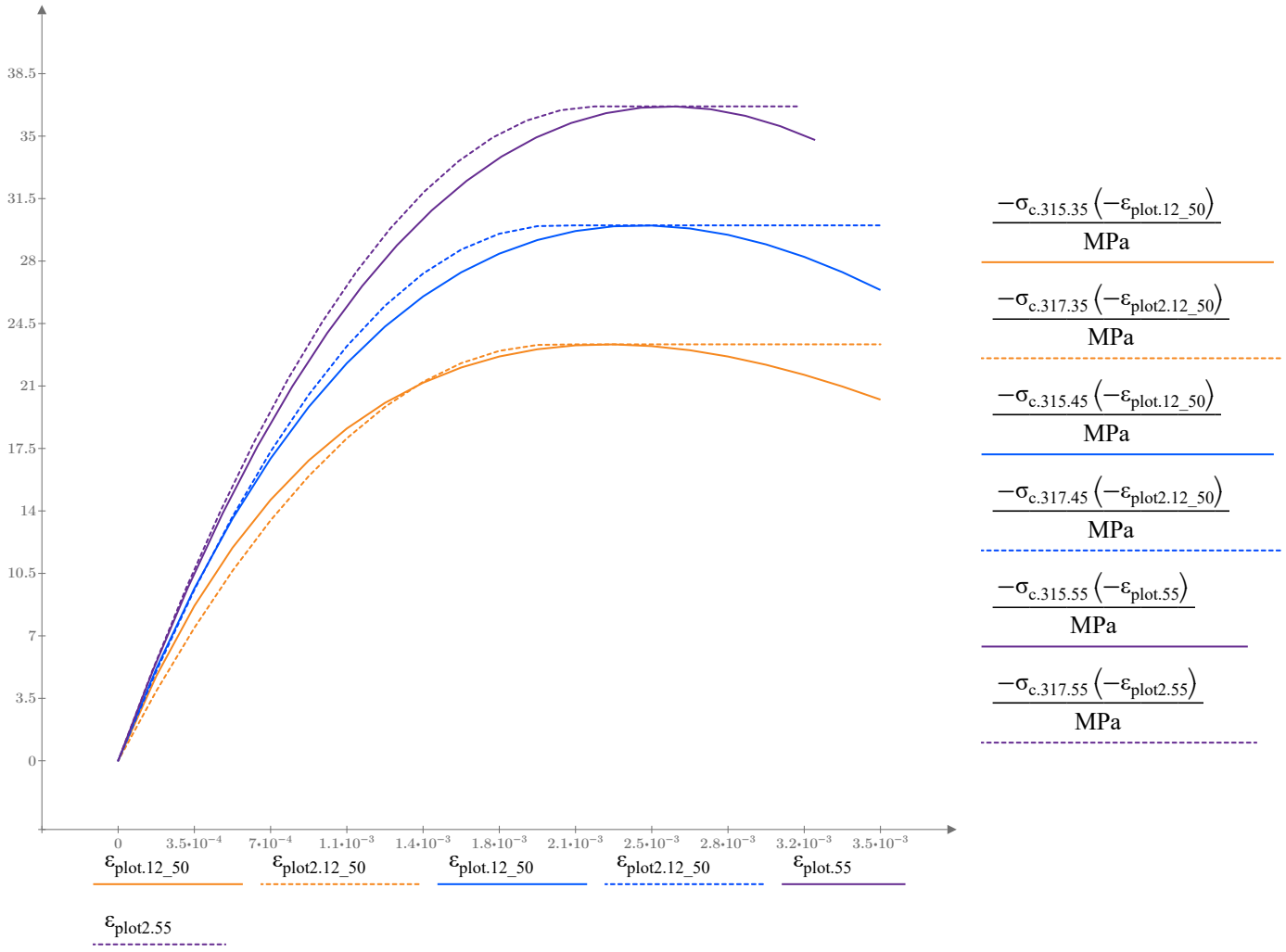

C Appendix: Crack band width

Fracture energy

According to CEB FIB 2010

$f_{ck} := 45\ \boldsymbol{MPa}$

$$G_F := 73\ \frac{\boldsymbol{N}}{\boldsymbol{m}} \cdot \left(\frac{f_{ck}}{\boldsymbol{MPa}} + 8\right)^{0.18} = 149.174\ \frac{\boldsymbol{N}}{\boldsymbol{m}}$$

Crack band width

Width of column $b := 1\ \boldsymbol{m} \quad h := 1\ \boldsymbol{m}$

Height of column $l_0 := 10\ \boldsymbol{m}$

Concrete cover thickness $d' := 0.125\ \boldsymbol{m}$

Effective height of cross section $d := h - d' = 0.875\ \boldsymbol{m}$

Characteristic compression strength $f_{ck} := 45\ \boldsymbol{MPa}$

Mean tensile strength $f_{ctm} := 0.30 \cdot \left(\frac{f_{ck}}{\boldsymbol{MPa}}\right)^{\frac{2}{3}} \cdot \boldsymbol{MPa}$

Characteristic tensile strength $f_{ctk} := 0.7 \cdot f_{ctm}$

Modulus of elasticity concrete $E_{cm} := 36\ \boldsymbol{GPa}$

Bar diameter $\phi := 25\ \boldsymbol{mm}$

Number of bars $n := 7$

Area of one row of reinforcement $A_s := n \cdot \frac{\pi \cdot \phi^2}{4} = \left(3.436 \cdot 10^3\right)\ \boldsymbol{mm}^2$

$A'_s := A_s$

Modulus of elasticity steel $E_s := 200\ \boldsymbol{GPa}$

Modular ratio $\alpha := \frac{E_s}{E_{cm}} = 5.556$

Horizontal force $H_{Ed} := 383\ \boldsymbol{kN}$

Moment $M := H_{Ed} \cdot l_0 = 3830\ \boldsymbol{kN} \cdot \boldsymbol{m}$

Normal force $N_{Ed} := -6000\ \boldsymbol{kN}$

Compression zone (guess until concrete stress at neutral axis = 0 $x := 0.29704055\ \boldsymbol{m}$

Transformed concrete area $A_{II} := b \cdot x + (\alpha - 1) \cdot A'_s + \alpha \cdot A_s = 0.332\ \boldsymbol{m}^2$

Center of gravity

$$x_{tp} := \frac{b \cdot x \cdot \frac{x}{2} + (\alpha - 1) \cdot A'_s \cdot d' + \alpha \cdot A_s \cdot d}{A_{II}} = 0.189\ m$$

Moment of inertia state II

$$I_{II} := \frac{b \cdot x^3}{12} + b \cdot x \cdot \left(x_{tp} - \frac{x}{2}\right)^2 + (\alpha - 1) \cdot A'_s \cdot \left(x_{tp} - d'\right)^2 + \alpha \cdot A_s \cdot \left(d - x_{tp}\right)^2 = 0.012\ m^4$$

Concrete stress at neutral axis

$$\sigma_c := \frac{N_{Ed}}{A_{II}} + \frac{M + N_{Ed} \cdot \left(\frac{h}{2} - x_{tp}\right)}{I_{II}} \cdot \left(x - x_{tp}\right) = -0.13\ Pa$$

Close to zero, OK!

Concrete stress at steel level

$$\sigma_c := \frac{N_{Ed}}{A_{II}} + \frac{M + N_{Ed} \cdot \left(\frac{h}{2} - x_{tp}\right)}{I_{II}} \cdot \left(d - x\right) = 78.844\ MPa$$

Steel stress

$$\sigma_s := \alpha \cdot \sigma_c = 438.022\ MPa$$

Effective height

$$h_{eff} := min\left(2.5 \cdot \left(h - d\right), \frac{h - x}{3}, \frac{h}{2}\right) = 0.234\ m$$

Effective area

$$A_{c.eff} := b \cdot h_{eff}$$

Effective reinforcement ratio

$$\rho_{p.eff} := \frac{n \cdot A_s}{A_{c.eff}} = 0.103$$

Factors

$$k_1 := 0.8 \qquad k_2 := 0.5 \qquad k_3 := 7 \cdot \frac{\phi}{d'} = 1.4$$

$$k_4 := 0.425 \qquad k_t := 0.4$$

Maximum crack distance

$$s_{r.max} := k_3 \cdot d' + k_1 \cdot k_2 \cdot k_4 \cdot \frac{\phi}{\rho_{p.eff}} = 0.216\ m$$

Strain difference

$$\Delta\varepsilon := \frac{\sigma_s - k_t \cdot \frac{f_{ctk}}{\rho_{p.eff}} \cdot \left(1 + \alpha \cdot \rho_{p.eff}\right)}{E_s} = 0.002$$

$$> \qquad 0.6 \cdot \frac{\sigma_s}{E_s} = 0.001$$

OK!

Crack width

$$w_k := s_{r.max} \cdot \left(\Delta\varepsilon\right) = 0.456\ mm$$

Mean crack distance

$$s_{rmean} := \frac{s_{r.max}}{1.7} = 127.296\ mm$$

D Appendix: Deformation calculation

Deformationsberäkning

Fast inspänd pelare

$$M := H\left(\frac{l_0}{2} - x\right)$$

$$\delta'' := \frac{-M}{EI}$$

BC:s

$\delta(0)$
$\delta'(0)$
$\delta'(l_0)$ All equal to zero

$$\delta'' := \frac{-H \cdot l_0}{2\ EI} + \frac{H \cdot x}{EI}$$

$$\delta' := \frac{-H \cdot l_0 \cdot x}{2\ EI} + \frac{H \cdot x^2}{2\ EI} + c_1$$

$\delta'(0)$ --> $c_1 := 0$

$$\delta := \frac{-H \cdot l_0 \cdot x^2}{4\ EI} + \frac{H \cdot x^3}{6\ EI} + c_2$$

$\delta(0)$ --> $c_2 := 0$

$$\delta := -\frac{H \cdot l_0^3}{12\ EI}$$

Konsolpelare

$$M := H\left(l_0 - x\right)$$

$$\delta'' := \frac{-M}{EI}$$

BC:s

$\delta(0)$
$\delta'(0)$ All equal to zero

$$\delta'' := \frac{-H \cdot l_0}{EI} + \frac{H \cdot x}{EI}$$

$$\delta' := \frac{-H \cdot l_0 \cdot x}{EI} + \frac{H \cdot x^2}{2\ EI} + c_1$$

$\delta'(0)$ --> $c_1 := 0$

$$\delta := \frac{-H \cdot l_0 \cdot x^2}{2\ EI} + \frac{H \cdot x^3}{6\ EI} + c_2$$

$\delta(0)$ --> $c_2 := 0$

$$\delta := -\frac{H \cdot l_0^3}{3\ EI}$$

E Appendix: DIANA curves

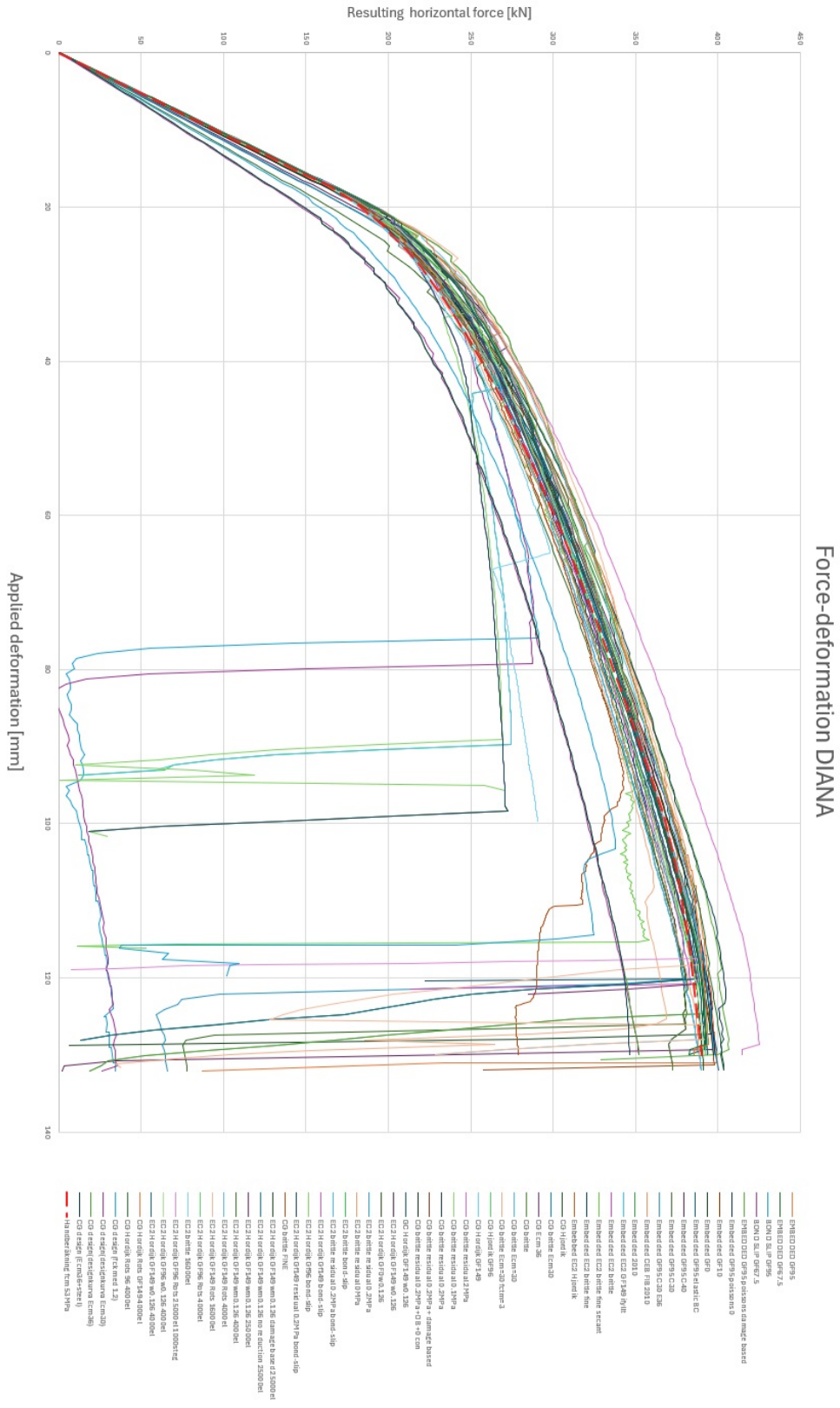

Figure E.1: Force-displacement curves from DIANA.

DEPARTMENT OF ARCHITECTURE AND
CIVIL ENGINEERING
CHALMERS UNIVERSITY OF TECHNOLOGY
Gothenburg, Sweden 2025
www.chalmers.se

CHALMERS
UNIVERSITY OF TECHNOLOGY